1-29-2015

Optically Micro-fabricated Linear and Freeform 3-D Extracellular Matrix Scaffolds for Tissue Engineering

Lawrence P. Cunningham
University of Connecticut - Storrs, lawrencecunningham@gmail.com

Optically Micro-fabricated Linear and Freeform 3-D Extracellular Matrix Scaffolds for Tissue Engineering

Lawrence Patrick Cunningham, Ph.D.

University of Connecticut, 2015

This work was aimed at advancing multi-photon excited, freeform fabrication technology with nano-scale and sub-micron precision as an enabler for tissue engineers to investigate cellular response to a biomimetic, bio-active extracellular matrix. We demonstrated that sub-micron and micron scale Collagen and Fibronectin structures can be fabricated via multi-photon excited photochemistry using a modified Benzophenone dimer and Rose Bengal while maintaining the biomimetic ECM structures' bioactivity. We confirmed that three-photon excitation produces significantly smaller features at comparable excitation wavelengths as a consideration to better approach focal adhesion size.

Bioactivity of MPE cross-linked FN and Collagens I and II was established via immunofluorescence and fibroblast adhesion. Additionally, the relative rates of degradation in these cross-linked matrices are consistent with the known activities of these enzymes.

Morphology measurements of fibroblasts grown on these proteins include log(Area), Perimeter, Area/Perimeter^2 were considered as proxies for cell response. Fibroblast perimeters are statistically different when associated with the Collagen I

microenvironment. Among fibroblasts grown on MPE structures of Collagen I, Fibronectin, BSA and the BSA Monolayer, the stress fiber distributions on Collagen I (all fiber lengths) are highly significantly different ($p < 1x10^{-4}$) than the distribution of stress fibers of cells on BSA Lines. This suggests contact guidance only for cells on BSA Lines but yet a combination of contact guidance and chemical signaling (RGD) with cells on Collagen I Lines. This supports additional overall orientation findings based on fibroblasts' fitted ellipse major axis direction for Collagens I, II and Fibronectin.

Stress fiber distribution on BSA Monolayer differed significantly from those on BSA structures ($p = 0.01$). This underscores the effects of pure contact guidance alone provided by the BSA fibers compared to the combined contact guidance and ECM cues provided by the FN, and collagen structures.

A method similar to rapid prototyping or three-dimensional printing was accomplished to resolve cellular response at the submicron level by fabricating biomimetic, bioactive extracellular matrices in a freeform three-dimensional (3D) manner. To the best of our knowledge, simultaneous 3D spatial and chemical control of collagen scaffold synthesis at the micrometer and sub-micrometer size scales has not been fully demonstrated.

Optically Micro-fabricated Linear and Freeform 3-D Extracellular Matrix Scaffolds for Tissue Engineering

Lawrence Patrick Cunningham

B.A., University of Vermont, 1981

M.S., University of Vermont, 1991

A Dissertation

Submitted in Partial Fulfillment of the

Requirements for the Degree of Doctor of Philosophy

At the

University of Connecticut

2015

APPROVAL PAGE

Doctor of Philosophy Dissertation

Optically Micro-fabricated Linear and Freeform 3-D Extracellular Matrix Scaffolds for Tissue Engineering

Presented by

Lawrence Patrick Cunningham, M.S.

Major Advisor _____
Paul Campagnola, Ph.D.

Associate Advisor _____
Liisa T. Kuhn, Ph.D.

Associate Advisor _____
Ji Yu, Ph.D.

University of Connecticut

2015

Acknowledgements

I would like to begin my thanking my wife for her support and encouragement for my endeavoring in this work.

In addition, I would like to thank my major advisor, Professor Paul Campagnola, as well as my committee members, Professors Liisa Kuhn and Jun Yi as well as our collaborator Professor George Pins of Worcester Polytechnic Institute and Professor Cyr M'lan, in the Department of Biostatistics at the University of Connecticut.

Together they have been a great resource of knowledge. They have helped me develop my research skills. I am grateful for their instruction, patience and support during this graduate education.

Multiphoton excited fabricated nano and micro patterned extracellular matrix proteins direct cellular morphology

I also wish to acknowledge American Chemical Society, John Wiley and Sons, and The Optics Society for permission to use or reprint content for Chapters 2, 3 and 5, respectively. The appropriate citations are found at the beginning of these chapters and in Appendix B.

Table of Contents

Abbreviations

3T3	mouse embryonic fibroblast cell line
BHK	Cells derived from baby hamster kidneys
BPD	Benzophenone dimer developed for crosslinking acid soluble collagens (where RB fails to generate singlet oxygen)
BSA	Bovine serum albumen
CSP	Cardiac side population cells
ECM	Extracellular Matrix
FA	Focal adhesion
FG	Fibrinogen
FN	Fibronectin
GFP	Green Fluorescent Protein
GLM	Generalized Linear Model
HSD	Tukey's Studentized Range
MDCK	Madin-Darby canine kidney cells
MPE	Multiphoton Excitation
MSV-85	Murine sarcoma virus two transformed cell line with a flat morphology
M-W-W	Mardia-Watson-Wheeler Test
PMMA	Polymethyl Methacrylate
RB	Rose Bengal

RGD	Tripeptide sequence in proteins comprised of Arg-Gly-Asp (RGD) making an attachment site which, together with the integrins that serve as receptors for them, constitute a major recognition system for cell adhesion.
SF	Stress Fiber
SV3T3	Swiss 3T3 cell line. Transformed cell lines with a flat morphology
TMPTA	Trimethylolpropane triacrylate, a trifunctional monomer used in the manufacture of plastics
TPE or 2PE	Two Photon Excitation
TPEF	Two Photon Excitation Fluorescence (or Fabrication)

List of Figures

List of Tables

Chapter 1

Specific Aims and Background

1.0 Specific Aims

The major thrust of this work is to establish multi-photon excited, freeform fabrication technology with nano-scale and sub-micron precision as an enabler for tissue engineers to investigate cellular response to a biomimetic, bio-active extracellular matrix.

To achieve this overall objective, the following aims are defined below.

Aim #1: To establish that Minimum Feature Sizes of MPE cross-linked Collagen are biologically appropriate for cell signaling investigations. This is discussed in Chapter 2, section 2.3.1.

Hypothesis: If focal adhesions form on MPE fabricated protein submicron structures with cell signaling peptide sequences such as RGD containing Collagen Type I, Fibrinogen and Fibronectin, then we may investigate biomimetic ECM response with optimal spatial precision.

Alternate existing methods of patterning shapes using ECM proteins have large size scales and limited free form spatial capabilities. Freeform MPE fabrication can be used for larger structures comprised of a matrix of finer structures. The laser scanning process can be controlled having the implication that the cross link density is controllable. Aim 1 requires that these optimally sized structures be, in fact, bioactive. This is identified as Aim 2.

Aim #2: To determine the Bioactivity of MPE cross-linked proteins via (A) Immunofluorescence, (B) Bioactivity via Cell Adhesion and (C) via Enzymatic Degradation of Collagen. This is discussed in Chapter 2, sections 2.3.2 to 2.3.4.

Hypotheses: (A) If a MPE-fabricated structure fluoresces when a fluorescently-labeled secondary antibody is added to the structure with a specific primary antibody, then the fluorescence provides evidence of post MPE-fabrication bioactivity. (B) If MPE-cross-linked collagen can be used to mimic in vivo behavior, excellent specificity for cellular adhesion (such as fibroblasts, in this case), would be expected, relative to the neutral background. (C) If MPE-cross-linked collagen is enzymatically degraded in a manner consistent with known, relative rates of collagen degradation, we can be assured of bioactivity compared to the native form with the benefit of understanding natural biodegradation rates of collagen based implants. We hypothesized that the least change in heights before and after would be seen in samples with the matrix having the highest initial crosslink density.

Establishing that biocompatible, bioactive sub-micron and micron scale structures can be fabricated from Types I, II and IV collagen suggests that the multiphoton fabrication process may be a powerful methods for cell-size scaffolding directly from collagen.

Aim #3: To explore the relative roles of topography and biochemistry that govern cell adhesion and spreading on ECMs patterns fabricated directly from cross-linked proteins. This is discussed in Chapters 3 and 4.

Hypothesis: If MPE fabricated structures are created that lack the biochemical cueing know to be contained within ECM proteins, then we can observe differences in

fibroblasts' morphological responses when comparing similar structures that have these biochemical cues. Cells on the BSA patterns should not be affected by a cell signaling mechanism but rather be constrained by physical guidance and orient between linear structures. By contrast, we hypothesize that cells will adhere on FN and FG structures due to inherent cell signaling mechanisms. We hypothesize that the cross-linked, matrix protein structures are expected to direct cell adhesion and spreading and that the topography and ECM cues would lead to different forms of guidance.

Chapter 3 details our efforts growing fibroblasts on cueing and non-cueing structures. Cueing ECM proteins used include Collagen I, Fibrinogen and Fibronectin which all contain the Arg-Gly-Asp (RGD) tripeptide which is involved in Focal Adhesions between cell membrane and the extracellular matrix. The non-cueing protein used is Bovine Serum Albumen which is use both as a non-cueing protein structure but as a non-specific, adsorbed monolayer as a neutral background on the microscope slide. Fibroblasts were grown on similarly shaped structures with the varied proteins responses. The cells' resulting shapes were fitted to ellipses. Major and minor axes were measured as was the angle of the major axis above the linear structures. This permitted a statistical comparison of fibroblast response to the different micro-environments.

Chapter 4 confirms an experimental observation in Chapter 3 concerning Fibroblast capability to sense a topographic cue by growing within parallel BSA linear structures. Fibroblasts grown on linear structures of Collagens I and II and Fibronectin show statistically different orientations compared to those grown on BSA linear structures.

Aim #4: To investigate the relationships between a focal adhesions and stress fibers with respect to a bioactive, biomimetic extracellular matrix in terms of likelihood of attachment of focal adhesion on varied spatial and biochemical microenvironments, stress fiber length and orientation, cell morphology. This is discussed in Chapter 4.

Hypotheses: *If α5 integrins are involved in fibroblast adhesion to Fibronectin MPE-fabricated linear structures, then this can be confirmed by immunofluorescence. Once establishing that integrins are the basis for the ECM-cell response, their stress fibers magnitude and direction can be studied to see if response differs in any of the combinations of protein type owing to chemical cueing of RGD containing protein structures. Additionally, fibroblast focal adhesion likelihood of occurrence should be greater than that of fibroblast focal adhesion counts on Fibronectin and to an even greater extent BSA structures.*

A specific primary antibody can be added to detect the integrin on the microscope slide's surface (including monolayer and FN linear patterns) and can be subsequently probed with a fluorescent-conjugated goat anti-mouse secondary antibody. Fluorescence indicates the unique response to the *α5* subunit. We anticipate different response with cells on BSA versus the ECM proteins discussed. Of additional interest is to observe differences or similarities between the ECM proteins' responses. Logistic Models are summarized in Table 3 of Chapter 4.

Aim #5: To advance this multi-photon excited, freeform fabrication technology in itself by integrating concepts and used in rapid prototyping or three-dimensional printing

to develop simultaneous 3D spatial and chemical control of collagen scaffold synthesis at the micrometer and sub-micrometer size scales. This is discussed in Chapter 5.

Hypothesis: *It is possible to develop CAD-based rapid, freeform 3-D fabrication with cross-linked layers that does not incur damage from overexposure at the co-registered locations.* Such 3-D structures can be used for an array of applications including cell sorting, bio-sensing and direct 3-D ECM fabrication.

1.1 Background

1.1.1 Introduction

Our work is aimed at advancing multi-photon excited, freeform fabrication technology with nano-scale and sub-micron precision as an enabler for tissue engineers to investigate cellular response to a biomimetic, bio-active extracellular matrix. Crosslinking via the xanthene Rose Bengal will not work for Collagens as Collagens are soluble at low pH where Rose Bengal is not photoactivatable at low pH. We aim to demonstrate that sub-micron and micron scale structures can be fabricated from collagen via multi-photon excited photochemistry using a modified benzophenone dimer and determine if resulting structures retain bioactivity. With this work we strive to accomplish a method to resolve cellular response at the submicron level by fabricating biomimetic, bioactive extracellular matrices in a freeform three-dimensional (3D) manner. This requires advancing the methods in multi-photon laser scanning from simple back and forth laser scans into defined freeform shapes in a manner which renders 3D structures. This would entail integrating similar concepts used in rapid prototyping or three-dimensional printing. To the best of our knowledge, simultaneous 3D spatial and chemical control of collagen scaffold synthesis at the micrometer and sub-micrometer size scales had not been fully demonstrated.

1.1.2 Cell Response to Topography

After detailed examination of cells' reactions to various grooved substrata, O'Hara [1] theorized the mechanism responsible for orientation of the cells was due to the orientation of sites of focal adhesion, and that this in turn would influence the orientation of microfilament bundles within the cells. In studying cell response to topography using

lithographically etched steps Clark [2] found that the degree to which a cell is impeded in its movement is dependent on the size of the topographic feature that it encounters. In this study, the effect of increasing step height on a cell's ability to cross and align is a gradual, until large step sizes are employed. Their data indicates that the alteration of a cell's behavior by a topographical feature follows a probabilistic pattern. Clark [3] studied contact guidance of cells using electronics miniaturization techniques to fabricate grooved substrates of varying dimensions (4-24 fan repeat, 0.2-1.9 pm depth). Topographical guidance of three cell types (BHK, MDCK and chick embryo cerebral neurones) was examined on these grooved substrates. An alignment within 10° of the groove direction was used as a guidance criterion. The repeated spacing had a small effect but that groove depth proved to be much more important in determining cell alignment. Cell alignment increased with increasing depth. BHK cells and MDCK cells interacted differently with grooved substrata. Additionally, it was observed that the response of MDCK cells depended on whether or not the cells were isolated (single) or part of an epithelial cell island (attached). Substrate topography is thus shown to be considered to be a vital cue in cellular migration. Cytoskeletal organization, cell adhesion and the interaction with other cells were postulated as being factors determining a cells susceptibility to topography.

1.1.3 Cell Adhesion, Morphology, Migration

When Ali and Hynes [4] added purified fibronectin (which was referred to at that time as LETS protein) to platelets that lacked fibronectin with little effect on cell growth rate. However, it had a major effect on cell adhesion and morphology as well as on cell migration and spreading [5, 6].

Willingham [7] also reported effects on cell adhesion and motility using antibodies on fibroblast myosin and indirect immunofluorescence microscopy. This study found no correlation between the presence of bundles of microfilaments and normal growth control. Normal cell line cultured on a poorly adhesive substratum resulted in small microfilament bundles. Similarly, a mutant cell line with normal growth but a rounded shape due to defective adhesiveness to substratum showed no bundle formation. However, two transformed cell lines (Swiss SV3T3 and Balb MSV-85) having a flat morphology showed extensive bundle formation. When a transformed cell line known to have insufficient adhesiveness was treated with a major surface glycoprotein of normal cells (CSP), there an increase in cell adhesiveness to substratum occurred. Cells formed extensive microfilament bundles without compromising growth. They conclude in this early study that distributions of microfilament bundles are related to cell-substratum adhesiveness and cell shape but not to growth properties.

1.1.4 Extracellular Matrix Organization and Cytoskeletal Actin

Zhang Q [8] created a *parallel* distribution of FN fibrils on cell surface that have underlying bundles of actin filaments and FA proteins. When cytochalasin (a fungal metabolite that binds to actin filaments, blocking polymerization and the elongation of actin) was employed to disrupt microfilaments, the outcome was a parallel disruption of the fibrillar FN matrix on the outside. This supports the strong correlation between extracellular matrix organization and cytoskeletal actin.

Zhang Q [9] identified the critical component in serum as a lipid that stimulates RhoA activity, as well as initiating other signaling pathways, namely Lysophosphatidic acid (LPA). This work demonstrates that microtubule depolymerization activates RhoA. Inhibiting RhoA activity or actin–myosin interaction was shown to prevent FN matrix assembly leading to the suggestion that it is the *tension* generated by the cytoskeleton that contributes to the assembly of a FN fibrillar matrix (Zhang Q [9]; Zhong CL [10]). Zhong CL [10] demonstrated that microtubule depolymerization activates RhoA. FN matrix assembly is shown to depend on RhoA-mediated contractility. It is suggested in this work that the role of the cytoskeleton and contractility in matrix assembly is to stretch FN, so as to expose these sites. Tension on FN exposes cryptic self-assembly sites. These studies provide evidence that ECM organization clues depend on the integrity of the cytoskeletal.

Additional studies have provided evidence for cryptic self-assembly sites within FN (Christopher RA [11]; Hocking DC [12]; and Ingham KC [13]). Strong evidence that cells exert tension on FN fibrils has been provided through the use of green fluorescent protein (GFP)-tagged FN. These experiments demonstrate that live cells can impose sufficient tension on FN fibrils to generate considerable stretch. Upon detachment, FN fibrils under tension were observed to contract rapidly to a quarter of their stretched length [14].

Tension generated by the actin cytoskeleton affects the assembly and organization of the ECM and, in turn, the organization of the ECM influences many aspects of cell behavior. FN matrix assembly is shown to depend on RhoA-mediated contractility and tension on FN exposes cryptic self-assembly sites. These all suggest that the role of the cytoskeleton and contractility in the matrix assembly is to stretch FN, so as to expose

these sites. This has been illustrated in studies showing that cell growth is diminished for cells adhering to an abnormal FN matrix assembled from truncated FN [15] where assembly of FN matrix from an FN mutant (deleted in the first 7 type III domains) inhibits cell cycle progression. Additionally, Mercurius KO [16] found supporting evidence for cells in which FN fibril assembly were blocked. The study concluded that inhibiting the FN matrix assembly by either a peptide or antibody would in turn inhibit cell cycle progression in vascular smooth muscle cells.

1.1.5 Guiding Cell Response – Topographic and Chemical Signaling

In designing new biomaterials, specific chemical and topographical cues will be important in guiding cell response. Filopodia are cellular actin-driven structures which are suspected to be involved in cell sensing of the three-dimensional environment. Work by Dalby [17] quantifies filopodia response to cylindrical nano-columns made of PMMA (100nm diameter, 160nm high) produced by colloidal lithography. Actin cytoskeleton morphology was observed by fluorescence microscopy and filopodia morphology by electron microscopy (scanning and transmission). Results showed that fibroblasts produced more filopodia per mm of cell perimeter. In addition, filopodia was observed to interact with the cells' nano-environment.

Cell adhesion responses are also involved in pathologies involving blood clotting, inflammatory deficits and as well as cancer metastasis ((Bunting [18]; McEver [19]; Brakebusch [20]). In addition, cell adhesion to adsorbed adhesive proteins mediate attachment and activation of neutrophils and macrophages, regulating subsequent host implant inflammatory responses (Anderson [21]; Shen [22]).

1.1.6 Fabrication Techniques

Much effort has recently occurred in developing two dimensional, micro-scale fabrication techniques for proteins and polymers for use in directing cell adhesion and growth. These efforts share the purpose of producing biomimetic and functional devices for biosensors, implants, and researching fundamental areas of cell biology, including the regulation of cell function with experimentally varied changes in the surface chemistries. Photolithography is a mature technology, producing features on the 200 nm size scale. Photolithographic fabrication has two important limitations with respect to these cell biology applications. First, photolithography is not optimal for fabricating vertical features of any complexity as lithography is essentially a two dimensional process. Second, photolithography has a limited ability to fabricate with multiple materials, including biomaterials. Variations of soft lithography, such as micro-contact printing, is becoming widely used for protein and cellular patterning (Lom [23]; Ito [24]; Mrksich [25], Xia [26]; Kung [27]; James [28]; Boateng [29]), however it also has limitations as a biological fabrication method. Although some axial control exists, it too, is essentially a two dimensional process, and seems have limited capability in producing sub-micron features. In addition, the stamping chemistries are not completely general. Electro-spinning can create micron scale structures from proteins. However, this has limited flexibility in the shapes that can be produced. To complement the suite of technologies, dip pen nanolithography (Demers [30] has promising fabrication method developments for functionalizing and patterning surfaces at the sub 100 nm scale and may prove to be a useful complement to our submicron 3D methods.

The fabrication processes used in our work presented here uses a photo-polymerization which occurs via a multi-photon process, where excitation of a photo-initiator proceeds through one or more virtual states. The simultaneous absorption probability through a virtual state is given by P^n/τ^{n-1}, where P represents the laser pulse energy, n is the number of absorbed photons, and τ is the laser pulse width. It is specifically the dependence on τ that necessitates the use of ultrafast lasers for multi-photon polymerization. The use of femtosecond lasers has the advantage of providing a low average laser power which avoids photo-damage in biological samples. Multi-photon excitation path involving a virtual state was predicted in 1931 by Maria Göppert-Mayer [31]. The diagram in Figure 1 depicts the two-photon excitation for the photo-initiator rose bengal (RB). The S1 state can be reached via a single-photon excitation of 550 nm or in our case, via a multi-photon approach with two 800 nm simultaneous photons. Multi-photon excitation at 800 nm reaches the S2 electronic state going through a virtual state which subsequently decays non-radiatively (10^{-12} s) with near unit efficiency as the S1 state. Inter-conversion of the S1 population to the long-lived (1 ms) T1 electronic state, with an efficiency of greater than 98%, becomes the final reactive state. The formation of a long-lived triplet state can initiates a free-radical polymerization mechanism in the presence of a co-initiator [32].

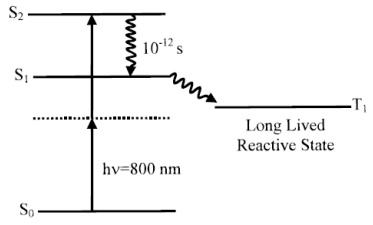

Figure 1: The two-photon excitation for the photo-initiator rose bengal (RB)

The multi-photon excitation process for submicron photo-polymerization has enabling advantages. Primarily, the polymerization is confined to only the focal volume. This is due to the fact that simultaneous absorption of multiple photons requires a very high photon flux, which is only present at the point of focus. This allows for precise spatial fabrication in solution by avoiding nonspecific polymerization outside of the focal volume. Second, there is reduced photo-bleaching of the photo-activatable dyes used for polymerization. Third, there is no linear near- IR absorption out of the plane in most bio-macromolecule samples [33]. The longer wavelength photon provides a greater penetration depth, allowing for fabrication of objects below the surface of biological samples and many other materials.

Future work must address the necessity that biomimetic extracellular matrix (ECM) scaffolds must replicate native tissue microstructures appropriate to cellular microenvironments (1-10 um) and organ-scale structures with cellular resolution (10-1000 um) to optimally maintain in vivo-like cellular function (Bhatia [34] and [35]).

We show that 3D proteins matrices can be fabricated with a variety of photo-chemistries and will demonstrate, by several means, that biological activity is maintained. We further advance this application in terms of fabricating scaffolds and patterned surfaces consisting of combinations of ECM proteins for directed cell growth. It is straightforward to pattern collagen composites as compared to the efforts of those achieved by 2D soft lithography and chemical means (Lickorish [36], Chen [37]). We have utilized both the xanthene Rose Bengal and a recently reported dimer of Benzophenone [38] as activators of biomimetic, bioactive tissue scaffolds. In addition, we use existing optical methods and developed new optical methods with appropriate

photo-chemistries to fabricate relevant ECM structures and quantify cellular response to this biomimetic microenvironment. With these methods, we validate the hypothesis that these optically cross-linked ECM scaffold proteins are bioactive.

Should precisely prescribed structures be fabricated under tightly controlled dimensions and at submicron scale, then experimental designs should elicit a measureable cellular response. As these biomimetic, extracellular matrices are fabricated at the at the submicron level, resolution of response would be commensurate in scale to elicit response of specific integrins. The use of MPE for fabricating nano and micron scaled cross-linked protein structures will offer a flexible method for studying the topographic factors and cell-matrix interactions that drive cell adhesion, spreading, differentiation, and proliferation. Our subsequent efforts are directed at systematically varying feature sizes, topographies, and protein composition to characterize the effects of surface morphology on cellular functions. Pitts, Howell [38] demonstrated that soluble proteins could be cross-linked, layer by layer, into three dimensional matrices by Multi-photon Excitation (MPE) in the presence of photo-activators, such as Rose Bengal [38, 39]. Recently, the synthesis of a new photo-activator, a dimer of Benzophenone (BPD), has been reported (Pitts, Howell et al. 2002) which demonstrates its use for multi-photon excited, three-dimensional photonic fabrication of proteins, most significantly collagen. This BPD photo-activator is demonstrated as a way to cross-link collagens, (or more accurately, tether of two with a dimer molecule covalently linking two proximal collagens) resulting in a cross-linking process which produces structures on the micron and submicron size scales. The BPD complements Rose Bengal which is a classic photo-activating xanthene. Rose Bengal, when acting as a photo-initiator in solution, excites

dissolved oxygen to its singlet state within the femto-liter scale focal volume of the multiphoton laser scan. Singlet oxygen facilitates the crosslinking of the proximal proteins in the plume of the MPE laser's scan. Collagens would not be cross-linkable using Rose Bengal alone. Rose Bengal and a co-initiator system would need to be into one molecule to crosslink collagen. Collagens have been difficult to cross-link photo-chemically, and these results which suggest that the new activators will be suitable for cross-linking collagens and additional proteins for the *de novo* assembly of biomimetic tissue scaffolds.

Chapter 2

Multiphoton Excited Fabrication of Collagen Matrixes Cross-Linked by a Modified Benzophenone Dimer: Bioactivity and Enzymatic Degradation

Multiphoton Excited Fabrication of Collagen Matrixes CrossLinked by a Modified Benzophenone Dimer: Bioactivity and Enzymatic Degradation

Swarna Basu,†,‡ Lawrence P. Cunningham,† George D. Pins,§ Katie A. Bush,§ Rosa Taboada," Amy R. Howell," Jun Wang,⊥ and Paul J. Campagnola*,†

† University of Connecticut Health Center.
‡ Current address: Department of Chemistry, Bryn Mawr College, 101 North Merion Ave., Bryn Mawr, PA 19010.
§ Worcester Polytechnic Institute.
" Department of Chemistry, University of Connecticut.
⊥ GlaxoSmithKline.

I wish to acknowledge the American Chemical Society for their permission to reprint (adapt) for the following work (citation below) for this chapter.

Basu S, Cunningham LP, Pins GD, Bush KA, Taboada R, Howell AR, Wang J, Campagnola PJ., Multiphoton excited fabrication of collagen matrixes cross-linked by a modified benzophenone dimer: bioactivity and enzymatic degradation., Biomacromolecules. 2005 May-Jun;6(3):1465-74.

ABSTRACT

The use of Multiphoton excited (MPE) photochemistry to fabricate model tissue engineering scaffolds directly from types I, II, and IV collagen is presented. A modified dimer of benzophenone (BPD) provides photoactivation and becomes incorporated into the resulting collagen matrixes. Unlike xanthene photochemistries, the BPD can be used in acidic environments, where most collagens have the greatest solubility. The minimum feature sizes are investigated by using two- and three-photon excitation, where the latter provides for superior "resolution" and suggests that collagen structures can be fabricated on the size scales of focal contacts. The resulting structures display excellent retention of bioactivity as evidenced by highly specific cell adhesion as well as immunofluorescence labeling. Structural and chemical aspects of the collagen matrixes are probed through measuring the enzymatic degradation through specific and nonspecific proteases, as the resulting relative rates are consistent with the activity of these enzymes. Degradation rates can also be controlled through varying the cross-link density in the matrixes, which is achieved through tuning the exposure dose during the fabrication process. The degradation rates are also found to be consistent with swelling/shrinking measurements and thus the average mesh size of the matrixes. In all cases the enzymatic degradations are well-fit single exponentials, suggesting that the matrixes can be fabricated with a priori knowledge of their structural properties. These results when coupled with the resulting bioactivity suggest that the MPE fabrication process may be a powerful tool for the creation of cell-sized tissue engineering scaffolds.

2.1 Introduction

Recent advances in materials science have led to the implementation of techniques for tissue engineering that can create biocompatible and bioactive structures that are on the size scale of cells and tissues. These structures can be used for applications such as directed cell growth on extracellular matrixes (ECM)[1] and cell encapsulation for in vivo repair.[2-4] Biocompatible tissue scaffolds can also be constructed to serve as active analogues of the ECM, where cells can attach, proliferate, and ultimately synthesize their own matrix molecules. Designing highly functional scaffolds for tissue engineering requires a fundamental understanding of the mechanisms by which the three-dimensional architecture and the biochemical composition of the tissue scaffolds modulate cellular adhesion, proliferation, and differentiation, as well as the regeneration of native tissue functions. Such tissue engineering scaffolds should replicate native tissue microstructures, not only at the cellular scale (10-100 μm) but also at the submicrometer scale (100-500 nm) of ECMs and basement membranes and do so with biomolecular complexity.

Since collagen is an important primary protein that forms topological complex ECMs, there has been considerable recent effort in fabricating cellular/collagen scaffold hybrid structures and examining their resulting activity. These efforts have utilized both two- and three-dimensional methods. For example, Desai used a layer by layer microfluidics approach to examine the effects of cell contraction on matrix structures comprised of type I collagen and Matrigel, where the matrixes were created through self-assembly of the collagen in basic solution.[5,6] Similarly, Pins used microfabrication strategies to create microtextured collagen membranes and dermal analogues with precisely defined topographic features to modulate keratinocyte function on the surfaces of cultured skin equivalents.[7,8] Microcontact

printing and photolithography have also been widely used to fabricate substrates that direct cell adhesion.[9-14] Recently several studies have also examined the cytoskeletal structure of cells on patterned surfaces with nano- and microscale architecture created from polymers.[1,15,16] While these studies have provided considerable insight into the creation of artificial scaffolds, it would be advantageous to create three-dimensional scaffolds directly from cross-linked collagen. To the best of our knowledge, simultaneous 3D spatial and chemical control of collagen scaffold synthesis at the micrometer and sub-micrometer size scales has not been fully demonstrated. This combination of fabrication modalities would have enormous potential for tissue engineering.

In general, cross-linking of collagen-based biomaterials often helps to improve the resistance of these materials toward degradation, especially by enzymes. Chemical cross-linking may also reduce the immunogeneticity of collagen and can be used to control the degradation upon implantation when used for medical applications.[17] Clinically, glutaraldehyde is the most commonly used chemical agent for cross-linking biological tissues, but it may result in poor biocompatibility.[18] Furthermore, limited spatial control is available through purely chemical schemes. The use of photochemical cross-linking provides spatial control; however, most conventional photochemical schemes are essentially two-dimensional in nature, as axial control is limited for linear (one-photon) excitation.

To overcome these difficulties, we have introduced the use of multiphoton excited (MPE) photo-cross-linking of proteins as a new 3D biofabrication method.[19-23] In this current work, we have used this methodology to fabricate photo-cross-linked collagen (types I, II, and IV) structures on the sub-micrometer and micrometer size scales and have studied some of the resulting structural and functional aspects of these model scaffolds. This photochemical

approach is analogous to that of multiphoton excited fluorescence, where, in the latter, intrinsic three-dimensionality, and thus optical sectioning, is obtained by confinement of the excitation to the plane of focus. In the present case, MPE photochemistry is used to *fabricate structures one plane at a time.* The confinement that results from the need for high peak powers affords the sequential fabrication in adjacent focal planes without overwriting or damaging preexisting layers. Because the fabrication is performed on a microscope platform, sub-micrometer feature sizes are readily obtainable using medium and high numerical aperture (NA) lenses. Since collagen matrixes (and other protein matrixes) are cross-linked under physiological conditions, the resulting products have excellent biocompatibility. For example, we recently assayed the biological activity of several proteins (alkaline phosphatase, fibrinogen, and fibronectin) cross-linked via MPE Rose Bengal photochemistry, and in all cases excellent compatibility was achieved.[21, 23]

In this paper, we extend this line of research to the fabrication and characterization of multiphoton cross-linked collagen structures (types I, II, and IV) that are relevant for tissue engineering applications. In general, these forms of collagen are difficult to cross-link by conventional photochemistries, such as Rose Bengal activation. This arises, in part, because many forms of collagen are only acid soluble, with the exception of type IV collagen, however, and because the Rose Bengal chromophore protonates at pH < 7 and is no longer photoactive. Thus, new approaches are necessary for efficient photo-cross-linking of collagen. For example, Chaikof and co-workers synthesized a type I collagen-methylacrylate conjugate and then linked the proteins together via free radical vinyl polymerization using eosin photochemical activation.[24] As an alternative to introducing polymeric groups into the cross-linked collagen matrix, we recently reported the synthesis

and optical characterization of a new photoactivator consisting of two modified benzophenone moieties linked together via a flexible amine tether.[20] Proteins have long been cross-linked using benzophenone chemistry in a two-step process by first chemically conjugating a benzophenone to a protein (typically via a maleimide), followed by a photochemical step. The latter excites the π to π * transition and creates a ketyl diradical that binds a second protein molecule.[25] This approach has been used to study structural aspects of many proteins, including myosin,[26] troponin,[27] and actin.[28] Our tact is fundamentally different in that each benzophenone monomer of the benzophenone dimer (BPD) is simultaneously photoactivated and then binds to a respective protein molecule and thus becomes incorporated into the cross-linked matrix. By contrast, in Rose Bengal activation, the dye relaxes to the ground state following production of singlet oxygen and is thus regenerated and available for further steps.[29, 30]

We previously reported the synthesis of the BPD and showed it was successful in cross-linking type I collagen. In that work, no attempts were made to investigate any of the properties of the resulting structures. In this paper we extend the work to characterizing cross-linked structures (using the BPD) from several types of collagen (I, II, and IV) in terms of their physical, biological, chemical, and structural properties (supramolecular). We begin by comparing the minimum feature sizes obtainable by both two- and three-photon absorption and demonstrate the latter provides superior "resolution". To have applications as tissue scaffolds and ECMs, the resulting protein matrixes must display retention of the collagen bioactivity. This is especially important in the current case because a new photochemistry is employed. To this end, bioactivity is demonstrated both in terms of immunofluorescence as well as directed cell adhesion of dermal fibroblasts on sub-

micrometer cross-linked linear structures. We next examine the enzymatic degradation of the cross-linked collagen matrixes using several proteases. In general, tissue engineering scaffolds are susceptible to degradation over time, and it is important to study the effect of several different enzymes of differing activity on the degradation rates. Furthermore, examining the degradation by different proteases reveals chemical information regarding how the matrixes were assembled. Specifically, it is desirable to have the cross-linked collagen molecules to retain as much of the native structure as possible. Furthermore, degradation measurements can provide insights into the cross-link density[31] and provide data on the resulting mechanical properties.[32] Here we investigate the degradation of matrixes cross-linked via MPE of the benzophenone dimer by specific and nonspecific proteases and find that the results are consistent with the known activityof these enzymes. Additionally, the relative rates can be correlated with the cross-link density and mesh size of the matrix. These results give us confidence that BPD cross-linked collagen matrixes can be created with some a priori knowledge of their properties and may be useful as new devices.

2.2 Experimental Section

2.2.1 Materials.

Octadecyltrichlorosilane (OTDS; Gelest, Morrsiville, PA), anhydrous toluene (Aldrich, St. Louis, MO), type I and type II collagen (Sigma, St. Louis, MO), bovine serum albumin (BSA; Sigma), Rose Bengal (Sigma), type II collagen-FITC (fluorescein isothiocyanate) conjugate (Sigma), Texas Red-labeled BSA, type IV collagen-Oregon Green conjugate (Molecular Probes, Eugene, OR), collagenase, pepsin, and trypsin (Sigma) were

used without further purification. The benzophenone dimer was synthesized as described previously.[20] For the immunofluorescence staining of type I and type II collagen, mouse anti-human collagen type I monoclonal antibody, mouse anti-collagen type II monoclonal antibody (Chemicon, Temecula, CA), and labeled goat anti-mouse IgG antibodies (Molecular Probes) were also used as received.

2.2.2 Fabrication/Imaging Apparatus.

A home-built laser-scanning nonlinear optical microscope was used for both the multiphoton excited fabrication of the collagen structures as well as two-photon fluorescence diagnostic imaging. The design and performance of the microscope have been previously described.[33] The multiphoton excitation is achieved through a femtosecond near-infrared titanium sapphire oscillator (Mira 900-F, Coherent, Santa Clara, CA) that is pumped by a 5 W Verdi Nd:YVO4 (Coherent). The laser is coupled to an upright microscope (Axioskop, Zeiss, Jena, Germany) that is equipped with both bright field and fluorescence optics. A 20x, 0.75 numerical aperture (NA) objective lens (Zeiss) was used for the fabrication. An oil immersion objective lens (40x, 1.3 NA; Zeiss) was used to measure lateral and axial dimensions of the cross-linked structures.

Two-photon excited fluorescence is used both as an online diagnostic of the fabrication process and for postfabrication imaging of physical dimensions, immunofluorescence, and enzymatic degradations. The fluorescence is detected in a non-descanned epi-illumination configuration, as this leads to greatly improved sensitivity over confocal detection (as a pinhole is not needed for nonlinear excitation). The fluorescence is separated from the laser by a 525 nm long pass dichroic mirror and two BG39 color glass filters (8 OD blocking) and detected in single-photon counting mode. The code for

operating this instrument for both the scan control and simultaneous data acquisition was written entirely using LabVIEW 6.1 (National Instruments, Austin, TX) in the form of a graphical user interface code and is freely available on our website at http://www.cbit.uchc.edu/ faculty_nv/campagnola/fabrication.html.

Typical pulse energies at the sample were approximately 500 pJ/pulse. We define the exposure dose in terms of integrating the pulse energy in each pixel across the dimensions of the fabricated structures over the number of repetitive scans. The concentrations of the proteins and photoactivators were as follows: type I collagen (3 mg/mL, 0.2 N acetic acid), type II collagen (2.8 mg/mL, 0.2 N acetic acid), type IV collagen (2 mg/mL, water), BSA (5 mg/mL, water), BPD (2.5 x 10^{-4} M, water), and Rose Bengal (1 mM, water). Preparations were created on silanized microscope slides (see below), under cover slips that were separated from the slide using glass spacers, such that the enclosed volume was approximately 50 *4u*L. Three-dimensional rectangular structures (60 *4*μm x 40 *4*μm x 5 *4*μm) and 100 *4*μm parallel linear structures (700 nm wide, 3 *4u*m high) of collagen were fabricated for all the measurements in this work.

2.2.3 Preparation of Silanized Surfaces.

We have found that the MPE cross-linking of collagen and other proteins on hydrophobic surfaces is more facile and robust than on a hydrophilic glass substrate. This is presumably due to the decreased water content on the surface. Here a chemisorbed, self-assembled organosilane (ODTS) monolayer is used to provide a stable, hydrophobic surface. The glass microscope slides were sonicated in a 1:1000 dilution of detergent (Aldrich Micro 90C) in deionized water for 15 min. This detergent contains no phosphates, silicates, borates, halogenated hydrocarbons, or phenols. The slides were then

washed with deionized water for another 15 min. The surface was dried with nitrogen or argon and plasma-cleaned at 0.3 Torr pressure for 3 min. The slides were soaked for 24 h in deionized water and dried once again with nitrogen or argon. The slides were then soaked overnight in a solution of 0.5% (v/v) ODTS in anhydrous toluene and care was taken to maintain an inert, moisture-free environment. After soaking, the slides were washed three times with anhydrous toluene to remove any residual ODTS, dried with nitrogen or argon, and heated for 30 min at 120 °C to complete the formation of the Si-O bond.

Collagen can then be MPE cross-linked directly onto the resulting silanized surface or onto this surface linked to a BSA monolayer. The latter preparation was used for the cell-adhesion experiments, where the silanized slides were soaked in a 10 mg/mL solution of BSA and rinsed several times with deionized water.[34,35] The adsorbed BSA then provides a stable, homogeneous foundation upon which proteins in solution may be cross-linked and, further, provides a background surface to reduce nonspecific cellular adhesion.

2.2.4 Fabrication and Enzymatic Degradation of Collagen Matrixes.

The wavelengths used for multiphoton excited cross-linking were 780 and 850 nm, where these nominally correlate to three- and two-photon excitation of the BPD, respectively, and 800 nm for two-photon excitation of Rose Bengal (only for type IV collagen). Fluorescently labeled collagen (FITC type II and Oregon Green type IV) was photo-cross-linked at 780 nm for the protease degradation experiments. The fabricated structures were rinsed with distilled water to remove any residual photoactivator; then an aqueous solution of the enzyme was added. The rate of digestion was determined by monitoring the decrease in two-photon excited fluorescence intensity (830 nm excitation),

where this was measured across the center of the sample by line scan imaging and then averaging the total intensity over several scans. These measurements were taken at intervals over a 30-60 min time course.

2.2.5 Cell Culture and Adhesion.

For the cell adhesion assays, primary human dermal fibroblasts were isolated from neonatal foreskins and cultured in Dulbecco's modified eagles medium (DMEM; Gibco BRL, Gaithersburg, MD) supplemented with 10% fetal bovine serum (FBS; Atlanta Biologicals, Lawrenceville, GA) and penicillin/streptomycin (100 U/(100 μg/mL); Gibco). Briefly, sections of dermis from human neonatal foreskins were cut and placed onto scored areas of standard tissue culture dishes. The sections were allowed to dry for 30 min and then were incubated in DMEM with 10% FBS and penicillin/streptomycin (100 U/(100 μg/ mL)) at 37 °C and 10% CO2 until the culture dishes were confluent with fibroblasts. The fibroblasts were then removed by trypsin and expanded in culture. Passages 3-9 were used for cell-adhesion experiments.

Silicone gaskets were used to create individual wells for the fabrication of the protein structures and subsequent cell plating. Slides were briefly rinsed in tissue culture medium to clean the surfaces. To seed the individual wells on the slides, 100 μL aliquots of tissue culture medium containing 6×10^4 cells/mL (final cell seeding density of 6×10^3 cells/ cm^2) were carefully pipetted into the center of each well. Cell-seeded slides were carefully transferred to a tissue culture incubator maintained at 37 °C and 10% CO2. After 3 h, the tissue culture plates containing the patterned slides were filled with 10 mL of DMEM supplemented with 10% FBS. To document cell adhesion, the patterned slides were viewed on a Nikon Eclipse TS100 inverted epi-fluorescence

microscope coupled with a SpotRT CCD camera (Diagnostic Instruments, Sterling Heights, MI).

2.3 Results and Discussion

2.3.1 Minimum Feature Sizes of MPE Cross-Linked Collagen.

For tissue engineering applications, it is desirable to fabricate protein structures with minimum feature sizes on the same scale of focal contacts or □300 nm. Here we demonstrate the achievable feature sizes obtainable with two-and three-photon excited cross-linking of collagen with the benzophenone dimer. Due to the cooperative nature of the process, the resolution resulting from multiphoton absorption is not governed by the Abbe' diffraction limit. Theoretical point spread functions (PSF) have predicted that, at the same wavelength, three-photon excitation will have a smaller three-dimensional PSF than that of two-photon excitation.[36,37] This finding is due to the need for higher peak excitation power in the former, which reduces the focal volume over which excitation can occur. In previous work, we demonstrated that for MPE polymerization this was indeed the case:[19] linear structures were fabricated from the triacrylate TMPTA using Rose Bengal (two-photon) and 9-fluorenone-2-carboxylic acid (three-photon) activation, both at 780 nm, and it was seen that the minimum features resulting from three-photon absorption were approximately half those created from two-photon excitation.

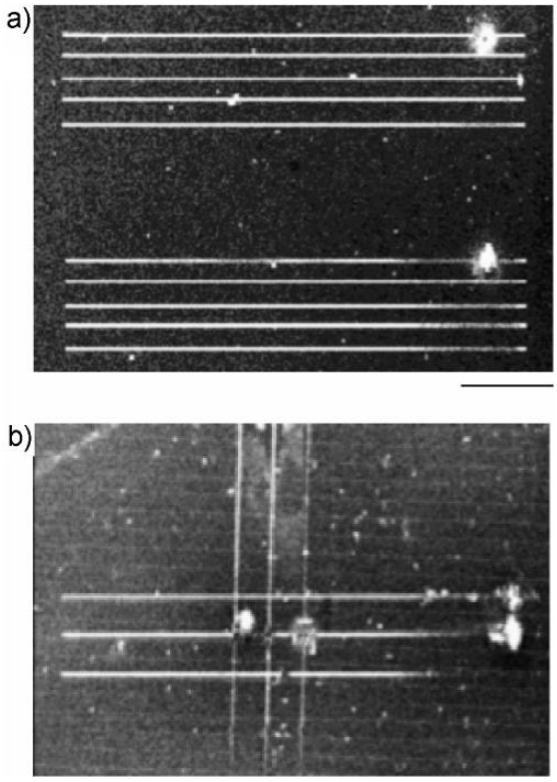

Figure 1. Three-photon excited fluorescence images of multiphoton cross-linked type I collagen, where the contrast arises from the benzophenone dimer: (a) two sets of parallel linear structures and (b) a set of orthogonal linear patterns. Scale bar) 20 μm.

We previously showed that absorption spectrum of the BPD molecule has two prominent bands, the π *to* π * transition (~260 nm) as well as a lower energy charge-transfer transition (~360 nm) that is highly solvatochromic.[20] A power dependence of fluorescence intensity was performed to determine the absorption order, and it was found that the resulting log-log plots at 780 and 850 nm had respective slopes of 2.84 and 2.17, corresponding to predominantly three- and two-photon absorption, respectively. Excitation of either transition results in photo-cross-linking, and on the basis of the identical emission spectrum, we concluded that the resulting photochemistry proceeds through the same relaxed state. Here the minimum widths of linear structures (type I and II

collagen) are compared for 780 nm (three-photon) and 850 nm (two-photon) excitation. Figure 1a shows the three-photon excited fluorescence image of two sets of equally spaced cross-linked linear structures of type I collagen fabricated at 0.75 NA, where each is approximately 100 μm in length. The contrast arises from the fluorescence of the incorporated benzophenone dimer (~1% fluorescence quantum yield) in the protein matrix. The widths were then measured using fluorescence imaging at higher NA and magnification (40×, 1.3 NA). We have previously determined that this optical configuration at 800 nm has a two-photon lateral PSF of ~450 nm and thus has sufficient resolution to measure these feature sizes.[33] This method has indeed previously produced good agreement with width measurements from higher resolution scanning electron microscopy (SEM) imaging.[22] The resulting widths are tabulated in Table 1, and it is observed that both type I and type II collagen lines fabricated by two-photon and three-photon excitation had respective widths of approximately 1 μm at 780 nm and 1.5 μm at 850 nm.

Table 1. Minimum Feature Sizes of Photo-Cross-Linked Collagen

protein	λ_{exc} (nm) (no. of photons)	width (μm)
type I collagen	780 (3)	1.06
type I collagen	850 (2)	1.58
type II collagen	780 (3)	0.98
type II collagen	850 (2)	1.48

This difference is far greater than can simply be attributed to the slightly shorter 780 nm excitation wavelength, since, even for a linear process, this would have accounted for only a 10% decrease in minimum feature size. Thus, we conclude that three-photon excitation does indeed produce significantly smaller features at comparable

excitation wavelengths. This trend is in good agreement with our previous results cross-linking TMPTA and BSA.[19]

These widths are somewhat larger than what we have observed with Rose Bengal photochemical activation of BSA.[33] This may arise from the more viscous nature of the collagen solution or perhaps be due to the different photochemical mechanism of the BPD. Still if these measured widths (0.75 NA excitation) are scaled to that which would be obtained with the use of a 1.4 NA lens, feature sizes approaching that of focal contacts would be achieved.

A future goal of this work is to simultaneously compare cell-adhesion specificity onto structures of more complex geometry. For example, observing the migration of fibroblasts to orthogonal fabricated lines of proteins, of the same or different proteins, that are in close proximity to one another could shed light on the specificity of the cells toward a particular protein and/or morphology. This can be accomplished by fabricating a grid of lines, in a "tic-tac-toe" form. As a first step, as shown in Figure 1b, a representative structure from type I collagen is fabricated by first fabricating a series of parallel cross-linked protein lines approximately 12 μm apart, then rotating the microscope stage by 90°, and fabricating another series of linear structures.

2.3.2 Determination of Bioactivity via Immunofluorescence.

One of the most important considerations of ultimately using this technology for tissue engineering or drug delivery applications is whether the cross-linked protein structures retain their biological activity following the intense peak powers required for MPE. For example, endogenous proteins may become denatured following undesired two-

and three-photon absorption. By performing a Michaelis-Menten analysis, we recently quantitatively demonstrated that the enzyme alkaline phosphatase did indeed retain its activity following cross-linking via two-photon excitation of Rose Bengal.[21] Because such quantitative assays are not available for most proteins, we have also employed immunofluorescence probing as a qualitative tool and showed that fibrinogen and fibronectin retained their bioactivity.[23]

The same approach is used here for assaying the activity of MPE cross-linked collagen by employing a standard two-step immunofluorescence protocol.[38] Type I and type II collagen matrixes (60 μm × 40 μm × 5 μm) were cross-linked via BPD photochemistry at both 850 nm (two-photon) and 780 nm (three-photon excitation).

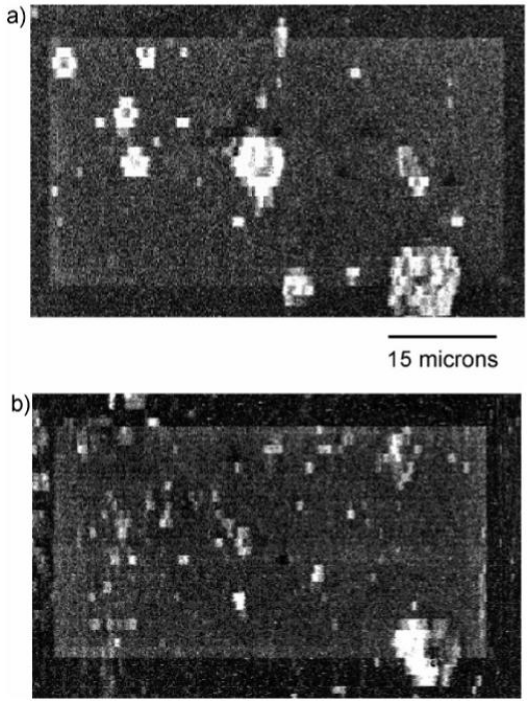

Figure 2. Two-photon excited immunofluorescence (FITC) images of (a) type I collagen and (b) type II collagen. Both were fabricated via three-photon excitation of the benzophenone dimer at 780 nm.

A primary antibody (mouse anti-human collagen type I monoclonal antibody, 20 μg/mL) was first added to cross-linked type I collagen. After incubation for approximately 30 min, the secondary antibody (FITC labeled goat anti-mouse IgG antibody, 10 μg/mL) was added. After another 45 min, the slide was washed with PBS buffer and a two-photon fluorescence FITC image (830 nm excitation) was acquired. Strong fluorescence from the cross-linked structures (both two- and three-photon fabricated) was observed and a representative immunofluorescence image of type I collagen (cross-linked at 780 nm) is shown in Figure 2a. This result is indicative of the successful binding of the immunofluorescent probe to the cross-linked structures, suggesting that the collagen was not significantly denatured by the fabrication process. Two negative controls were performed to eliminate the possibility of nonspecific binding: In the first, the primary antibody was replaced with 0.1% BSA, and, in the second, the secondary antibody was added in the absence of the primary. The control images each have a baseline fluorescence background from the incorporated benzophenone dimer photoactivator. Both of these controls then resulted in a fluorescence increase over this background of approximately 10%, indicating little nonspecific binding. By contrast, the addition of the primary and secondary antibody resulted in a 5-fold increase over the control data. A similar two-step approach (including the controls) was used for type II collagen, where the primary antibody was a mouse anti-collagen monoclonal antibody (2 μg/mL). Similarly, after addition of the secondary antibody, significant fluorescence enhancement relative to background in the protein matrix was observed, as shown in Figure 2b.

While not quantitative, the comparable levels of activity between the 850 and 780 nm MPE cross-linked structures from both types of collagen suggest that significant

denaturing did not occur during the fabrication process. This is important because it is well-known that multiphoton excitation at 780 nm can be damaging to live cells, where adverse effects have been ascribed to higher order absorption of endogenous proteins[39] and from plasma formation.[40] It was further shown that the probability for damage decreases at longer wavelengths.

2.3.3 Cell Adhesion.

Our interests in MPE fabricating collagen structures lie in creating scaffolds and ultimately implantable devices. As a first step, we began to study the adhesion of human dermal fibroblasts on cross-linked collagen (type I and type II). Parallel linear structures of collagen were MPE cross-linked (three-photon) on uniform BSA/ silanized surfaces. Since BSA is a nonspecific serum protein, only random cell adhesion would be expected on this surface. By contrast, if MPE cross-linked collagen can be used to mimic in vivo behavior, excellent specificity for adhesion of fibroblasts would be expected relative to the background. As shown in Figure 3, this was indeed born out. The top panel (Figure 3a) shows a phase-contrast image of a set of cross-linked type I collagen lines (of approximately 1 μm width) 3 h after plating with fibroblasts, and excellent specificity for cell adhesion is observed. The cells are numbered 1-6, and they are either covering one set of lines (cell 1), bridging two regions (cells 2 and 3), or aligning lamellapodia directly on the lines (cells 4-6). Similar behavior was observed for fibroblasts on MPE cross-linked type II collagen (data not shown). The control of the BSA/ silanized surface without collagen is shown in Figure 3b, and it is observed that the cell adhesion that did occur was random. As an additional control, similar sized BSA linear structures were cross-linked onto the BSA/silanized background, and no specific adhesion to the cross-linked structures

was observed (data not shown). This demonstrates that the excellent specificity of the fibroblasts to the cross-linked collagen results from the biological activity, rather than simply from morphological differences. By contrast, some previous studies have demonstrated that cells such as fibroblasts will orient in response to fibrils in aligned collagen gels,[41] to ECM proteins and peptides patterned on biocompatible materials[13,14,42,43] and to microscale topographic features.[15,44-48] However, this study demonstrates that cells cultured onto MPE fabricated collagen structures can distinguish between the effects of the sub-micrometer surface topography and that of the ECM protein itself.

To be more rigorous in our conclusions regarding biocompatibility, we need to consider the possibility that the benzophenone dimer might have phototoxic and/or cytotoxic effects. Unlike Rose Bengal photochemical activation, the BPD does not require singlet oxygen for its cross-linking mechanism. However, some singlet oxygen will be generated during triplet-state formation. On the other hand, singlet oxygen has lifetimes in solution ranging from nanosecond to microseconds before deactivation occurs.[49] Thus it is not a persistent species, and, further, even the long-lived (microsecond) form can only propagate, at a maximum, a few micrometers from the point of excitation. Moreover, a quenching species such as ascorbic acid could be added without affecting the desired photochemistry.

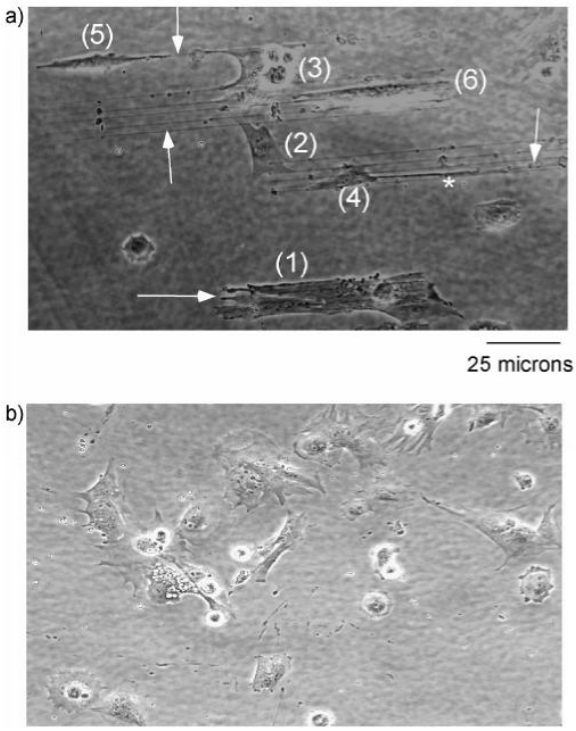

Figure 3. (a) Phase contrast image of directed adhesion of dermal fibroblasts on parallel sets of linear structures of type I collagen fabricated via three-photon of the benzophenone dimer at 780 nm. The linear structures demarked by arrows are approximately 1 μm in width. Fibroblasts extend along and bridge the sets. The lamella-podium of 4 is denoted by an asterisk (*). (b) Control image of fibroblasts on the BSA/silanized surface, where the adhesion is random.

Although benzophenone is used in topical applications such as sun blocking agents, it is potentially toxic in live cells. Specifically it has been shown to have estrogenic activity in MCF-7 and cytotoxic effects in cultured hepatocytes, where Nakagawa et al.[50] observed highly adverse effects for benzophenone concentrations of 1 mM within a few hours of treatment. However, these effects were greatly diminished or absent for concentrations of less than 100 μM. In this context we need to consider if leaching of the BPD out of the cross-linked matrix could have cytotoxic effects on cells adhered to the cross-linked collagen. In our experiments, the BPD concentration in solution was 200 μM. To achieve toxic concentration, virtually all of the BPD would have to come out of the

matrix and then endocytose into the cells. Since the BPD is covalently cross-linked into the protein (unlinked BPD is washed prior to culture), this outcome is unlikely. Furthermore, the cells on the cross-linked collagen surface shown in Figure 3a remained alive in culture during the week-long observation time. Thus we can conclude that at concentration levels used here, BPD has good biocompatibility for the fabrication of scaffolds for live cells.

2.3.4 Enzymatic Degradation of Type II Collagen.

Enzymatic degradations are often used to characterize the chemical and mechanical properties of cross-linked structures. For example, such measurements can provide data on the extent of cross-linking[31] and how this affects the mechanical properties such as the compressive modulus.[32] Performing degradation measurements can also shed light on how implantable cross-linked biomaterials might degrade in vivo. Furthermore, comparing the relative rates of degradation with different proteases of differing activity can give an indication of the extent that the cross-linked structure reproduces that of the native form.

It is important to investigate these issues in the present case since the fabrication of the collagen matrixes employs a new photoactivator. To this end, relative degradation rates of BPD cross-linked collagen matrixes are measured using the proteases pepsin, trypsin, and bacterial collagenase. Pepsin and trypsin are both digestive proteases differing by target hydrolysis sites. Pepsin hydrolyzes only peptide bonds with a preference toward peptide bonds that contain an aromatic residue on either side, while trypsin targets peptide bonds that have carboxyl groups donated by arginine and lysine. Collagenase is typically used to digest connective components in tissue samples and, similar to pepsin, is fairly

nonspecific in attacking cleavage sites. We will show that the relative rates of degradation in these cross-linked matrixes are consistent with the known activities of these enzymes.

Our approach is to fabricate matrixes from dye-labeled collagen (FITC type II and Oregon Green type IV) with three-photon excitation of the BPD. The enzymatic degradation is measured by monitoring the decrease in fluorescence intensity of the labeled collagen over time, where the temporal dependence of the signal is indicative of the fraction of cross-linked collagen being digested. The possibility that the decline in fluorescence was due to photobleaching of the dye was eliminated by the control experiment where the cross-linked collagen matrixes were imaged in the absence of enzyme under analogous conditions. No appreciable decline in fluorescence intensity was seen in these measurements.

FITC-conjugated type II collagen matrixes of dimensions 60 μm × 40 μm × 5 μm were cross-linked at 780 nm at an integrated exposure dose of 15 μJ. The enzyme concentrations were as follows: pepsin, 0.04% in 10 mM HCl; collagenase, 10 mg/mL in 1mM Ca^{2+}. For each enzyme, the pH for each protease solution was chosen as the optimal value recommended by the supplier. Note that while the fluorescence quantum yield of fluorescein is pH-dependent, the results are self-consistent as only the relative rates between the proteases are being compared. Furthermore, the proteases are used at different concentrations because they each have different respective activities based on their specificity constants. The value in each case corresponds to the limit of excess concentration based on this activity, and the relative rates between the proteases can then be compared directly.

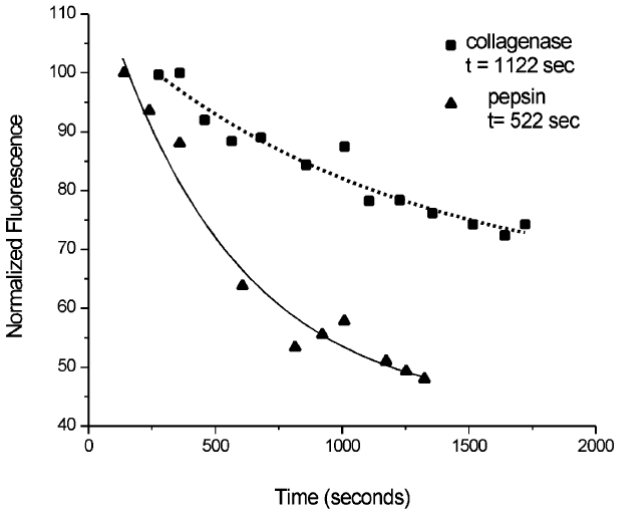

Figure 4. Enzymatic degradations of type II collagen cross-linked by the benzophenone dimer at 780 nm. The data for collagenase and pepsin are show with the corresponding single-exponential fits. In both cases incomplete degradation was observed, suggesting an increase in cross-link density relative to the native form.

Table 2. Relative Enzymatic Degradation Rates of Cross-Linked Collagen

protein	concn (mg/mL)	three-photon photoactivator (laser dose (μJ))	enzyme	t [a] (s)
type II collagen	2.8	BPD (15)	pepsin	522
			trypsin	591
			collagenase	1122
type IV collagen	2	BPD (75)	pepsin	382
		BPD (150)	pepsin	680
		RB (75)	pepsin	1885

[a] t = decay rate.

Figure 4 shows the decay curves with the exponential fits for the in vitro degradation using collagenase and pepsin, where respective time constants of 1122 and 522 s are obtained. The analogous experiment was also performed with trypsin, and the decay constants for the three proteases are tabulated in Table 2. In all cases, the data were well-fit to single-exponential decays, as would be expected for enzymatic degradation. Because the obtained decay constants depend on the extent of cross-linking and the

collagen concentration in the matrix, no significance can be ascribed to the absolute values of the time constants. Moreover, these values would most likely be different in vivo than in our in vitro conditions. However, since the collagen matrixes were fabricated under the same conditions, the relative rates of degradation of these enzymes can be compared to examine if these are consistent with their respective activities. While the number of cleavage sites in photo-cross-linked collagen may not be equivalent to that in native collagen, the BPD cross-linking occurs through a ketyl diradical that will target carbon double bonds and is thus not likely to affect the peptide bonds targeted by these species. Type II collagen is degraded faster by the protease pepsin (τ = 522 s) than by the similarly acting collagenase (τ = 1122 s). This result can be explained by considering the fact that the observed degradation rate will also depend on the ability of the enzyme to diffuse into and within the cross-linked matrix. We have previously shown[22,23] that dyedextran conjugates of different sizes (10 kDa vs 70 kDa) in multiphoton cross-linked protein matrixes (BSA, fibronectin, and fibrinogen) exhibit diffusion coefficients that scale properly as a function of their sizes (molecular weight). Similarly, while collagenase (68-125 kDa) will have a comparable number of sites to attack in type II collagen, its larger size and slower diffusion into the matrix decreases its degradation rate relative to pepsin (34 kDa). Trypsin degraded type II collagen at a rate similar to pepsin (591 s vs 522 s), as would be expected due to its comparable size. Since the degradation is related to the manner in which the matrix was assembled, knowledge of protease activity is crucial for the creation of tissue scaffolds that reproduce the native structure of collagen to the fullest extent possible.

It should be noted that in all these measurements, complete degradation was never observed (40-50% degradation). Pek et al.[32] also recently reported incomplete degradation

of collagen cross-linked with NHS-EDAC. By contrast, they observed complete degradation of both native collagen and that cross-linked with a thermal treatment. This effect can be attributed to a change in the structural and mechanical properties due to the additional chemical cross-linking. Similarly, we are also increasing the cross-link density of the collagen matrix relative to that of the native collagen through the addition of the covalent bonds formed by the photoactivation with the BPD. This might also suggest that some sites in the collagen are no longer accessible to the proteases following cross-linking with the BPD.

As enzymatic degradation of a protein results in the breaking of bonds, the structural properties of the matrix, such as the cross-link density and average mesh size, are expected to change following digestion. For example, Pek et al.[32] measured swelling ratios for a type I collagen chondroitin sulfate matrix and found that enzymatic (collagenase) degradation resulted in increased ability of the structure to swell, which is indicative of a decreased cross-link density. In prior work[22,23] on cross-linked BSA, fibrinogen, and fibronectin we approximated the cross-link density or average matrix mesh/pore size by measurement of the swelling ratios of the (hydrated) cross-linked protein matrix to the "dehydrated" (using methanol) matrix in conjunction with a modified Flory-Rehner analysis.[51] The mesh size, ξ, is related to the swelling/shrinking ratio Q_V by the hydrodynamic radius, r_0:

$$\xi = Q_V^{1/3} r_0 \qquad (1)$$

The measurements were performed on protein matrixes cross-linked at different laser exposure doses, where the premise was that, at higher laser dose, the structure will become more highly cross-linked and will swell/shrink to a lesser extent. Indeed, we found that the structures created using higher laser exposure swelled less, due to the decreased mesh size. This analysis was also in good agreement with transmission electron microscopy (TEM) imaging of BSA matrixes created over the same range of laser dose.[22] Uniform meshes were not observed and no average pore size could be assigned due to these variations.

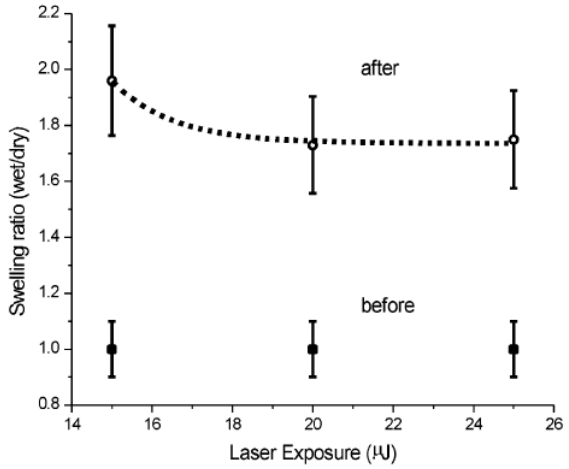

Figure 5. Swelling ratios of type II collagen matrixes cross-linked by the benzophenone dimer with differing exposure doses before and after pepsin digestion. The increased ability to swell postdigestion represents a decrease in cross-link density in the matrix and is indicative of the pepsin degradation activity.

However the "surface coverage" of cross-linked protein measured in the TEM sections was higher for structures fabricated with higher laser dose, and this modality thus provides an additional measure of the cross-link density. Here a similar analysis is used to determine whether the cross-linked type II collagen matrix underwent changes in average mesh size following enzymatic degradation with pepsin. As the hydrodynamic radii are not known for all proteins, and since we are most interested in comparing the

relative changes under different conditions, only the volume changes, Q, are measured and reported. Type II collagen matrixes were fabricated via BPD cross-linking at three integrated laser doses (15, 20, and 25 μJ). After the structures were soaked in water, the axial heights of the "wet" or "swollen" structures were then measured at 1.3 NA by using the fluorescence of the incorporated BPD. The heights of the "dry" structures were measured after repeated methanol washes and air-drying for 15 min. Subsequent rehydration reproduced the initial wet heights. Since swelling is taking place in three dimensions, $Q_v^{1/3}$ is simply taken as the ratio of the heights. These measurements were then repeated after digestion with pepsin. The swelling ratios of pre- and postdigested type II collagen are shown in Figure 5 for the three integrated laser doses, where the ratios are normalized to unity for the predigested matrix. The pre- and postdigestion swelling ratios decreased from 2 to 1.7 with increasing laser exposure (decreasing average mesh size). These data indicate that the enzymatic treatment was indeed decreasing the concentration of cross-linked collagen in the matrixes. Furthermore, the matrix with the highest initial cross-link density underwent the least degradation. This may arise from decreased diffusion of the pepsin due to the decreased average mesh size.

2.3.5 Photo-Cross-Linking and Enzymatic Degradation and Type IV Collagen.

Type IV collagen is a basement membrane protein which forms a lattice network to which other proteins such as laminin and fibronectin bind. Thus the ability to cross-link 3D structures from this molecule has relevance for tissue engineering applications.

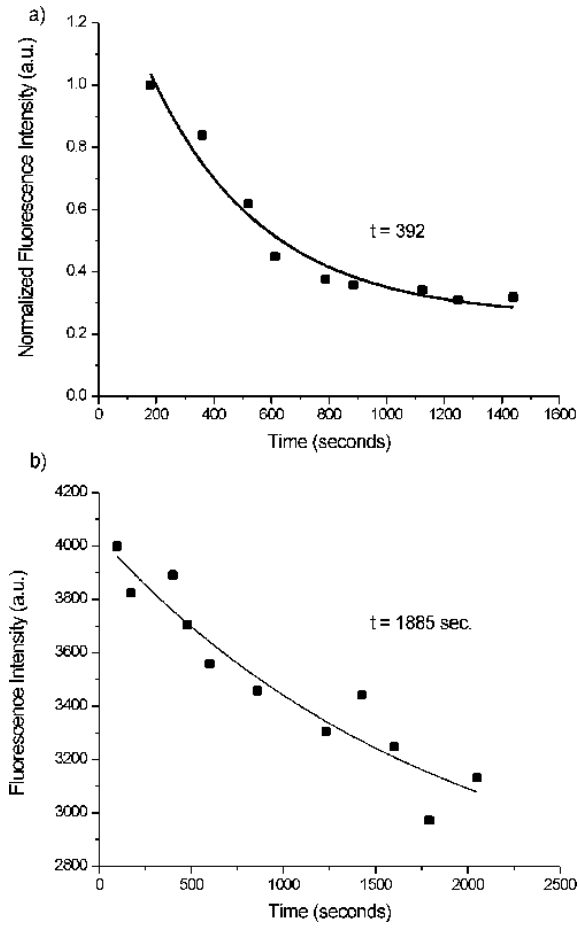

Figure 6. Comparison of pepsin digestion of type IV collagen cross-linked via (a) the benzophenone dimer via three-photon excitation at 780 nm and (b) two-photon excitation with Rose Bengal photochemistry at 800 nm. The large differences in degradation rates are likely due to the different photochemical mechanism that targets different residues.

Here we demonstrate the ability to cross-link type IV collagen via two different photochemistries (Rose Bengal and the benzophenone dimer) and characterize their respective degradation kinetics by pepsin to determine if these are consistent with the respective cross-linking mechanisms. One of the main considerations when using Rose Bengal (or other xanthenes) as a photoinitiator is its inactivity at acidic pH, where many forms of collagen have their highest solubility. Attempts to cross-link solutions of

neutralized type I and II collagens with Rose Bengal failed to produce stable structures. By contrast, two-photon excitation of Rose Bengal did indeed form stable cross-linked structures at pH 7.0. To quantitate the relative degradation rates of pepsin on cross-linked type IV collagen (Oregon Green labeled), comparable matrixes of dimensions 60 μm × 40 μm × 5 μm were fabricated via Rose Bengal and the BPD photochemistry at 780 nm with the same laser exposure dose. The enzymatic degradation was carried out in the same manner as described in the preceding section. The resulting pepsin degradation curves are shown in Figure 6, parts a and b, respectively, where much slower kinetics are observed for the Rose Bengal (τ = 1885 s) vs the BPD cross-linked structure (τ = 392 s).

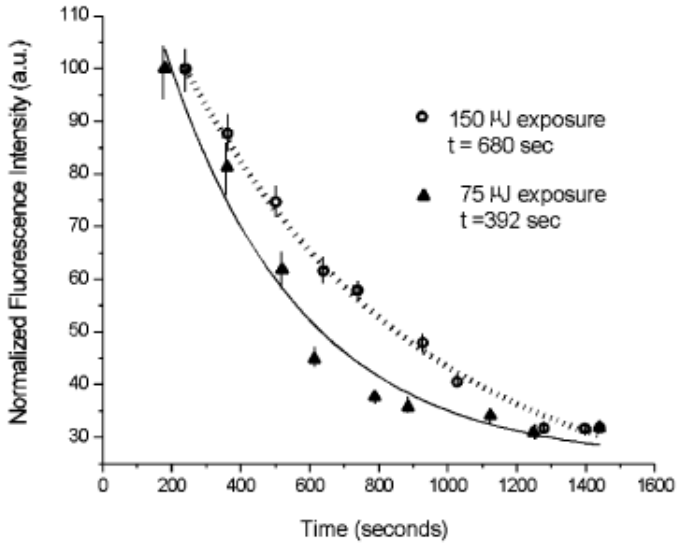

Figure 7. Comparison of pepsin digestion of type IV collagen cross-linked via the benzophenone dimer at 780 nm at integrated exposure doses of 75 (392 ± 85 s) and 150 μJ (680 ± 80 s). The increased exposure dose results in increased cross-link density in the matrix and slower degradation rate.

This large difference in degradation rate is likely due to the different cross-linking mechanism of Rose Bengal and the BPD. In the former, photo-cross-linking proceeds via efficient triplet-state production (>99%) and facile energy transfer to create singlet oxygen

radicals (>80%, depending on conditions).[29] By contrast, the BPD becomes incorporated into the protein matrix, where it is likely the ketyl radicals attack carbon-carbon double bonds in the protein. This would leave the peptide bonds still available for pepsin digestion. By contrast, singlet oxygen cross-linking can likely target many functional groups in proteins, including free amines.[30] Thus, the matrix produced by Rose Bengal cross-linking would have fewer available peptide bonds and slower degradation kinetics would be expected, and this is observed. Due to large differences in absorption cross-section (approximately 5-fold for one-photon absorption),[20] photo-crosslinking via the BPD would require more integrated dose than Rose Bengal to achieve the same collagen cross-link density. Thus at equal cross-link density, the difference in the relative degradation rates would be even more pronounced.

We showed above (Figure 5) that increasing the integrated laser exposure led to increased cross-linking. Here we show that increasing the extent of cross-linking (decreasing mesh size) decreases the relative degradation rate of type IV collagen by pepsin. The pepsin degradation kinetics for matrixes cross-linked at exposure doses of 75 and 150 μJ are shown in Figure 7. The degradation rate of the matrix with the higher cross-link density was nearly a factor of 2 slower than that of the less cross-linked structure (680 ± 80 s vs 392 ± 85 s). We have shown in prior work that increasing the laser exposure both increases the cross-link density as well as increases the protein concentration in the matrix.[22] The differences in degradation rates can thus be attributed to the same effect that the diffusion of the pepsin within the matrix will be slower for the structured cross-linked at the higher exposure dose. Similar to the case of type II collagen discussed previously, the degradation for the matrixes cross-linked at both exposure doses were well-fit by

single-exponential kinetics. From this result, we infer that type IV collagen matrixes can also be fabricated via MPE of the benzophenone dimer with a priori knowledge of the resulting physical properties, including cross-link density and susceptibility to enzymatic degradation.

2.4 Conclusions

We have demonstrated that sub-micrometer and micrometer scale structures can be fabricated from types I, II, and IV collagen via multiphoton excited photochemistry using a modified benzophenone dimer. The resulting structures have excellent biocompatibility as determined by immunofluorescence measurements as well as directed cell adhesion. The structures can be degraded by several proteases with relative rates consistent with the known activities of these enzymes. Furthermore, the relative rates of degradation of the collagen matrixes can be controlled by adjustment of the cross-link density during the fabrication process. These results indicate that collagen structures can be fabricated with structural and chemical similarities to those of native collagen and suggest that the multiphoton fabrication process may be a powerful tool for the creation of cell-sized tissue scaffolds directly from collagen.

Acknowledgment. Support under NIH Grant R01 EB000263 is gratefully appreciated. We thank Matthew Veilleux for technical assistance.

References

(1) Flemming, R. G.; Murphy, C. J.; Abrams, G. A.; Goodman, S. L.; Nealey, P. F. *Biomaterials* **1999**, *20*, 573-588.

(2) Desai, T. *Med. Eng. Phys.* **2000**, *22*, 595-606.

(3) Bhatia, S. N.; Chen, C. S. *Biomed. Microdev.* **1999**, *2*, 131-144.

(4) Wilkinson, C. D. W.; Riehle, M.; Wood, M.; Gallagher, J.; Curtis, A. S. G. *Mat. Science Eng. C* **2002**, *19*, 263-269.

(5) Tan, W.; Desai, T. A. *Biomaterials* **2004**, *25*, 1355-1364.

(6) Tan, W.; Desai, T. A. *Tissue Eng* **2003**, *9*, 255-267.

(7) Downing, B. R.; Cornwell, K. G.; Toner, M.; Pins, G. D. *J. Biomed. Mat. Res.* **2005,** 72A: 47-56.

(8) Pins, G. D.; Toner, M.; Morgan, J. R. *FASEB J.* **2000**, *14*, 593-602.

(9) Chen, C. S.; Mrksich, M.; Huang, S.; Whitesides, G. M.; Ingber, D. E. *Science* **1997**, *276*, 1425-1428.

(10) Bhatia, S. N.; Balis, U. J.; Yarmush, M. L.; Toner, M. *Biotechnol. Prog.* **1998**, *14*, 378-387.

(11) Folch, A.; Toner, M. *Biotechnol Prog* **1998**, *14*, 388-392.

(12) Kane, R. S.; Takayama, S.; Ostuni, E.; Ingber, D. E.; Whitesides, G. M. *Biomaterials* **1999**, *20*, 2363-2376.

(13) Patel, N.; Padera, R.; Sanders, G. H. W.; Cannizzaro, S. M.; Davies, M. C.; Langer, R.; Roberts, C. J.; Tendler, S. J. B.; Williams, P. M.; Shakesheff, K. M. *FASEB J.* **1998**, *12*, 1447-1454.

(14) Zhang, S.; Yan, L.; Altman, M.; Lassle, M.; Nugent, H.; Frankel, F.; Lauffenburger, D. A.; Whitesides, G. M.; Rich, A. *Biomaterials* **1999**, *20*, 1213-1220.

(15) Dalby, M. J.; Riehle, M. O.; Yarwood, S. J.; Wilkinson, C. D.; Curtis, A. S. *Exp Cell Res* **2003**, *284*, 274-282.

(16) Teixeira, A. I.; Abrams, G. A.; Bertics, P. J.; Murphy, C. J.; Nealey, P. F. *J. Cell Sci.* **2003**, *116*, 1881-1892.

(17) Nimni, M. E.; Cheung, D. T.; Strates, B.; Kodama, M.; Sheikh, K. In *Collagen, Vol. III.*; Nimni, M. E., Ed.; CRC Press: Boca Raton, FL, 1988; pp 1-38.

(18) Huang-Lee, L. H.; Cheung, D. T.; Nimni, M. E. *J. Biomed. Mat. Res.* **1990**, *24*, 1185-1201.

(19) Pitts, J. D.; Campagnola, P. J.; Epling, G. A.; Goodman, S. L. *Macromolecules* **2000**, *33*, 1514-1523.

(20) Pitts, J. D.; Howell, A. R.; Taboada, R.; Banerjee, I.; Wang, J.; Goodman, S. L.; Campagnola, P. J. *Photochem Photobiol* **2002**, *76*, 135-144.

(21) Basu, S.; Campagnola, P. J. *Biomacromolecules* **2004**, *5*, 572-579.

(22) Basu, S.; Wolgemuth, C. W.; Campagnola, P. J. *Biomacromolecules* **2004**, *5*, 2347-2357.

(23) Basu, S.; Campagnola, P. J. *J Biomed Mater Res* **2004**, *71A*, 359-368.

(24) Brinkman, W. T.; Nagapudi, K.; Thomas, B. S.; Chaikof, E. L. *Biomacromolecules* **2003**, *4*, 890-895.

(25) Ledger, M. B.; Porter, G. *J. Chem. Soc.: Faraday Trans. 1* **1972**, *68*, 539-553.

(26) Agarwal, R.; Rajasekharan, K. N.; Burke, M. J. *J. Biol. Chem.* **1991**, *266*, 2272-2275.

(27) Leszyk, J.; Collins, J. H.; Leavis, P. C.; Tao, T. *Biochemistry* **1987**, *26*, 7042-7047.

(28) Tao, T.; Lamkin, M.; Scheiner, C. J. *Arch. Biochem. Biophys.* **1985**, *240*, 627-634.

(29) Neckers, D. C. *J. Photochem. Photobiol. A* **1989**, *47*, 1-29.

(30) Balasubramanian, D.; Du, X.; Zigler, J. S. J. *Photochem. Photobiol.* **1990**, *52*, 761-768.

(31) Burdick, J. A.; Chung, C.; Jia, X.; Randolph, M. A.; Langer, R. *Biomacromolecules* **2005**, *6*, 386-391.

(32) Pek, Y. S.; Spector, M.; Yannas, I. V.; Gibson, L. J. *Biomaterials* **2004**, *25*, 473-482.

(33) Sridhar, M.; Basu, S.; Scranton, V. L.; Campagnola, P. J. *Rev. Sci. Instrum.* **2003**, *74*, 3474-3477.

(34) Huang, T. T.; Geng, T.; Akin, D.; Chang, W. J.; Sturgis, J.; Bashir, R.; Bhunia, A. K.; Robinson, J. P.; Ladisch, M. R. *Biotechnol Bioeng* **2003**, *83*, 416-427.

(35) Mooney, J. F.; Hunt, A. J.; McIntosh, J. R.; Liberko, C. A.; Walba, D. M.; Rogers, C. T. *Proc Natl Acad Sci U S A* **1996**, *93*, 12287-12291.

(36) Gu, M.; Sheppard, C. J. R. *J. Microscopy* **1995**, *177*, 128-137.

(37) Hell, S. W.; Stelzer, E. H. K. *Optics Comm.* **1992**, *93*, 277-282.

(38) Zoumi, A.; Yeh, A.; Tromberg, B. J. *Proc Natl Acad Sci U S A* **2002**, *99*, 11014-11019.

(39) Hopt, A.; Neher, E. *Biophys J* **2001**, *80*, 2029-2036.

(40) Konig, K.; So, P. T. C.; Mantulin, W. W.; Gratton, E. *Opt. Lett.* **1997**, *22*, 135-136.

(41) Dunn, G. A.; Ebendal, T. *Exp Cell Res* **1978**, *111*, 475-479.

(42) Chen, C. S.; Mrksich, M.; Huang, S.; Whitesides, G. M.; Ingber, D. E. *Biotech. Prog.* **1998**, *14*, 356-363.

(43) Parker, K. K.; Brock, A. L.; Brangwynne, C.; Mannix, R. J.; Wang, N.; Ostuni, E.; Geisse, N. A.; Adams, J. C.; Whitesides, G. M.; Ingber, D. E. *FASEB J* **2002**, *16*, 1195-1204.

(44) Berry, C. C.; Campbell, G.; Spadiccino, A.; Robertson, M.; Curtis, A. S. G. *Biomaterials* **2004**, *25*, 5781-5788.

(45) Dalby, M. J.; Yarwood, S. J.; Riehle, M. O.; Johnstone, H. J.; Affrossman, S.; Curtis, A. S. *Exp Cell Res* **2002**, *276*, 1-9.

(46) Meyle, J.; Gultig, K.; Nisch, W. *J Biomed Mater Res* **1995**, *29*, 81-88.

(47) Walboomers, X. F.; Ginsel, L. A.; Jansen, J. A. *J Biomed Mater Res* **2000**, *51*, 529-534.

(48) James, C. D.; Davis, R. C.; Kam, L.; Craighead, H. G.; Isaacson, M.; Turner, J. N.; Shain, W. *Langmuir* **1998**, *14*, 741-744.

(49) Schweitzer, C.; Schmidt, R. *Chem. Rev.* **2003**, *103*, 1685-1757.

(50) Nakagawa, Y.; Suzuki, T.; Tayama, S. *Toxicology* **2000**, *156*, 27-36.

(51) Leach, J. B.; Bivens, K. A.; C. W. Patrick, J.; Schmidt, C. E. *Biotech. Bioeng* **2003**.

Chapter 3

Multiphoton excited fabricated nano and micro patterned extracellular matrix proteins direct cellular morphology

Multiphoton excited fabricated nano and micro patterned extracellular matrix proteins direct cellular morphology

George D. Pins,[1] Katie A. Bush,[1,2] Lawrence P. Cunningham,[3] and Paul J. Campagnola[3]

[1]Department of Biomedical Engineering, Worcester Polytechnic Institute, Worcester, Massachusetts 01609
[2]Department of Biomedical Engineering and Medical Physics, Graduate School of Biomedical Sciences at the University of Massachusetts Medical School, Worcester, Massachusetts 01655
[3]Department of Cell Biology and Center for Cell Analysis and Modeling, University of Connecticut Health Center, Farmington, Connecticut 06030

Contract grant sponsor: NIH; contract grant number: R01 EB000263
Contract grant sponsor: WPI (Steadman-Smith Fellowship)

I wish to acknowledge the John Wiley and Sons for their permission to reprint (adapt) for the following work (citation below) for this chapter.

Pins GD, Bush KA, Cunningham LP, Campagnola PJ., Multiphoton excited fabricated nano and micro patterned extracellular matrix proteins direct cellular morphology., J Biomed Mater Res A. 2006 Jul;78(1):194-204.

ABSTRACT

We use multiphoton excited (MPE) photochemistry to fabricate patterned extracellular matrices (ECM) and to investigate the morphology of human dermal fibroblasts adhered to the resulting photocrosslinked linear structures of fibronectin (FN), fibrinogen (FG), and bovine serum albumin (BSA). These proteins were chosen to systematically investigate the roles of topography and ECM biochemistry on cell spreading, as fibroblasts bind directly to both FN and FG at RGD sites through known integrins, whereas BSA provides no comparable ECM cues for cell binding. MPE crosslinked patterns are created from parallel linear structures 600 nm in width, 200 m in length, and spaced by either 10 or 40 pm. Immunofluorescence staining of FN and FG was used to assay the functionality of crosslinked proteins. The metrics of orientation, elongation, and cell perimeter were used to quantitate the resulting cellular behavior on the crosslinked protein patterns. These parameters all reflect statistical differences for cells on BSA, relative to the similar statistical behavior on fibronectin and fibrinogen. Cells on the BSA patterns are constrained by physical guidance and orientation between linear structures. In contrast, cells adhered on both FN and FG had a greater propensity to spread across adjacent structures, indicating the importance of cell matrix interactions. Focal adhesion staining of cells adhered to the protein structures revealed similar trends. These findings are consistent with our hypothesis that these crosslinked matrix protein structures are expected to direct cell adhesion and spreading and that the topography and ECM cues lead to different forms of guidance.

Keywords: cell adhesion; ECM; scaffolds; nanofabrication; tissue engineering

3.1 INTRODUCTION

It is now well-appreciated that the control of cellular functions is to a large extent governed by cells interacting with protein matrices (e.g., the extracellular matrices (ECM)), which have an extremely complex structure in the submicron or nanoscale range (100– 300 nm).[1,2] A major challenge for tissue engineering lies in fabricating scaffolds that replicate the native 3D architecture with the appropriate biochemical composition to successfully modulate cellular adhesion, proliferation, and differentiation, as well as to regenerate native tissue functions.[3–5] This goal requires the development of new fabrication technologies, as well as the acquisition of detailed fundamental understandings of cellular responses to nano and microtopographic features.[6] Recently, several investigators have studied fibroblast and epithelial cell functions on surfaces containing synthetic topographic features with dimensions that mimic those found on native basement membrane structures.[7–9] For example, Den Braber et al. fabricated microgrooved silicone substrates with groove and ridge widths that ranged from 1 to 10 pm and groove heights of 0.45 or 1.0 pm.[10] They observed that cells cultured on surfaces with ridge widths of ~4.0 pm were highly orientated and elongated along the surface grooves. Furthermore, these results showed that ridge widths affected cell function more than groove height. In contrast, Britland et al. found that when BHK cells were cultured on fused silica substrates with grooves ranging in height from 0.1 to 6.0 pm that cell alignment was most pronounced in grooves that were 6 m deep.[11] Recently, Nealey and coworkers examined corneal epithelial cells' functions on the surfaces of synthetic substrates with nano-topographic features comparable to those observed on basement membranes.[12,13] The results of these studies showed that cells elongated and aligned along patterns of grooves and ridges with feature

dimensions as small as 70 nm in width, 150 nm in height, and 400 nm in pitch spacing. However, this alignment was most pronounced in grooves that were at least 800 nm in width and 600 nm in height. These apparently disparate reports on the most important geometrical factors highlight the complexity of the problem in understanding cell-topography interactions.

While these studies have provided insight into the topographic factors that modulate cellular adhesion, proliferation, and differentiation in native tissue, the ECM provides additional cues that are important for proper functionality.[1,14] While the optimal fabrication technique would provide simultaneous control over these factors, most current technologies do not offer these combined capabilities. To help remedy these shortcomings, we developed a nano/microfabrication method based on multiphoton excited (MPE) photochemical crosslinking of proteins and polymers.[15,16]

The method is analogous to the more familiar multiphoton excited fluorescence imaging of live cells and tissues where optical sectioning is obtained by confinement of the excitation to the plane of focus, greatly reducing *out of plane* photobleaching and photodamage.[17,18] Several researchers have recognized that this same sectioning capability of MPE can be used for nano and microfabrication, where 3D objects can be fabricated in one plane at a time, without overwriting previous layers.[19–28] Most of this work has centered on the microfabrication of polymer resins, with the research being directed at 3D storage and nanophotonics applications.

We have previously reported our efforts on the fabrication and subsequent physical and chemical characterization of 3D protein matrices created from bovine serum albumin (BSA), fibronectin (FN), fibrinogen (FG), conconavalin A, and alkaline

phosphatase.[29–31] Remarkably, all of these proteins retained their biological activity following MPE crosslinking. In a more recent study, we further demonstrated the use of this methodology to fabricate photocrosslinked linear and matrix structures directly from collagen (types I, II, and IV) on the submicron- and micron-sized scales.[32]

Here we describe our initial efforts to systematically characterize cell adhesion and spreading on linear patterns of crosslinked matrix molecules. We specifically investigate the effects of pattern spacing and ECM protein composition on the morphology of adhered cells. The spreading of dermal fibroblasts was measured on MPE fabricated patterns composed of BSA, FN, and FG that were spaced at 10 or 40 pm increments. Since human fibroblasts bind directly to both FN and FG at RGD sites through known integrins,[33–35] spreading on these surfaces is expected to be governed by both topographic interactions as well as ECM cues provided by the crosslinked proteins. By contrast, crosslinked BSA lines were used to examine the role of topography in the absence of biochemical specificity. Morphological analyses show that cells adhered to the crosslinked FN and FG structures show statistically different spreading behavior than those on BSA, indicating the role of cell–matrix interactions in the former case. Similarly, focal adhesion staining further supports the importance of these interactions. Collectively, these findings indicate that topography and ECM cues lead to different forms of guidance and spreading for fibroblasts adhered to crosslinked matrix proteins.

3.2 MATERIALS AND METHODS

3.2.1 Materials

Octadecyltrichlorosilane (OTDS; Gelest, Morrisville, PA), anhydrous toluene (Aldrich, Sigma, St. Louis, MO), bovine serum albumin (Sigma), Rose Bengal (Sigma), human fibronectin (Sigma), and bovine fibrinogen (Sigma) were used as received. The HFN7.1 hybridoma supernatant was obtained from the Developmental Studies Hybridoma Bank developed under the auspices of the NICHD and maintained by the University of Iowa, Department of Biological Sciences, R.J. Klebe, contributor. The primary fibrinogen antibody (American Diagnostica, Greenwich, CT), the fluorescent secondary antibody Alexa fluor 488 F(ab')2 fragment of goat antimouse IgG (Molecular Probes, Eugene, OR) , and the vinculin primary antibody (Sigma) were used as received. The benzophenone dimer (BPD) photoactivator was synthesized as described previously.[36]

3.2.2 Fabrication instrument

The fabrication and imaging instrument (shown schematically in Figure 1) is a custom-designed laser-scanning nonlinear optical microscope whose features have been previously described.[37] The laser for MPE is a femtosecond near-infrared titanium-sapphire oscillator operating at 800 nm. The laser is coupled to an upright microscope, equipped with bright field and fluorescence optics, and average powers at the sample were between 30 and 50 mW. A 20X, 0.75 numerical aperture (NA) objective lens was used for the fabrication and resulted in lateral and axial resolutions (i.e. minimum feature sizes) of approximately 0.75

and 2.5 pm, respectively.[31] Scan-synchronized two-photon excited fluorescence is used as an online diagnostic of the fabrication process and for immunofluorescence measurements on crosslinked proteins. The code for operating this instrument for both the scan control and simultaneous fluorescence image acquisition was written entirely using LabVIEW 7.

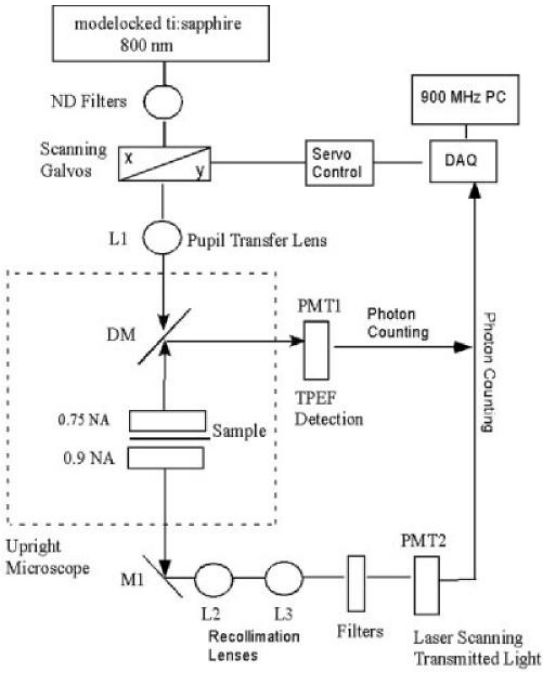

Figure 1. Optical schematic representation of the fabrication microscope. L1 (pupil transfer lens, 50 mm fl), L2 (300 mm fl), and L3 (100 mm fl) recollimate the forward directed signals. PMT1 and PMT2 are Hamamatsu 928 and 7421, respectively. M1 is a broad-band aluminum mirror. DM, 525 nm long wave pass dichroic mirror. The upright microscope is a Zeiss Axioskop. The galvo scanners are from GSI Lumonics and the DAQ board is from National Instruments.

3.2.3 Surface preparation and photochemistry

To compare the morphology of fibroblasts on the MPE crosslinked protein patterns, these must be fabricated on a nonspecific background surface. To this end, a chemisorbed, self-assembled eighteen-carbon organosilane (ODTS) monolayer was prepared to provide a stable, hydrophobic surface that adsorbs a monolayer of BSA.[38] We have previously reported the procedure in detail and only provide the most salient features

here. Plasma cleaned glass microscope slides were soaked in a solution of 0.5% v/v ODTS in anhydrous toluene in an inert, moisture-free environment. The slides were then washed with anhydrous toluene to remove any residual ODTS, dried with N_2, and heated for 30 min at 120°C to complete the formation of the Si—O bonds. The silanized slides were soaked in a 10 mg/mL solution of BSA to form the background and then were rinsed. Fibrinogen (1 mg/mL) and BSA (10 mg/mL) are crosslinked via 2-photon excitation with Rose Bengal (RB; 1 m*M*) at 800 nm. The photochemistry proceeds through the generation of singlet oxygen which then attacks residues containing aromatic groups and free amines.[39,40] The resulting radical protein then links to a second protein molecule. Fibronectin (1 mg/mL) is crosslinked via 3-photon excitation of the BPD at 780 nm. This reagent inserts into either carbon—hydrogen, or carbon— carbon bonds, and becomes part of the crosslinked network.[36] This reagent is particularly effective for crosslinking minimally soluble ECM proteins, and was initially developed in our laboratory for crosslinking collagen.[36] Additionally, preliminary data suggested that superior fibroblast adhesion was obtained on fibronectin crosslinked with the BPD rather than RB.

3.2.4 Fabrication design strategy

We examine cell morphology on MPE crosslinked BSA, FN, and FG. BSA was chosen since it provides no ECM cues, and any cell adhesion and guidance is expected to be governed only by topography. By contrast, FN and FG are known to provide ECM cues to fibroblasts through RGD binding motifs.[33,34] Fabricated linear patterns were created with pitch widths (i.e. line separations) of 10 and 40 pm. These sizes were chosen as they represent dimensions both smaller than, and approximately equal to that of fibroblasts, respectively. Line lengths are 200 pm and sufficiently long to allow adequate spreading

along the patterns. Line widths are approximately 600 nm, and approximate the size of small clusters of focal adhesions.

3.2.5 Characterization of feature functionality via immunofluorescence

Immunofluorescence staining was performed to assay the functionality of the crosslinked FN and FG. MPE fabricated patterns of human FN were labeled with the primary antibody HFN7.1 that binds specifically to the RGD and/or PHSRN cell binding domains on the FN.[41] The HFN7.1 supernatant was added undiluted over the FN patterns. After 30 min, the patterns were washed with phosphate buffered saline (PBS). The fluorescent secondary antibody was added at a concentration of 1 pg/mL to the preparation for 15 min. The sample was washed thrice with PBS and imaged via two-photon excitation at 800 nm. MPE fabricated patterns of FG were labeled using the polyclonal FG primary antibody at a concentration of 1 pg/mL. The protocol for washing and adding the secondary fluorescent antibody was the same as with FN. In both cases, two negative controls were performed to eliminate the possibility of nonspecific binding. In the first, the primary antibody was replaced with 0.1% BSA, and in the second, the secondary fluorescent antibody was added in the absence of the primary.

3.2.6 Culture of human cells

Human dermal fibroblasts used in all experiments were derived from neonatal foreskin using a protocol described previously.[42] To isolate fibroblasts, foreskin tissue was trimmed to remove excess fatty tissue, rinsed with sterile PBS, and diced into small fragments. The fragments were allowed to adhere to the bottom of a tissue culture plate in a humidified 10% CO_2 atmosphere at 37°C for 1 h, and were then covered with

Dulbecco's Modified Eagle's Medium (DMEM; Gibco BRL, Gaithersburg, MD) supplemented with 10% fetal bovine serum (FBS; Atlanta Biologicals, Lawrenceville, GA) containing penicillin/streptomycin (100 U/ 100 pg per mL; Gibco). After 14 days, confluent fibroblasts were harvested with 0.05% trypsin/ethylenediamine tetracetic acid solution and subcultured in DMEM containing 10% FBS and penicillin/streptomycin.

3.2.7 Cell adhesion protocol

To create individual wells for cell culture assays, adhesive silicone isolators (9.0 mm inner diameter) were affixed to the surfaces of the patterned slides. After the isolators were placed on the surfaces, the slides were rinsed three times in DMEM containing 10% FBS and penicillin/streptomycin to clean the surfaces. Slides were placed in tissue culture plates and 100 pL of tissue culture medium containing fibroblasts was seeded in the center of each well on the slide. The final cell density in each individual well was 38,000 cells/ml. Each well was individually inspected to assure cells were uniformly distributed on the patterned surfaces. Tissue culture plates containing cell-seeded slides were transferred to a tissue culture incubator maintained at 37°C and 10% CO_2. After 3 h, the slides were removed from the incubator and submerged in 10 mL of tissue culture medium.

3.2.8 Morphological analyses of cell spreading

To quantitate the effects of the patterned BSA, FN, and FG surfaces on cell morphology, images of cells were analyzed using Image J Analysis software (public domain software, downloaded from: http://rsb.info.nih.gov/ij/). Phase contrast images of

individual cells were converted to binary images and initially traced by hand in Image J. Demonstrative examples of the measurements are shown in the phase contrast images in Figure 2. To approximate the elongation ratio (L/B) of the cells, the perimeter shapes were fitted to an ellipse (E) defined by maximum length (L) and cell breadth (B) perpendicular to the maximum length. The angle of orientation (O) for each cell, relative to patterned ECM protein lines, was calculated by extending the maximum length of the ellipse and measuring the distended angle relative to the axis of the pattern. The probability for cells spreading across multiple lines was determined by counting the number of cells that intersected differing numbers of patterned lines and then binning the results.

3.2.9 Statistical analysis

Statistical comparisons between sample groups were made using Sigma Stat Version 3.10 (Systat Software, Richmond, CA). One-tailed Student's *t*-tests were performed to determine significant differences between pitch widths, and analyses of variances (ANOVA) were performed to determine significant differences between proteins at the pitch widths. Wherever specifically noted, statistical analyses were performed on ranks due to unequal variance among the sample populations. Mann-Whitney analysis on ranks was substituted for the one-tailed Student's *t*-test and Kruskal-Wallis one-way analysis with Dunn's Test for ranks was substituted for the ANOVA, where unequal treatment group sizes were observed. p values 0.05, for both the equal and unequal variance tests, indicated a significant difference between the groups. The number

of sample cells varied for each protein and pitch width due to the probability of individual cells landing on the patterned surfaces.

3.2.10 Focal adhesion staining

Fibroblasts were stained with an antibody for vinculin to visualize focal adhesions. Slides with cells seeded on the surfaces were rinsed with PBS and treated with a fixing solution for 10 min consisting of PBS, 4% formaldehyde, and 0.2% of Triton X-100 (Sigma). Fixed slides were rinsed to remove fixative and a solution consisting of PBS with 1% BSA and 0.1% NaN_3 was applied for 10 min to reduce nonspecific binding. The fixed and blocked cells were then incubated with the antibody at a 1:40 dilution (0.24 mg/mL) for 45 min. The cells were rinsed and incubated with the secondary Alexa 546-conjugated goat antimouse antibody at a 1:40 dilution (0.05 pg/mL). Fluorescence images (608–683 nm) were taken with a 20X, 0.5 NA lens and were captured using an RT Color Spot camera.

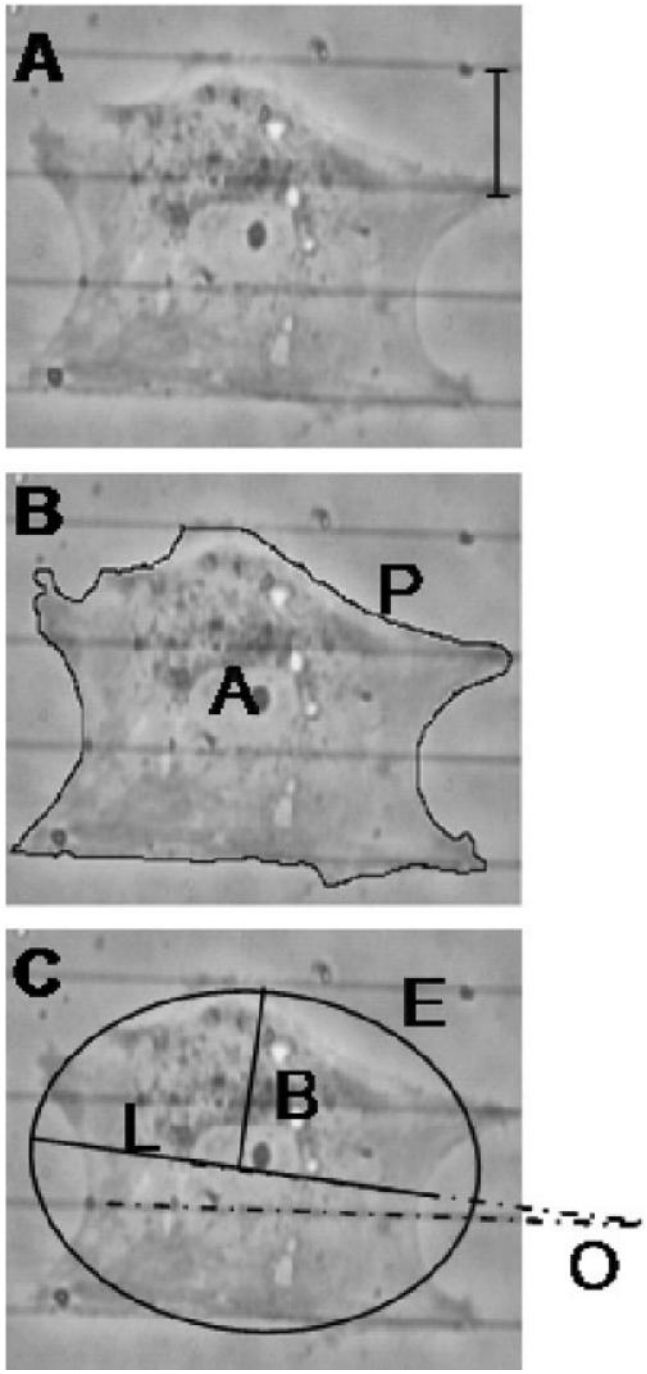

Figure 2. Micrographs illustrating techniques for analyzing cell morphology on MPE protein matrices. (a) Phase contrast images of dermal fibroblasts are recorded 3 h after the cells are seeded on the surfaces of ECM patterns. (b) Image analysis software is used to measure the perimeter (P) of each cell. (c) Each cell is also fitted with an ellipse (E) to measure the maximum length (L) of the ellipse as well as the breadth (B) perpendicular to the maximum length. The angle of orientation (O) is measured as the arc between the maximum length of the cell (L) and the direction of the ECM pattern. Scale bar represents 20 pm.

3.3 RESULTS

3.3.1 Morphology of patterns

The overall morphology of the crosslinked individual linear structures and patterns of lines can be visualized by fluorescence microscopy. BSA and FG are crosslinked via RB activated photochemistry, and some residual RB remains adhered to the protein structure (which is washed prior to cell adhesion). The RB has a small (<1%) fluorescence quantum yield and this is used as imaging contrast. Fibronectin is crosslinked by the BPD which becomes part of the matrix. It similarly has sufficient fluorescence intensity for imaging contrast. Figure 3(a,b) shows the 2-photon excited fluorescence image (20X) of a series of crosslinked FN (10 m pitch width) and FG lines (40 m pitch width), respectively. The linear patterns were determined to be 200 pm in length. An accurate measure of the width of individual lines was made by higher resolution (60X, 1.4 NA) 2-photon fluorescence imaging and an example for FG is shown in Figure 3(c), where the feature width is -700 nm. This value is in good agreement with theoretical predictions of 2-photon fluorescence resolution using Point Spread Function calculations.[43] If these measured widths (0.75 NA excitation) are scaled to that which would be obtained with the use of a 1.4 NA lens, feature sizes approaching that of single focal adhesions (300 nm) would be achieved. To obtain an estimate of the axial dimensions of the linear structures, the step height was measured using a 1.3 NA, 40X objective. This resulted in a minimum height of 2.5 pm for structures fabricated with the 0.75 NA lens and is also in good agreement with theoretical predictions.[43]

3.3.2 Determination of bioactivity via immunofluorescence

An important aspect of optical fabrication using proteins is determining whether biological activity is maintained, following the MPE process. It is well known that live cells can be readily damaged by the high peak powers required for two-photon absorption, which can occur by higher order absorption and/or plasma formation.[44,45] We first validate the functionality of the crosslinked FN and FG using immunofluorescence staining. The human antibody HFN7.1 binds specifically to the RGD and/or PHSRN fibronectin cell binding domains and effectively blocks cell binding.[41] A representative resulting immunofluorescence image for crosslinked human FN structures (one rectangular and four lines of 10 pm pitch width) is shown in Figure 4. This staining resulted in a signal to background ratio of 10:1 over the negative controls (see Methods) without the HNF7.1. Two further controls were performed to validate these measurements. First, a monolayer of fibronectin was adsorbed to a self-assembled monolayer of ODTS and strong fluorescence was observed. Second, bovine FN was crosslinked by the same photochemistry and no fluorescence signal was observed above the background when the protein was stained with the HFN7.1 Since this antibody only binds to human FN,[41] we conclude that the crosslinked protein retains function known that live cells can be readily damaged by the high peak powers required for two-photon absorption, which can occur by higher order absorption and/or plasma formation.[44,45] We first validate the functionality of the crosslinked FN and FG using immunofluorescence staining. The human antibody HFN7.1 binds specifically to the RGD and/or PHSRN fibronectin cell binding domains and effectively blocks cell binding.[41] A representative resulting immunofluorescence image for crosslinked human FN structures (one

rectangular and four lines of 10 pm pitch width) is shown in Figure 4. This staining resulted in a signal to background ratio of 10:1 over the negative controls (see Methods) without the HNF7.1. Two further controls were performed to validate these measurements. First, a monolayer of fibronectin was adsorbed to a self-assembled monolayer of ODTS and strong fluorescence was observed. Second, bovine FN was crosslinked by the same photochemistry and no fluorescence signal was observed above the background when the protein was stained with the HFN7.1 Since this antibody only binds to human FN,[41] we conclude that the crosslinked protein retains function of the cell binding sites with high specificity. We previously reported the activity of multiphoton cross-linked FG via immunofluorescence,[30] and have repeated the measurements here with an additional primary antibody and observed similar levels of activity.

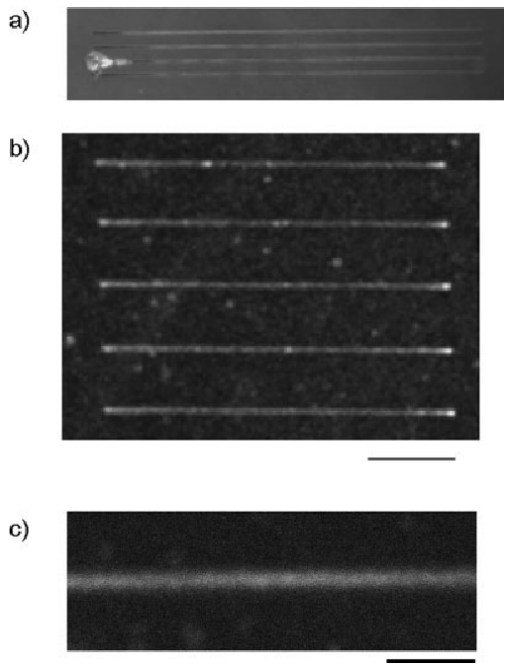

Figure 3. Two-photon excited fluorescence images of crosslinked proteins. The contrast arises from the photoactivator. (a) 10 pm spaced 200 pm long linear patterns of FN; scale bar = 50 pm. (b) 40 pm spaced linear patterns of FG; scale bar = 50 pm. (c) High resolution (60X, 1.4 NA), high zoom (10X) image of fibrinogen line; scale bar = 5 pm. The feature width is 600 nm.

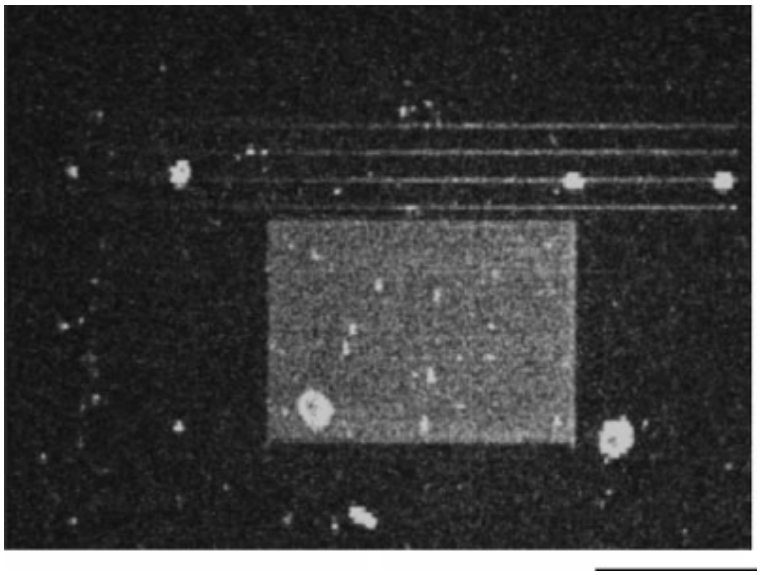

Figure 4. Immunofluorescence staining of 3-photon crosslinked human fibronectin structures stained with the monoclonal antibody HFN7.1. The rectangular structure was used to obtain an accurate signal to background measurement, where a value of 10:1 was obtained relative to the negative controls. Scale bar = 50 μm.

3.3.3 MPE patterns direct cell adhesion and spreading

The spreading of dermal fibroblasts was compared on crosslinked patterns of BSA, FN, and FG with pitch widths (line separations) of 10 and 40 μm. Representative phase contrast images are shown in Figure 5. The images suggest, that for the 10 μm pitch widths, the cells adhered onto BSA are predominantly constrained by geometrical factors and align between the linear structures (top row, left hand column). By contrast, the corresponding data for 10 μm pitch FN and FG show more spreading (middle and bottom rows, left hand column). To quantitatively compare these behaviors, we use the orientation, elongation, and perimeter size parameters described in the Methods (see Figure 2), as well as the probability that cells spread across 2 or more crosslinked lines. For the orientation parameter, an angle of less than 10° with respect to the

direction of the lines on a surface is considered to be highly aligned.[10,13,46] The data are summarized in Table I and plotted in Figure 6(a), where the adjoining lines signify data points that are statistically distinct. The symbol "*" indicates a significant difference where $p < 0.05$, Mann-Whitney Analysis; and the symbol "#" indicates significant differences where $p < 0.05$, Kruskal-Wallis one way Analysis with Dunn's Test for ranks. We see that the cells are most aligned on the BSA linear structures, with a mean angle of 10°. This result may seem counter-intuitive but points to the difference in guidance arising from the purely topographic interaction on crosslinked BSA in comparison with the cell-specific interactions on FN and FG. In the former, the cells are more physically constrained, and in the latter, the cells spread across the patterns resulting in a higher angle and seemingly less orientation. This is further borne out by the statistical similarity in the 10 and 40 μm pitch width data for both the FN and FG patterns ($p = 0.896$ for FN patterns, $p = 0.130$ for FG patterns, both analyzed using Student's *t*-test), where considerable spreading is observed, and the cells extend across multiple linear structures. By contrast, the cells on the BSA lines are much less aligned on the lines of 40 μm pitch widths (-10° vs 30°), presumably because the cells are less physically constrained between the lines.

We also use the elongation parameter as an additional measure of cell spreading, where this is calculated by the ratio of the maximum length (L) of the ellipse to the cell breadth (B) perpendicular to L. The data are plotted in Figure 6(b), where the control corresponds to cells randomly adhered to a monolayer of BSA on the ODTS surface. We observed that the cells that adhered to the crosslinked BSA patterns with 10 μm pitch width had a greater extent of elongation (L/B = 7) than those adhered to the crosslinked BSA of 40

μm pitch width (*indicates significant differences where $p < 0.05$, Mann-Whitney Analysis). These results suggest that the fibroblasts are confined between the 10 μm linear structures of BSA and spread directly along the topographical features, whereas at 40 μm there is reduced elongation (L/B = 3.9) due to lack of physical constraints. In contrast, the elongation of the fibroblasts adhered to crosslinked FN and FG features were not significantly different between the 10 and 40 μm pitch width (FN: $p = 0.103$, Student's *t*-test; FG: $p = 0.992$, Mann-Whitney). Additional measurements indicate a significant increase in cellular perimeter values [Fig. 6(c)] for both FN and FG on 10 μm patterns in comparison with 40 μm patterns (FN, $p = 0.014$; FG, $p = 0.045$, Student's *t*-test (**)). Further analyses show that fibroblasts cultured on 10 μm FN patterns had significantly greater perimeters than cells cultured on 10 μm BSA patterns or control surfaces (## indicates significant differences where $p < 0.05$, One-way ANOVA with Tukey posthoc analysis). The cellular perimeter values are increased due to the increase in the number of protrusions on the smaller pitch width patterns, which could result from the increased cell–matrix interactions or increased topographical features. At 40 μm pitch width, there were no significant differences of cellular elongation observed in response to the three different proteins ($p = 0.971$, Kruskal-Wallis) nor any difference in perimeter values ($p = 0.975$, Kruskal-Wallis). This data suggests that fibroblasts are attempting to spread across the patterns as opposed to directly spreading along the topographical features. These data are thus self-consistent with the orientation parameters shown in Figure 6(a).

A final metric we use to analyze the spreading behavior is the probability that the fibroblasts extend across and intersect two or more crosslinked lines. We only examine the 40 m pitch width, as the 10 m spacing is smaller than the width of a typical cell. The data are

plotted in Figure 6(d) as the percentage of total cells as a function of the number of lines intersected. Here, a value of one line represents the case of interaction with only a single line. We find that the fibroblasts on FN and FG have greater probability of bridging to 2, 3, or 4 lines than those on BSA. For example, the majority of cells on crosslinked BSA do not interact with more than one line, whereas, 2 interactions is the most probable outcome for FG, and nearly so for FN. These results are self-consistent with the orientation and elongation parameters indicating that fibroblasts adhered on the cell-specific FN and FG patterns preferentially spread across pitch spacing, rather than being simply aligned between them. These findings collectively indicate that the spreading on these crosslinked protein surfaces is governed by cell– matrix interactions as well as topographic factors, and these factors have different influences on the cell morphology.

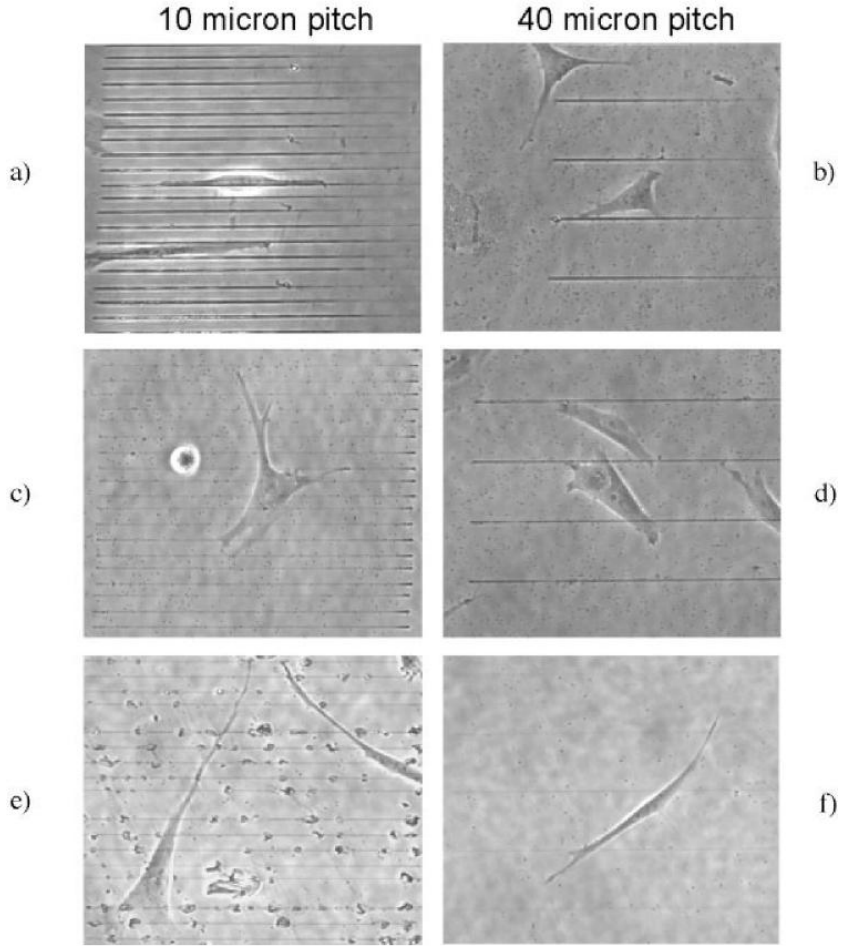

Figure 5. Phase contrast micrographs show fibroblast morphologies 3 h after cells were seeded onto MPE patterned matrices composed of BSA (a) and (b), FG (c) and (d), or FN (e) and (f). MPE patterned matrices were spaced with uniform pitch widths of 10 m (a), (c), and (e) or 40 m (b), (d), and (f).

3.3.4 Focal adhesion staining

Focal adhesion staining for vinculin was used to isolate the role of ECM cues on the spreading of the fibroblasts on the crosslinked proteins. Figure 7 shows the corresponding phase contrast image (top panel) which shows the positions of the lines, and the focal adhesion staining (bottom panel) for cells on BSA, FN, and FG. Punctate fluorescence (denoted by arrows) on the lines is seen only for cells on FN and FG,

suggesting a strong influence of ECM cues guiding cell morphology. This finding is consistent with the morphological analysis of cell spreading described above.

TABLE I
Analyses of Morphometric Data

	Pitch Width (μm)		
	0 (control)	10	40
Area (μm^2)			
BSA	1607.5 ± 180.74 (13)	1291.91 ± 157.05 (25)	1475.08 ± 119.13 (68)
FG		2398.99 ± 356.86 (16)	1791.01 ± 244.87 (36)
FN		1778.33 ± 307.25 (8)	1419.89 ± 194.5 (12)
Perimeter (μm)			
BSA	257.03 ± 21.27 (13)	263.94 ± 20.63 (25)	258.7 ± 12.57 (68)
FG		331.18 ± 28.27 (16)	265.78 ± 17.13 (36)
FN		403.73 ± 62.97 (8)	246.83 ± 22.24 (12)
Major length (μm)			
BSA	80.19 ± 7.63 (13)	97.67 ± 9.29 (25)	77.04 ± 3.82 (68)
FG		96.99 ± 8.67 (16)	81.31 ± 5.28 (36)
FN		99.44 ± 8.32 (8)	72.17 ± 6.97 (12)
Minor length (μm)			
BSA	27.14 ± 3.5 (13)	17.87 ± 2.13 (25)	24.98 ± 1.46 (68)
FG		32.37 ± 4.44 (16)	27.31 ± 2.63 (36)
FN		23.04 ± 3.24 (8)	25.59 ± 1.93 (12)
Elongation (μm)			
BSA	3.79 ± 0.68 (13)	7.16 ± 1.01 (25)	3.9 ± 0.35 (68)
FG		3.91 ± 0.67 (16)	3.87 ± 0.47 (36)
FN		5.17 ± 1.04 (8)	3.23 ± 0.56 (12)
Orientation (degrees)			
BSA		9.96 ± 2.7 (25)	28.77 ± 3.11 (68)
FG		26.83 ± 6.03 (16)	39.3 ± 4.65 (36)
FN		40.49 ± 10.67 (8)	42.92 ± 7.17 (12)

Cell morphology patterns, where values are reported as means with standard error of the means and the parenthesis show number of analyzed cells.

3.4 DISCUSSION

A primary benefit of the MPE nano/microfabrication method is the intrinsic biocompatibility that is achieved by fabricating 3D patterns of ECM proteins in an aqueous environment rather than using synthetic polymers as structural templates. Immunofluorescence labeling of FN and FG both indicated a high level of retention of bioactivity. Similarly, a high degree of specificity for fibronectin for the human antibody HFN 7.1 was observed. These findings of excellent biocompatibility are consistent with

our previous findings for the biological activity of crosslinked collagen[32] and alkaline phosphatase.[29]

Since FN is photocrosslinked with a modified benzophenone dimer that becomes part of the crosslinked matrix, we also must consider any possible cytotoxic effects arising from this reagent. Although benzophenone is used in topical applications such as sun blocking agents, it is potentially toxic in live cells. Specifically it has been shown to have estrogenic activity in MCF-7 and cytotoxic effects in cultured hepatocytes, where Nakagawa et al. observed highly adverse effects for concentrations of 1 m*M*.[47] However, these effects were greatly diminished or absent for concentrations of less than 100 I.L*M*. In the current context we need to consider if leaching of the BPD out of the crosslinked matrix could reach sufficient concentration to have cytotoxic effects on cells adhered to the crosslinked collagen. In our experiments, the BPD concentration in solution was 200 I.L*M*. To achieve toxic concentration, virtually all the reagents would have to come out of the matrix and then endocytose into the cells. Since the BPD is covalently crosslinked into the protein (unlinked dye is washed prior to culture), this outcome is unlikely.

Having established the bioactivity of the surfaces, we have examined the spreading of dermal fibroblasts on crosslinked BSA, FN, and FG in order to understand the relative roles of topography and ECM cues. We find that the spreading is quantitatively different on the nonspecific BSA in contrast to the ECM proteins FN and FG. On BSA patterns, the cellular orientation appears to be governed by physical constraints, where the cells primarily align parallel to linear structures. On FN and FG patterns the cells are more highly spread across the crosslinked linear structures.

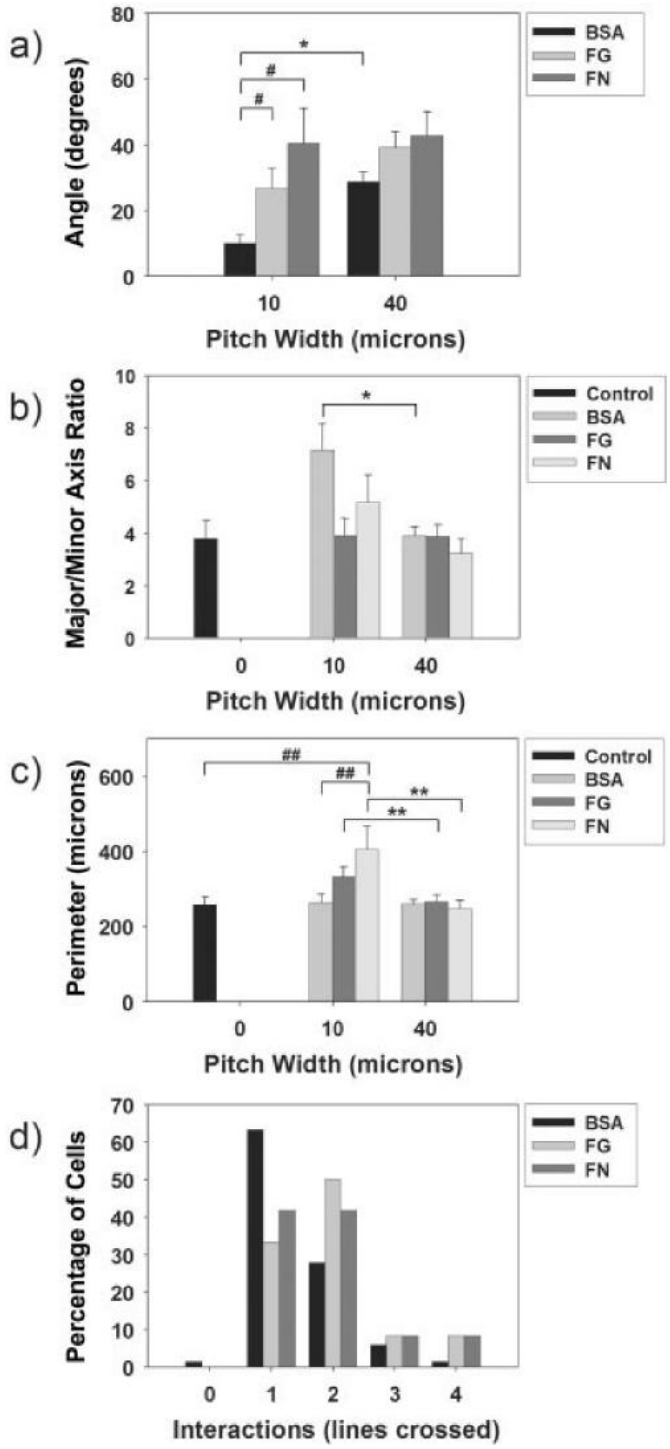

Figure 6. Analyses of morphological data of cells on crosslinked BSA, FG, and FN. The control is a monolayer of BSA on a self-assembled monolayer of organosilane. The bar graphs show (a) orientation, (b) elongation, (c) perimeter, and (d) probability for cell spreading across multiple lines. The lines connect statistically distinct points (all $p < 0.05$) where significant differences are indicated by Mann-Whitney analysis (*), Student's *t*-test (**), Kruskal-Wallis one-way Analysis with Dunn's Test for ranks (#), and One-way ANOVA with Tukey for posthoc analysis (##). Error bars are standard error.

The morphological analyses obtained for orientation and elongation parameters as well as the cellular propensity to spread across two or more lines are all self-consistent with this assessment. Furthermore, the appearance of punctate focal adhesion staining directly on the FN and FG lines, and its absence on BSA structures also supports the conclusion that the ECM cues are important in governing cell function. Due to the alignment observed on BSA, we can also conclude that the topographies of the crosslinked proteins are important. These findings are consistent with those found by other researchers[10,13,48] on the importance of the relative sizes and separations of grooves and ridges on cell spreading. However, the specific findings of each paper are highly dependent upon the details of the fabrication method used, and thus far it is difficult to reach broad, unifying conclusions regarding the most important topographic factors that direct cell morphology on the surfaces.

While these studies on synthetic templates have provided considerable insight into the creation of artificial scaffolds, it is highly advantageous to create three-dimensional scaffolds directly from crosslinked ECM proteins. To the best of our knowledge, simultaneous 3D spatial and chemical control of protein-based scaffold synthesis at the micron and submicron size scales has not been fully demonstrated. This combination of fabrication modalities has enormous potential for tissue engineering. While this paper has focused on fibrinogen and fibronectin, we have been successful in photocrosslinking a wide range of ECM and structural proteins, including collagens, laminin, myosin, tubulin, as well as growth factors. This array of proteins, coupled with the ability to fabricate with submicron-dimensions in three dimensions affords possibilities not available through other fabrication methods.

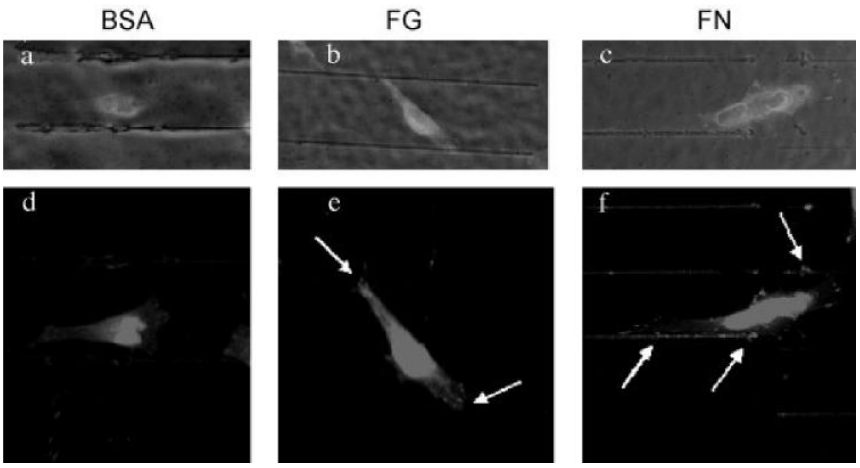

Figure 7. Focal adhesion staining with a monoclonal antibody for vinculin for cells on BSA (a) and (d); FG (b) and (e) and FN (c) and (f) patterns with a pitch width of 40 um. The top panel (a), (b), and (c) are the phase contrast images used to visualize the linear structures and the bottom panel. (d), (e), and (f) are the corresponding fluorescence images of the focal adhesions. Punctate fluorescence along the crosslinked patterns is observed on FN and FG, but not for BSA, indicating a different guiding mechanism.

3.5 CONCLUSIONS

We have begun to explore the relative roles of topography and biochemistry that govern cell adhesion and spreading on ECMs patterns fabricated directly from crosslinked proteins. We find statistically distinct cell spreading responses on crosslinked BSA patterns in contrast to the similar FN and FG structures, where the former shows physical or geometrical guidance, and the latter are dominated by cell–matrix interactions. Thus, the use of MPE for fabricating nano- and microscaled crosslinked protein structures offers a flexible method for studying the topographic factors and cell–matrix interactions that drive cell adhesion, spreading, differentiation, and proliferation. Our future efforts will be directed at systematically varying feature sizes, topographies, and protein composition to characterize the effects of surface morphology on cellular functions.

The HFN7.1 hybridoma supernatant was obtained from the Developmental Studies Hybridoma Bank developed under the auspices of the NICHD and maintained by the University of Iowa, Department of Biological Sciences, Iowa City, IA; R.J. Klebe, contributor.

3.6 References

1. Abrams GA, Goodman S, Murphy CJ. Nanoscale Topography of the Extracellular Matrix Underlying the Corneal Epithelium of the Primate. Invest Ophthal Visual Sci 1997;38:S505.
2. Abrams GA, Schaus SS, Goodman SL, Nealey PF, Murphy CJ. Nanoscale topography of the corneal epithelial basement membrane and Descemet's membrane of the human. Cornea 2000;19(1):57-64.
3. Tan J, Saltzman WM. Biomaterials with hierarchically defined micro- and nanoscale structure. Biomaterials 2004;25:3593-3601.
4. Tan W, Desai TA. Layer-by-layer microfluidics for biomimetic three-dimensional structures. Biomaterials 2004;25:1355-1364.
5. Tan W, Desai TA. Microfluidic patterning of cells in extracellular matrix biopolymers: effects of channel size, cell type, and matrix composition on pattern integrity. Tissue Eng 2003;9(2):255-67.
6. Curtis A, Wilkinson C. Topographical control of cells. Biomaterials 1997;18:1573-1583.
7. Dalby MJ, Riehle MO, Sutherland DS, Agheli H, Curtis AS. Use of nanotopography to study mechanotransduction in fibroblasts--methods and perspectives. Eur J Cell Biol 2004;83(4):159-69.
8. Flemming RG, Murphy CJ, Abrams GA, Goodman SL, Nealey PF. Effects of synthetic micro- and nano-structured surfaces on cell behavior. Biomaterials 1999;20:573-588.
9. Clark P, Connolly P, Curtis ASG, Dow JAT, Wilkinson CDW. Cell guidance by ultrafine topography in vitro. J Cell Sci 1991;99:73-77.
10. den Braber ET, de Ruijter JE, Ginsel LA, von Recum AF, Jansen JA. Quantitative analysis of fibroblast morphology on microgrooved surfaces with various grove and ridge dimensions. Biomaterials 1996;17:2037-2044.
11. Britland S, Morgan H, Wojiak-Stodart B, Riehle M, Curtis A, Wilkinson C. Synergistic and hierarchical adhesive and topographic guidance of BHK cells. Exp Cell Res 1996;228(2):313-25.
12. Teixeira AI, Abrams GA, Bertics PJ, Murphy CJ, Nealey PF. Epithelial contact guidance on well-defined micro- and nanostructured substrates. J. Cell Sci. 2003;116:1881-1892.
13. Teixeira AI, Nealey PF, Murphy CJ. Responses of human keratocytes to micro- and nanostructured substrates. J Biomed Mater Res 2004;71A(3):369-76.
14. Karuri NW, Liliensiek S, Teixeira AI, Abrams G, Campbell S, Nealey PF, Murphy CJ. Biological length scale topography enhances cell-substratum adhesion of human corneal epithelial cells. J Cell Sci 2004;117(Pt 15):3153-64.
15. Pitts JD, Campagnola PJ, Epling GA, Goodman SL. Reaction efficiencies for sub-micron multi-photon freeform fabrications of proteins and polymers with applications in sustained release. Macromolecules 2000;33:1514-1523.
16. Campagnola PJ, Howell AR, Delguidas D, Epling GA, Pitts JD, Goodman SL. 3-Dimensional sub-micron polymerization of acrylamide by multi-photon excitation of xanthene dyes. Macromolecules 2000;33:1511-1513.

17. Denk W, Strickler JH, Webb WW. Two-photon laser scanning fluorescence microscopy. Science 1990;248:73-76.
18. Zipfel WR, Williams RM, Webb WW. Nonlinear magic: multiphoton microscopy in the biosciences. Nat Biotechnol 2003;21(11):1369-77.
19. Lee W, Pruzinsky SA, Braun PV. Multi-Photon Polymerization of Waveguide Structures Within Three-Dimensional Photonic Crystals. Adv. Mater. 2002;14:271-274.
20. Zhou W, Kuebler SM, Braun KL, Yu T, Cammack JK, Ober CK, Perry JW, Marder SR. An Efficient Two-Photon-Generated Photoacid Applied to Positive-Tone 3D Microfabrication. Science 2002;296:1106-1109.
21. Olson CE, Previte MJ, Fourkas JT. Efficient and robust multiphoton data storage in molecular glasses and highly crosslinked polymers. Nat Mater 2002;1(4):225-8.
22. Witzgall G, Vrijen R, Yablonovitch E, Doan V, Schwartz BJ. Single-shot two-photon exposure of commercial photoresist for the production of three-dimensional structures. Optics Letters 1998;23:1745-1747.
23. Kawata S, Sun H-B, Tanaka T, Takada K. Microfabrication: Finer features for functional microdevices. Nature 2001;412:697-698.
24. Maruo S, Nakamura O, Kawata S. Three-dimensional microfabrication with two-photon-absorbed photopolymerization. Optics Letters 1997;22:132-134.
25. Kawata Y, Ishitobi H, Kawata S. Use of two-photon absorption in a photorefractive crystal for three-dimensional optical memory. Opt. Lett. 1998;23:756-758.
26. Kaehr B, Allen R, Javier DJ, Currie J, Shear JB. Guiding neuronal development with in situ microfabrication. Proc Natl Acad Sci U S A 2004;101(46):16104-8.
27. Cumpston BH, Ananthavel SP, Barlow S, Dyer DL, Ehrlich JE, Erskine LL, Heikal AA, Kuebler SM, Lee I-YS, McCord-Maughon D and others. Two-photon polymerization initiators for three-dimensional optical data storage and microfabrication. Nature 1999;398:51-54.
28. Strickler JH, Webb WW. Three-dimensional optical data storage in refractive media by two-photon point excitation. Optics Letters 1991;16:1780-1782.
29. Basu S, Campagnola PJ. Enzymatic Activity of Alkaline Phosphatase inside Protein and Polymer Structures Fabricated via Multi-photon Excitation. Biomacromolecules 2004;5:572-579.
30. Basu S, Campagnola PJ. Properties of crosslinked protein matrices for tissue engineering applications synthesized by multiphoton excitation. J Biomed Mater Res 2004;71A(2):359-68.
31. Basu S, Wolgemuth CW, Campagnola PJ. Measurement of Normal and Anomalous Diffusion of Dyes within Protein Structures Fabricated via Multi-photon Excited Crosslinking. Biomacromolecules 2004;5:2347-2357.
32. Basu S, Cunningham LP, Pins G, Bush K, Toboada R, Howell AR, Wang J, Campagnola PJ. Multi-photon Excited Fabrication of Collagen Matrices Crosslinked by a Modified Benzophenone Dimer: Bioactivity and Enzymatic Degradation. Biomacromolecules 2005;6:1465-1474.

33. Gailit J, Clarke C, Newman D, Tonnesen MG, Mosesson MW, Clark RA. Human fibroblasts bind directly to fibrinogen at RGD sites through integrin alpha(v)beta3. Exp Cell Res 1997;232(1):118-26.
34. Cutler SM, Garcia AJ. Engineering cell adhesive surfaces that direct integrin alpha5beta1 binding using a recombinant fragment of fibronectin. Biomaterials 2003;24(10):1759-70.
35. Charest JL, Bryant LE, Garcia AJ, King WP. Hot embossing for micropatterned cell substrates. Biomaterials 2004;25(19):4767-75.
36. Pitts JD, Howell AR, Taboada R, Banerjee I, Wang J, Goodman SL, Campagnola PJ. New photoactivators for multiphoton excited three-dimensional submicron cross-linking of proteins: bovine serum albumin and type 1 collagen. Photochem Photobiol 2002;76(2):135-44.
37. Sridhar M, Basu S, Scranton VL, Campagnola PJ. Construction of a laser scanning microscope for multiphoton excited optical fabrication. Rev. Sci. Instrum. 2003;74(7):3474-3477.
38. Mooney JF, Hunt AJ, McIntosh JR, Liberko CA, Walba DM, Rogers CT. Patterning of functional antibodies and other proteins by photolithography of silane monolayers. Proc Natl Acad Sci U S A 1996;93(22):12287-91.
39. Eaton DF. Dye sensitized photopolymerization. Advances in photochemistry 1986;13:427-487.
40. Balasubramanian D, Du X, Zigler JSJ. The reaction of singlet oxygen with proteins, with special reference to crystallins. Photochem. Photobiol. 1990;52:761-768.
41. Schoen RC, Bentley KL, Klebe RJ. Monoclonal antibody against human fibronectin which inhibits cell attachment. Hybridoma 1982;1:99-108.
42. Pins GD, Collins-Pavao ME, Van De Water L, Yarmush ML, Morgan JR. Plasmin triggers rapid contraction and degradation of fibroblast-populated collagen lattices. J. Invest. Dermatol. 2000;114:647-653.
43. Hell SW, Stelzer EHK. Fundamental improvement of resolution with a 4pi-confocal fluorescence microscope using two-photon excitation. Optics Comm. 1992;93:277-282.
44. Konig K, So PTC, Mantulin WW, Gratton E. Cellular response to near-infrared femtosecond laser pulses in two-photon microscopes. Opt. Lett. 1997;22:135-136.
45. Hopt A, Neher E. Highly nonlinear photodamage in two-photon fluorescence microscopy. Biophys J 2001;80(4):2029-36.
46. den Braber ET, de Ruijter JE, Ginsel LA, von Recum AF, Jansen JA. Orientation of ECM protein deposition, fibroblast cytoskeleton, and attachment complex components on silicone microgrooved surfaces. J Biomed Mater. Res 1998;40:291-300.
47. Nakagawa Y, Suzuki T, Tayama S. Metabolism and toxicity of benzophenone in isolated rat hepatocytes and estrogenic activity of its metabolites in MCF-7 cells. Toxicology 2000;156(1):27-36.
48. Dalby MJ, Yarwood SJ, Riehle MO, Johnstone HJ, Affrossman S, Curtis AS. Increasing fibroblast response to materials using nanotopography: morphological and genetic measurements of cell response to 13-nm-high polymer demixed islands. Exp Cell Res 2002;276(1):1-9.

Chapter 4

Morphological and Cytoskeletal dynamics on microfabricated crosslinked ECM Scaffolds

Morphological and Cytoskeletal dynamics on microfabricated crosslinked ECM Scaffolds

Lawrence P. Cunningham[1‡], Katie A. Bush[32], Cyr E. M'Lan[4], George D. Pins[†], and Paul J. Campagnola[1]

[1]Department of Cell Biology and Center for Cell Analysis and Modeling,
University of Connecticut Health Center, Farmington, Connecticut
[2] University of Massachusetts Medical School, Worcester, MA
[3]Worcester Polytechnic Institute, Department of Biomedical Engineering, Worcester, MA
[4] Department of Statistics, University of Connecticut, Storrs, Connecticut

Contract grant sponsor: NIH; contract grant number: R01 EB000263

ABSTRACT

This chapter investigates the relationship between stress fibers and focal adhesions with respect to a biomimetic, bioactive extracellular matrix in terms of likelihoodof focal adhesion attachment on varied spatial and biochemical microenvironments, stress fiber length and orientation, cell morphology. Using multiphoton-excited (MPE) photochemistry we fabricated parallel linear patterns with extracellular matrices (ECM) proteins fibronectin (FN), and Collagen I and bovine serum albumin (BSA) as a Control to investigate morphological and the directional response of human dermal fibroblasts grown on the photocrosslinked linear structures. We cells spread more on ECM protein proteins compare with BSA. Fibroblasts on BSA structures are not significantly associated with stress fiber orientation. Stress fibers on Collagen I will orient themselves significantly differently than those on BSA structures. Areas and Perimeters of fibroblasts differ significantly when grown on Collagen I versus BSA linear structures. Odds are less for focal adhesions to form on Collagen I compared with Fibronectin structures. We conclude that the different focal adhesion complex with Collagen I and fibroblasts facilitate stronger, stiffer stress fibers enhancing changes in cellular morphology compared with Fibronectin.

Keywords: Cell Adhesion, Extracellular Matrix, ECM, Scaffolds, Microfabrication, Tissue Engineering, Integrin, Focal Adhesions, Stress Fibers, Fibroblast

4.1.0 Introduction

The design of highly functional scaffolds for tissue engineering must begin with a fundamental understanding of the mechanisms by which the 3-D architecture and the biochemical composition of the tissue scaffolds modulate cellular adhesion, proliferation, and differentiation, as well as the regeneration of native tissue functions [40]. These scaffolds must replicate native tissue microstructures with cellular microenvironments (1-10 μm) as well as organ-scale structures with cellular resolution (10-1000 μm) to better maintain *in vivo*-like cellular function.[41, 42] Additionally, the control of cellular functions is largely modulated by cells interacting with ECMs, which have an extremely complex structure in the submicron or nanoscale range (100 – 300 nm). [43, 44] The ECM consist of filaments containing collagen, laminin, fibronectin and proteoglycans as well as other fibrils which form a complex nanometer sized topography (~2 nm to 200 nm) of fibers and ridges.[44-46] In addition to providing structural support, the ECM provide biophysical signals that direct cell migration, proliferation, differentiation as well as new tissue synthesis. [45, 47-52]

Recognizing the importance of the initial cell adhesion, recent efforts have attempted to create 3D nano/microstructured model systems from a variety of materials in order to replicate the topography of the ECM. The simplest forms have used photolithography to create nanogrooves and ridges on the size scales of the basement membrane and dermis and studied fibroblast and epithelial cell functions on these modified surfaces.[43, 52-59] These reports have conflicted in terms of identifying the most important geometrical factors in governing cell spreading and alignment, highlighting the complexity of the problem in understanding cell-topography interactions.

This may arise because traditional and soft lithographies are limited in their ability to create structures with complexity in all three dimensions. Other efforts have fabricated scaffolds from polymeric membranes designed to replicate basement membranes.[60, 61] While these scaffolds may present the topographic features similar to the native structure, they do not present the ECM cues required for specific cell-matrix interactions. Fundamental knowledge gained from cell-matrix studies using models that both the topography and biochemical cues of the native ECM would provide important insights into the design of functional tissue engineering devices.

To work towards this goal, we have developed a nano/microfabrication method based on multiphoton excited (MPE) photochemical crosslinking of proteins with submicron spatial control.[62, 63] The method is analogous to that of the well-known two-photon excited fluorescence (TPEF) imaging, where in the present case, the excitation, and thus the photochemistry, is restricted to the focal volume. [64-70] In contrast, conventional (i.e. one-photon excitation) photochemical crosslinking is essentially two dimensional in nature, as axial control is limited for this scheme. We have previously reported our efforts on the fabrication and subsequent physical and chemical characterization of protein matrices created from serum and ECM proteins using this technology. [71-73] Of note, based on antibody labeling, enzymatic activity, and cell adhesion, all of these proteins retained their biological activity following MPE crosslinking. In a previous paper we reported on our initial efforts to systematically characterize cell adhesion and spreading of dermal fibroblasts on linear fiber patterns of crosslinked matrix molecules (BSA, fibronectin (FN) and fibrinogen (FG)). Morphological analyses show that cells adhered to the crosslinked FN and FG structures

show statistically different spreading behavior than those on BSA, indicating the role of combined cell- matrix/topographic interactions in the former case. Collectively these findings indicate that topography and ECM cues lead to different forms of guidance and spreading for fibroblasts adhered to crosslinked matrix proteins.

Here we extend these studies to extend to more in depth morphological analysis, as well examining the cytoskeletal and integrin binding dynamics of dermal fibroblasts on fibers of FN, Type I collagen, and BSA. This approach allows the isolation of purely topographic guidance from that arising from a combination of topographic and biochemical cues. Here we correlate the spatial distribution of focal adhesions and stress fibers for cells adhered to the different protein. We specifically find differences for cells adhered to FN and Collagen in spreading and cytoskeletal organization, which may arise from differences in their respective roles in promoting migration and new matrix synthesis.

4.2.0 Experimental methods

4.2.1 Fabrication instrument, photochemistry and Surface preparation

The multiphoton fabrication and imaging instrument is a custom-designed laser-scanning system whose features have been previously described. [74]BSA (10 mg/ml) is crosslinked via 2-photon excitation with Rose Bengal (1 mM) at 800 nm. The photochemistry proceeds through the generation of singlet oxygen which then attacks residues containing aromatic groups and free amines.[75, 76] The resulting radical protein then links to a second protein molecule. Collagens I, II and Fibronectin (1 mg/ml) are crosslinked via 3-photon excitation of the benzophenone dimer at 780 nm. This reagent inserts into either carbon-hydrogen, or carbon-carbon bonds, and becomes

part of the crosslinked network.[38] Protein linear structures are fabricated on a nonspecific BSA background that is adsorbed to a chemisorbed, C-18 organosilane surface (ODTS, Gelest). Structures were fabricated on adsorbed BSA monolayers using removable silicone gaskets (isolators) on the glass. As the proteins are covalently bonded to the monolayer stable fixation to a neutral background is assured. The silicone isolators were removed and the slides were kept in sterile PBS until cell plating.

4.2.2 Cell culture and seeding

Human dermal fibroblasts used in all experiments were derived from neonatal foreskin using a protocol described previously [77]. To isolate fibroblasts, foreskin tissue was trimmed to remove excess fatty tissue, rinsed with sterile PBS, and diced into small fragments. The fragments were allowed to adhere to the bottom of a tissue culture plate in a humidified 10% CO_2 atmosphere at 37°C for 1 h, and were then covered with Dulbecco's Modified Eagle's Medium containing penicillin/streptomycin (100 U/100 µg per mL; Gibco). After 14 days, confluent fibroblasts were harvested with 0.05% trypsin/ ethylenediamine tetracetic acid solution and subcultured in DMEM containing 10% FBS and Penicillin / Streptomycin.

After silicone isolators were placed on the experimental surfaces, the slides were warmed to 37°C and rinsed three times in DMEM containing penicillin / streptomycin to clean the surfaces. Slides were placed in tissue culture plates and 100 µl of serum free culture medium containing fibroblasts was seeded in the center of each well on the slide. The final cell density in each individual well was 38,000 cells and each well was individually inspected to assure cells were uniformly distributed on the patterned

surfaces. Tissue culture plates containing cell-seeded slides were transferred to a tissue culture incubator for 3 hours and then fixed.

4.2.3 Focal adhesion, cytoskeletal, and nuclei staining

After incubation, fibroblasts were fixed and stained for focal adhesions (Anti-vinculin; Ted Pella), cytoskeletal actin (Rhodamine-Phalloidin; Invitrogen) and nuclei (Hoescht Nuclear Stain; Invitrogen). Slides were then rinsed with PBS and imaged fluorescently. To verify that the cell adhesion was via integrin binding, we employed the cross-linking/extraction biochemical method that has been previously described by Garcia and co-workers [78]. Fibroblasts were seeded on the MPE patterned FN slides and ligated integrins were cross-linked using DTSSP for 1 hour at room temperature and a 0.1% sodium dodecyl sulfate and phenylmethylsulfonyl fluoride solution in PBS was used to extract uncrosslinked cellular components. Crosslinked cellular components were rinsed with PBS, incubated in blocking buffer (5% FBS in PBS) for 1 hour and then probed with α5 specific primary antibody (Chemicon International Temecula, CA) in blocking buffer (1:1000 dilution) for an additional hour. The slides were then rinsed and probed with an Alexa 546-conjugated goat anti-mouse secondary antibody (Invitrogen) in blocking buffer (3:500 dilution) for 1 h at 37°C and then fluorescently imaged for presence of the α5 integrin subunit.

4.2.4 Cell morphology and cytoskeletal dynamics

We examined cell morphology and cytoskeletal dynamics on linear structures of multiphoton crosslinked FN, Type I Collagen and BSA. BSA provides no ECM cues, and any cell adhesion and guidance is expected to be governed only by contact guidance provided by the topography. Fabricated linear patterns were created with spacing of 10

µm, where this was consistent with our previous study. This spacing is of a scale significantly smaller than that of fibroblasts. Line lengths are 200 µm are sufficiently long to allow adequate spreading along the patterns The minimum feature sizes of fabricated collagen and fibronectin protein fibers are approximately 0.75 µm (fiber thickness) and 2.5 µm (fiber height), respectively. As the fiber widths are approximately 600 nm, they approximate the size of clusters of focal adhesions. Cell morphology on a monolayer of BSA was also employed as a negative control for a surface lacking both biochemical signaling and topographic response.

In this study, we preferred to not employ fluorescently labeled proteins for fabrication to prevent the possibility of the hindering signaling motifs (such as RGD) in the integrin-mediated processes of cell-matrix protein attachment. In addition, a focal adhesion on a protein structure that is fluorescently labeled might not be as readily identifiable. Images of stained preparations were taken at rhodamine and green fluorescent protein excitations wavelengths as well as white light.

Using Metamorph ™ software and coregistered triple-stained and brightfield TIF images, we measured the Area and Perimeter of human dermal fibroblasts that were touching another fibroblast (attached) or were not touching another fibroblast (single). This was done to determine if there was a difference in areas or perimeters that might be explained by other factors. One such explanation might be that cell-cell signaling effects cell morphometry in terms of area and perimeter.

Three dependent variables “Proteins” are BSA, Collagen I, and Fibronectin. BSA is regarded as a control in that MPE-fabricated BSA lines inherently lack biochemical

signals, is comprised of the same material as the neutral background monolayer, yet has the topography as FN and Collagen MPE-fabricated lines.

4.2.5 Focal Adhesion Response Studies

To understand the effect the biomimetic ECM has on fibroblast focal adhesion formation, we counted focal adhesions on a per cell basis and categorized according to attachment location. A focal adhesion could be formed on a fabricated protein line, on a stress fiber, simultaneously on a fabricated protein line and stress fiber, or on none of the above. A focal adhesion that forms on neither fabricated line, nor stress fiber is a Nascent focal adhesion that in these resulting data would be referred to as "not both" or "neither." To statistically evaluate the interactions between intracellular cueing (Cell Type, i.e., fibroblasts Attached to other fibroblasts versus Single fibroblasts), the role of topographical cues (use of BSA Monolayer and BSA Lines as controls) and protein composition of the linear structures, the frequency data of focal adhesions were collected and segregated into partitioning categories. These "per cell" partitioning categories are: the number of focal adhesions on a fabricated protein line ("Line"); simultaneously on both a stress fiber and a line ("Both"); stress fibers only ("SF"); and finally, on neither stress fibers nor lines ("Nascent").

To relate cell morphology to the cell's microenvironment we used three independent variables – Center, Cell Type and Protein Type. To interpret the results of our measurements taken of fibroblast morphology on fabricated ECM structures we performed statistical analyses (mostly Generalized Linear Models, or GLMs) which are broadly broken down into three areas. The first analysis seeks to relate the likelihood of four types of Focal Adhesion to cells measure at two different facilities (Cell Type),

fabricated Protein Type and the interaction of Cell Type and Protein Type. The second analysis seeks to relate the orientation of Stress Fibers to fabricated protein lines. The third analysis seeks to relate geometrical quantities of cells such as Area, Perimeter, and Isoperimetric Quotient (defined as Area/Square of Perimeter) to Center, Cell Type and Protein Type.

The first analysis seeks to relate four types of Focal Adhesion, namely those occurring on Protein Lines Only, Stress Fiber Only, Both Lines and Stress fibers, and Neither Lines and Stress fibers or Nascent to Cell Type (Attached to other fibroblasts or Single), Protein Type (FN, BSA or Collagen) and their interaction. Three GLMs had been formulated. The first GLM had Cell Type, Protein Type and their interaction as independent variables, the second GLM excluded the interaction, while the third only had Protein Type as an independent variable.

4.2.6 Stress Fiber Orientation Response Studies

The next analysis concerned the angular distribution of Stress Fibers with respect to different Protein Type lines. Concretely, the goals of this analysis were to see if there is a preference in any direction, as well as to see if the preferences changed for different Protein Types. To quantitate the effects of BSA monolayer, patterned BSA, Col I, and FN structures on cell morphology, fibroblasts were measured using Metamorph ™ Version 7.0 (Molecular Devices). The images are fluorescently stained to provide stress fiber origin and terminus. Metamorph ™ was used to measure magnitude and direction of each stress fiber. The area, perimeter, orientation, and stress fiber distributions were determined independently for isolated fibroblasts and those that contacted another cell. This was done to determine if there was a difference in cell response that might be

explained by cell-cell signaling effects rather than cell-matrix interaction. The statistics for morphological characterizations were performed using SAS 9 and differences of $p<0.05$ were considered to be significant.

The stress fiber distribution was analyzed using circular statistics (Oriana 3.0, Kovach Computing Services, Wales, U.K.), which provides a spatial histogram and circular statistical analysis of the stress fiber orientation over the entire cell with respect to the linear axis.[79] Here the mean resultant of the stress fibers, R, is a measure of orientation, given by:

$$R = \frac{1}{N}\sqrt{\sum_{j=1}^{N}\sin 2\theta_j + \sum_{j=1}^{N}\cos 2\theta_j} \qquad [1]$$

where N is the number of cells, and θ is the angle of the stress fiber.

4.2.7 Focal Adhesion Analysis: Logistic Procedure and Generalized Linear Models

With the total number of focal adhesions known (by counting), our rationale is to evaluate the likelihood of focal adhesion occurrence as likelihood of odds ratios. Using the logit of the odds ratio as the canonical function, we determine the likelihood of interactions between Cell Type (Attached versus Single cells); Protein type; and interactions within Cell Type and Protein Type (CellType*Protein) in terms of focal adhesion formation with statistical significance. If p is the probability of occurrence, then [p / (1-p)] is the corresponding "odds". The logit of the probability is the logarithm of the "odds" that is, logit (p) = log[p / (1-p)]. We combine the use of the logit and log odds with two probabilities, such as the probability of focal adhesions on lines and the probability of focal adhesion of stress fibers in the binomial (versus multinomial) case. It should be noted that the logit function has values that range from zero to unity.

Three Logistic Models were developed to assure robustness using SAS (version 9). The first model analyzed the effects of Cell Type (attached versus single), protein type (FN versus Collagen I), and Cell Type * Protein (interactions between protein and cell type combinations). The second model excludes Cell Type * Protein combined interaction and simply provides results about "Cell Type" and "Protein".

The third model only incorporated "Protein" data. The results from last model should represent the same outcome with a more fine-tuned probability as there is less noise in the system. In fact all three of our models yield a consistent result. These three models (using the logit function) are included in Appendix A. BSA Monolayer and BSA lines data were not included in the models. The Monolayer experiment, by design, lacks BSA lines. Clearly, as one cannot count focal adhesions on lines that do not exist, an alternate method of analyses would necessarily be employed. The data for BSA Lines lacked sufficient response for the model to work. This is actually expected as BSA lacks sufficient biochemical cueing and as a consequence would not warrant a robust data set of focal adhesion counts. The subsequent model was developed to be able to deal with the expected lack of focal adhesion response from BSA lines and the null data for focal adhesion counts on non-existing lines (BSA monolayer). To find the likelihood of the number of focal adhesions per cell, with BSA controls included, a Poisson distribution was used as a canonical function in the Generalized Linear Model, instead of the logit function which was employed with the linear models.

The fourth linear model (using the Poisson distribution) is included within Appendix A (therein, refer to Fourth Procedure, The Generalized Linear Model. This is used for Stress fiber. The Effect of Proteins on morphometry (Area, Perimeter) will be

evaluated using Generalized Linear Models data will be evaluated using Rao's spacing test, Kuiper's Test, and the pairwise Mardia-Watson-Wheeler Test orientation such as Stress Fiber Magnitude Statistics and Angular Statistics.

4.3.0 Results and Discussion
4.3.1 Validation of Integrin Binding

Immunostaining cells on fibronectin lines was positive for the α5 subunit. Positive immunofluorescence for the α5 integrin subunit was performed to assay the crosslinked FN's ECM signaling protein functionality. Cells were evaluated for integrin specificity on FN lines since similar results were obtained for the other extracellular matrix proteins evaluated. It was shown through staining of α5, an integrin responsible for binding to FN, that cellular interactions with the MPE FN lines were integrin-mediated. Note that the validation of integrin binding was not performed with collagen, as there are no published reports on this method to our knowledge. Having substantiated for integrin specificity for FN lines, we continue studying likelihood of focal adhesions on FN (and Collagen I which also contains RGD) and stress fiber formation.

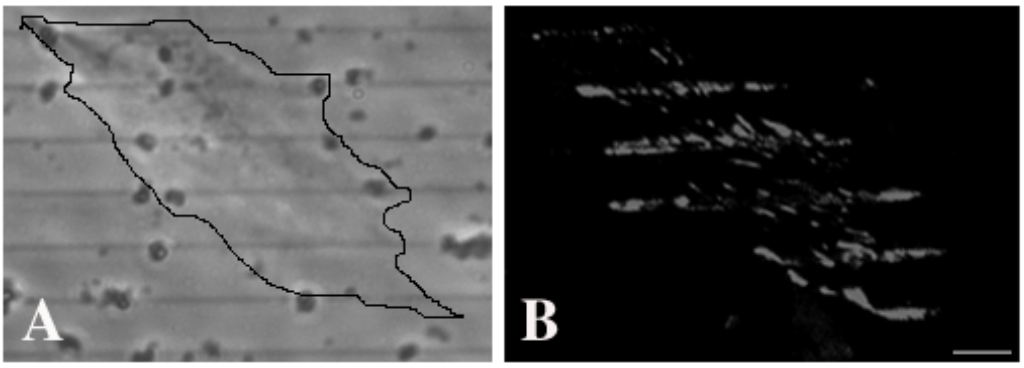

Figure 1. Integrin α5 integrin staining on MPE Fabricated Fibronectin Lines
(A) Traced shadow of Human Dermal Fibroblast grown on Fibronectin lines, Bright Field
(B) Immunostained cells on fibronectin fibers was positive for the α5 subunit via immunofluorescence.

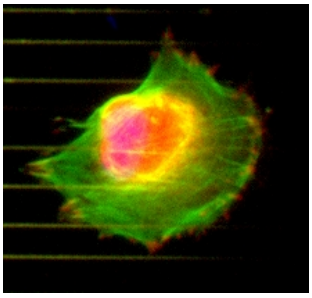

(A) BSA Monolayer

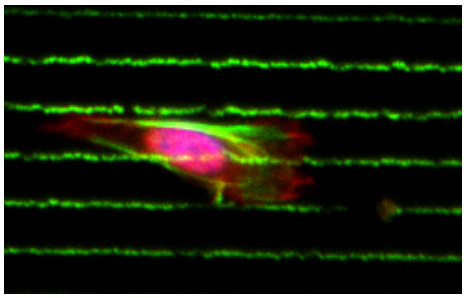

(B) BSA MPE-fabricated BSA Lines with 10 um spacing

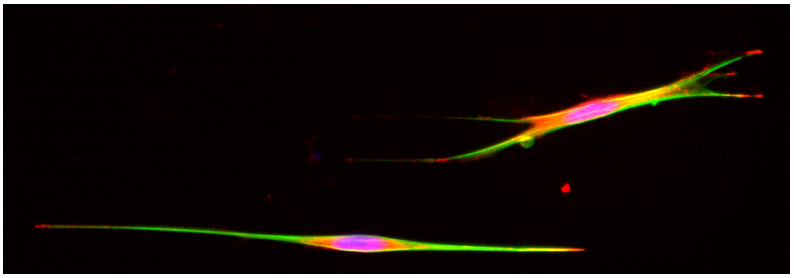

(C) Fibronectin lines with 10 um spacing

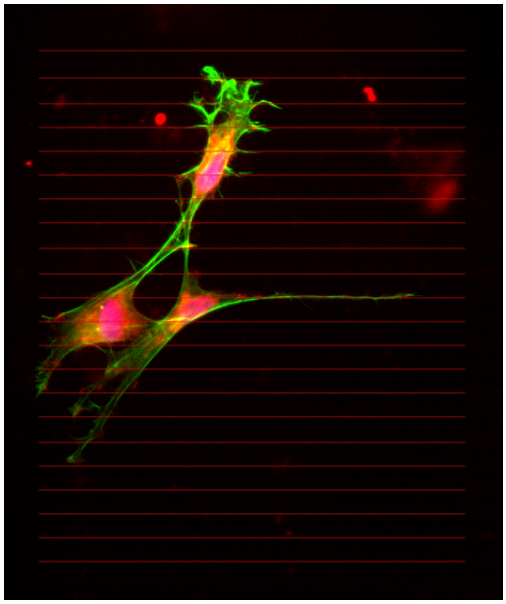

(D) Type I Collagen lines with 10 um spacing

Figure 2, Images of Cells on BSA, FN and Collagen I
Human Dermal Fibroblasts were cultured for three hours on separate adsorbed BSA monolayers upon which are covalently bound fabricated lines of Collagen I, Fibrinogen or BSA. Fibroblasts were also cultivated on a BSA monolayer.

4.3.2 Fibroblast Focal Adhesions to Collagen I, FN, BSA, and BSA Monolayer

In Figure 2 (left), the BSA lines and the BSA Monolayer serve as Controls. Fibroblasts are stained for actin fibers using rhodamine-phalloidin (pseudo-colored green) and antivinculin (pseudo-colored red) to show punctate staining marks the Focal Adhesion molecules. Focal Adhesion location, Area, Perimeter, Stress Fiber Magnitude and Direction were measured for each cell growing on the various proteins.

Fibroblasts (Top row, A and B) are shown growing on BSA lines. Image (A) on the left shows stress fibers radiating outward, without appreciable Focal Adhesions to the BSA lines. Note that the right edge of the cell is not on any BSA liners, but is spreading outward beyond the BSA lines where the only microenvironment is the BSA monolayer. The image on the right demonstrates fibroblast tendency to grow within lines, cued by topography, rather than extracellular chemical signaling, as previously shown [80]. In addition, it is interesting to note that there is a distinct the lack of Focal Adhesions on the BSA Lines. Fibroblasts are grown on MPE-fabricated BSA Lines and BSA Monolayer (as Controls). Fibroblasts on BSA Monolayer, lacking BSA lines is not pictured. The parallel lines are spaced 10 microns apart. Note that BSA structures are very easy to image, so structures need not be digitally highlighted. The image on the top left (A) shows stress fibers radiating outward, without appreciable Focal Adhesions to the BSA lines. The image on the right (B) demonstrates fibroblast tendency to grow within lines, cued by topography, rather than extracellular chemical signaling, as previously shown [80]. In addition, it is interesting to note that there is a distinct lack of Focal Adhesions on the BSA Lines. Fibroblasts growing on MPE-fabricated Fibronectin lines with 10 um spacing are shown in the middle picture (C). At the bottom picture (D), attached

fibroblasts are growing on MPE-fabricated Type I Collagen lines with 10 um spacing. The red lines (which were digitally added) indicate location of linear structures.

Distribution of Focal Adhesions

Protein (N)	Average Number of Stress Fibers per Fibroblast	% of Focal Adhesions on lines	% of Adhesions on Stress Fibers	% of Focal Adhesions on *both* lines and Stress Fibers
Collagen I (8)	8.6	61.4%	60.0%	45.0%
Fibronectin (24)	4	67.9%	59.8%	46.4%
BSA lines (5)	2.4	35.1%	5.4%	2.7%
BSA Monolayer (5)	9.6	68.6%	n/a	n/a

Table 1, entitled "Distribution of Focal Adhesions", depicts percentages of focal adhesion locations for fibroblasts on fabricated linear structures made of Collagen I, Fibronectin, BSA and BSA Monolayer. Focal adhesions in this experiment can be found associated with a fabricated line, on a stress fiber, on both, simultaneously, or on neither.

The Distribution of Focal Adhesions chart illustrates that the majority of focal adhesions in fibroblasts occurred on fabricated lines (61.4% Collagen I, 67.9% Fibronectin, and 35.1% BSA). Fibronectin appears to have a slightly greater effect on focal adhesion frequency compared to Collagen I. Both Collagen and Fibronectin have similar percentages of focal adhesions that occurred both on stress fibers and fabricated protein lines. Note that the values do not sum to 100% due to the adhesion sites neither on Stress Fibers nor lines. The reader may notice that values do not reach a maximum at 100% This is due to the fact that the unplotted values are adhesion sites neither on Stress Fibers nor lines, which may mean that the adhesion sites are Nascent adhesion molecules (i.e., in the process of making FAs).

Note that Collagen I, Fibronectin and the BSA monolayer have similar focal adhesion frequency on Stress Fibers. This is not true for the focal adhesion frequency on BSA lines. The lower frequency may speak to the topographic cues. It is worth noting that BSA optically crosslinks much more readily than the other proteins. The height of these BSA lines approach 5 microns, as opposed to the 1 micron height of FN and

Collagen 1. The fact that BSA lines facilitated any adhesion at all is not unexpected. We have previously reported a directional response to fibroblasts on BSA lines as a response to micro-environmental topography [80].

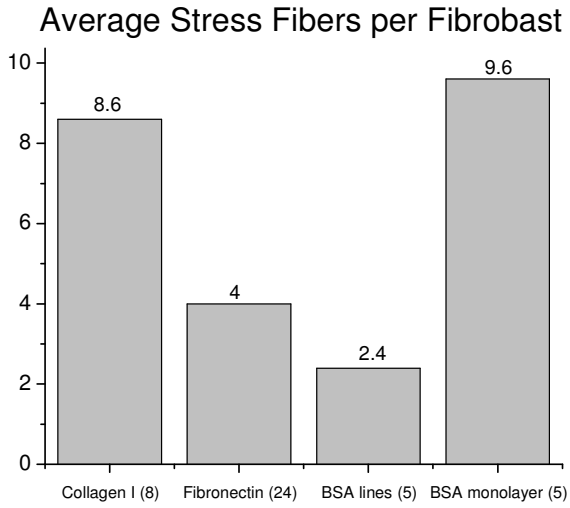

Figure 3, "Average Stress Fibers per Cell"The higher values of stress fibers seen in Collagen and BSA Monolayer generally include fibers of smaller length perhaps reflecting a "sensing" function. Though Collagen I and Fibronectin both have RGD sequences, Fibroblasts on Collagen I lines (as well as BSA Monolayer) have more than twice as many Stress Fibers per cell than cells on Fibronectin lines. Note Figure 3 does not take SF direction into account.

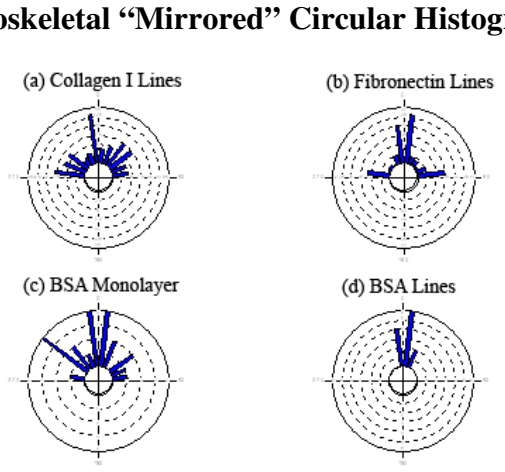

Figure 4: Circular Histograms of stress fibers direction for cells on CI, FN, BSA 10 µm lines and BSA monolayer are provided for visualization purposes. The zero degree position is at "twelve o'clock" on these Combined, opposing bins are shown "reflecting" stress fibers from quadrants II and III to bins in quadrants I and IV. This allows histogram bins to all exist above the horizontal.

4.3.3 Elongation and orientation

Seemingly unexpectedly, cells on BSA lines are visually more elongated than those adhered to the ECM proteins (Figure 5 a). However inspection of the images shows that the cells are more trapped between the BSA lines than associated with them. This is also borne out by the orientation data in Figure 5 b, where this parameter is defined by the angle of the long axis of the ellipse to the protein fiber axis. Here cells on the ECM protein lines show similar orientations to each other though different compared with BSA (~40˚ vs ~10˚ using Kruskal-Wallis One Way Analysis with Dunn's test for Rank ($P>0.05$), where the cells on BSA are more aligned in between the fibers. As we have shown previously for FN [80], cells on Collagens I and II have less apparent orientation with respect to a given protein line as they attempt to maximize their interactions with other adjacent lines. These results explicitly show the effects of pure contact guidance alone provided by the BSA fibers in comparison to the combined contact guidance and ECM cues provided by the FN, and collagen fibers, which is representative of the cell interactions on the native ECM. Given the similarity in molecular structure, it is expected that the spreading response on Collagen 1 and Collagen II would be similar. Having shown this, in the current chapter limits our analysis to Collagen I in addition to FN and BSA fibers.

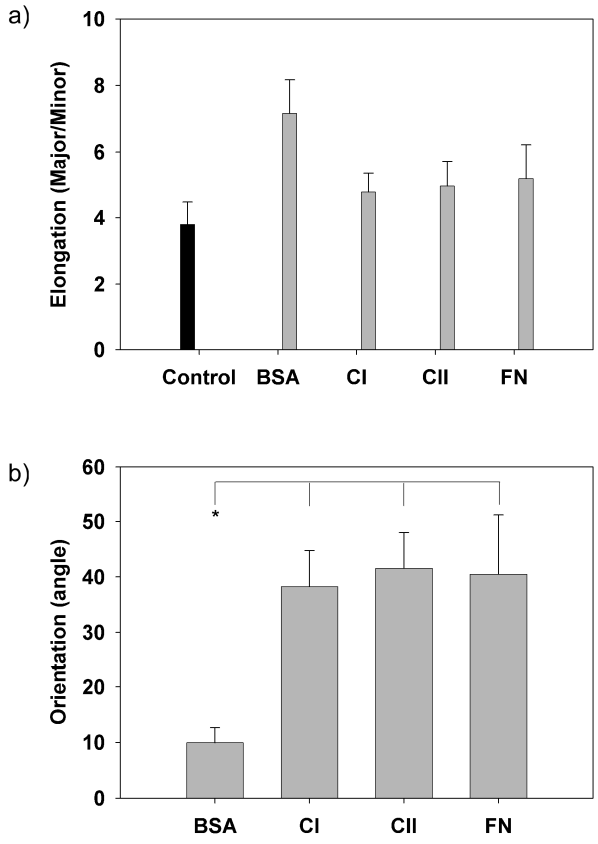

Figure 5: Elongation and orientation using a fitted ellipse with Major/Minor axes

Fibroblasts were grown on 10 micron lines of BSA, Collagen I (CI), Collagen II (CII) and Fibronectin (FN). The trends in Figure 6 above support the same trends for BSA and FN in Chapter 3 (Pins, et al., 2006, Figures 2 and 6). Fibroblast orientation on BSA lines is significantly different from Collagens I & II as Fibronectin, showing topographical guidance within 10˚. The work in Chapter 3 did not involve Collagen for these comparisons.

Specifically in common with the Chapter 3 figures we observe that Elongation (Ratio of fitted Major/Minor axis) of fibroblasts on FN is less than that of fibroblasts on BSA lines. In addition, we observe both in Chapter 3 and this chapter that the Orientation angle for Fibroblasts on BSA is lower than those on RGD-containing FN lines.

The similar responses of CI, CII and FN in Figure 6 may illustrate that more robust statistical methods may be required to observe effects of Fibroblasts on biomimetic extracellular matrices when comparing both with and without RGD-containing proteins.

Table 2: Summary Results of Stress Fiber Magnitude Statistics and Angular Statistics (refer to Table 3)

- Based on Rao's spacing test, these Proteins, in general terms, are significantly associated with stress fiber orientation at the $\alpha = 0.05$ level.
- Based on Kuiper's Test, unattached fibroblasts on Collagen I ($0.15 > p > 0.01$) and both unattached (single) ($p < 0.01$) and attached fibroblasts on FN ($p < 0.01$) are significantly associated with stress fiber orientation.
- Based on Kuiper's Test unattached (single) fibroblasts on "BSA" structures ($p > 0.15$) are not are significantly associated with stress fiber orientation.
- Based on the Mardia-Watson-Wheeler Test Stress Fiber Angular distribution of fibroblasts cultured on Collagen I lines was found to have a highly significant difference between stress fiber angles of fibroblasts cultured on BSA Lines ($p = 1.83E-04$).
- Mardia-Watson-Wheeler Test has its null hypothesis of identical distributions. Highly significant (* or **) and significant pairwise combinations are summarized below with protein / stress fiber length and significance.

Protein / SF Length	:	Protein / SF Length	significance
▪ BSA Lines / 0µm-max	:	Col I 0 - 25 µm	p = 0.027
▪ BSA Lines / >25 µm	:	Col I / >50 µm	p = 6.49E-05*
▪ BSA Lines / 0µm-max	:	Col I / 0 µm -max	p = 1.83 E-04*
▪ BSA Lines / >25 µm	:	Col I / 0 µm -max	p = 2.96 E-04*
▪ BSA mono/ 0µm-max	:	BSA Lines / 0µm-max	p = 0.01
▪ BSA mono / 0 – 25 µm	:	BSA Lines / 0µm-max	p = 0.022
▪ BSA mono/ 0µm-max	:	BSA Lines / >25 µm	p = 0.011
▪ BSA mono / 0 – 25 µm	:	BSA Lines / >25 µm	p = 0.04
▪ Col I / >25 µm	:	BSA Lines / 0µm-max	p = 6.2 E-05*
▪ Col I 0 - 25 µm	:	BSA Lines / >25 µm	p = 0.032
▪ Col I / >25 µm	:	FN / >25 µm	p = 0.034
▪ FN / 0µm-max	:	Col I / >25 µm	p = 0.034
▪ Col I / >25 µm	:	BSA mono/ >25 µm	p = 9.28E-05**

- Mardia-Watson-Wheeler Test shows <u>no</u> significant difference with stress fiber lengths on Fibronectin lines for SF length data binned into two groups, >25 µm and >50 µm .

Protein / SF Length	:	Protein / SF Length	~ significance
▪ FN / >25 µm	:	FN / >50 µm	p = .988

4.3.4 STRESS FIBER MAGNITUDE STATISTICS AND ANGULAR STATISTICS RESULTS AND DISCUSSION

In the Circular Histograms (Figure 5) above, we observe Stress Fibers in the Collagen I histogram (Figure 5 a) illustrate the strong tendency for some stress fibers to form and persist along the Collagen lines where the other stress fibers are fairly uniformly dispersed. (b) Stress Fibers angles Fibroblasts growing on Fibronectin lines, show a strong tendency to form parallel and perpendicular to the protein lines (i.e., align either along or reaching towards next fiber). (c) As expected, fibroblasts on a BSA monolayer have neither chemical nor topographical cueing and thus have more random orientation of stress fibers. (d) The majority of Stress Fibers for Fibroblasts grown on BSA Lines stay in between two parallel BSA lines.

For the angular distribution analysis, Rao's spacing test rejects the null hypothesis of uniformity for all three Protein Types (Collagen I, FN, BSA lines) at the 5% level. Using the pairwise Mardia-Watson-Wheeler Test, we examined angular distributions of stress fibers in fibroblasts grown on lines of Collagen 1, Fibronectin, BSA and the BSA Monolayer. Stress fiber length data was sorted into three bins for each protein: combined angular data for all stress fiber lengths; the subset of fiber lengths from 0 – 25 μm, and the subsets of fiber lengths >50 μm and 0-max μm.

The Mardia-Watson-Wheeler Test (Fisher [81], Batschelet [82], Zar [83]), also referred to as the Uniform Scores Test, is a non-parametric test for determining whether two or more distributions are identical. The test is based on samples being pooled together, sorted into a data set by increasing angles, and then evenly distributed around the circle by calculating a circular rank. If distributions are identical then the new circular rank for the samples should be evenly interspersed around the circle. Their resultant

vector lengths R should be short and similar. Any significant difference (i.e., at the 5% level) between the resultant vectors will lead to a large W test statistic and rejection of the null hypothesis of pairwise identical distributions.

Mardia-Watson-Wheeler (M-W-W) Test shows that the stress fiber distributions on Collagen I (all fiber lengths) are significantly different than the distribution of stress fibers of cells on BSA Lines (see * in the summary results of Table 3, above). This may suggest contact guidance only for cells on BSA Lines but yet a combination of contact guidance and chemical signaling (RGD) with cells on Collagen I Lines. The M-W-W Test also indicates that stress fibers on Collagen I of all length categories have *highly*, significantly different ($p < 1x10^{-4}$) orientations compared to stress fibers on BSA lines of all length categories (see ** in the summary results of Table 3, above).

The distributions of fibroblasts' individual stress fibers of all observed lengths on fibronectin and collagen both have distributions that are *not* significantly different than those on BSA monolayers ($p = 0.206$; $p = 0.222$, respectively). This supports the notion that stress fibers are outwardly migrating and are not encumbered by fibronectin or collagen lines as topographic barriers to migration. This supports previous overall orientation findings based on fibroblasts' fitted ellipse major axis direction in this chapter for Collagen I and Fibronectin as well as in Chapter 3 [80] which studied fibroblast orientation on fabricated lines of Collagens I and II.

Too few stress fibers for cells grown on with FN lines were observed that were less than 25 µm to analyze short fiber orientation. Fibers of all observable lengths growing on FN showed different orientations than fibers with lengths greater than 25 µm which are on Collagen I ($p=0.034$). Interestingly, we observed that the stress fiber

distribution on BSA Monolayer differed significantly from stress fibers on BSA Lines ($p = .01$).

The control BSA monolayer has neither topographic nor chemical signals. These results explicitly underscore the effects of pure contact guidance alone provided by the BSA fibers in comparison to the combined contact guidance and ECM cues provided by the FN, and collagen structures. These results imply that the ECM-integrin binding provides sufficient force (or signal) to migrate over these fabricated RGD-containing protein structures similar size. These also support the premise that RGD-containing proteins can model and remodel stress fibers that are stiff enough to facilitate migration along these topographical barriers.

We also investigated stress fiber distribution response comparing single fibroblasts versus fibroblasts that were attached to other fibroblasts. The Kuiper's Test was used which has a null hypothesis that the data fits the uniform test distribution (testing for cyclic variations). Kuiper's test rejects the null hypothesis of uniformity between distributions for unattached (single) fibroblasts on both unattached (single) on FN ($p < 0.01$) and attached fibroblasts on FN ($p < 0.01$), but *not* for unattached (single) fibroblasts on "BSA" structures ($p > 0.15$) and *not* for Single cells on Collagen I ($0.15 > p > 0.10$). Unattached fibroblasts on BSA lines and Collagen I lines have a more uniform distribution. Attached and Single fibroblasts on fibronectin lines do not have uniform stress fiber distributions. Thus, direction of stress fibers is significantly influenced by FN lines' microenvironment, whether or not the fibroblasts are attached or single. This is in contrast to conclusions involving MDCK cells [3], though that study investigated topographic cueing, not combined topographic and chemical signaling structures.

4.3.5 FIBROBLAST MORPHOLOGY RESULTS AND DISCUSSION

To interpret the results of our measurements taken of fibroblast morphology on fabricated ECM structures we performed statistical analyses (mostly Generalized Linear Models, or GLMs) which are broadly broken down into three areas. The first analysis seeks to relate the likelihood of four types of Focal Adhesion to cells measure at two different facilities (Cell Type), fabricated Protein Type and the interaction of Cell Type and Protein Type. The second analysis seeks to relate the orientation of Stress Fibers to fabricated protein lines. The third analysis seeks to relate geometrical quantities of cells such as Area, Perimeter, and Isoperimetric Quotient (defined as Area/Square of Perimeter) to Center, Cell Type and Protein Type.

The first analysis seeks to relate four types of Focal Adhesion, namely those occurring on Protein Lines Only, Stress Fiber Only, Both Lines and Stress fibers, and Neither Lines and Stress fibers or Nascent to Cell Type (Attached to other fibroblasts or Single), Protein Type (FN, BSA or Collagen) and their interaction. Three GLMs had been formulated. The first GLM had Cell Type, Protein Type and their interaction as independent variables, the second GLM excluded the interaction, while the third only had Protein Type as an independent variable.

In each of the three GLMs, the overall model was found to be significant, as indicated by the small p-values in the "Testing Global Null Hypothesis: BETA=0" section of the SAS output. Next, looking at the "Type 3 Effects" section in the SAS outputs, Protein Type was found to be significant in each of the three GLMs; furthermore the first GLM indicates that the Cell-Protein interaction is also marginally significant at the 5% level. Finally, the interpretation and the implications of the estimates and

confidence intervals for Odds Ratios from the SAS output showed across models in the Protein Type that by going from FN to Collagen Lines there are decreased odds of Focal Adhesion occurrence. The goal was to relate cell morphology to the cell's microenvironment, which was characterized by three independent variables – Center, Cell Type and Protein Type.

The next analysis concerned the angular distribution of Stress Fibers with respect to different Protein Type lines. Concretely, the goals of this analysis were to see if there is a preference in any direction, as well as to see if the preferences changed for different Protein Types.

4.3.6 Results of Focal Adhesion Analysis (Logistic Procedure and Generalized Linear Models)

Three models were developed using a Logistic Procedure. Logits modeled use the response variable describing the count of focal adhesions that occurred on stress fibers as the reference category. The first model analyzed the effects of cell type (attached versus single cells), protein type and the combination of these two. There was no difference in focal adhesion ratio between attached cells and single cells (Wald Chi-square = 4.5582, p = 0.2072). The proteins' data were significantly different (Wald Chi-square = 18.0140, p=0.0004). The combined analysis of cell type and protein interactions were marginally significant (Wald Chi-square = 1.8117, p = 0.0501). The implication of these findings illustrates that not only are there differences in focal adhesion response between proteins, but there is also an interaction within the cell type and protein type. Specifically, Single Cell –FN focal adhesion distribution differs from single cell – BSA lines which differs from Single Cell – Collagen I combinations. This may be due to intercellular interaction. However, the main point is that the protein type is the driving factor in the focal adhesion formation. A Maximum Likelihood estimate was performed in the first model. The likelihood of forming focal adhesions on both stress fibers and lines, lines only, or Nascent adhesion sites (focal adhesion sites on neither lines nor stress fibers) were not significant (P = 0.1617, p = 0.7041, 0.1323, respectively) compared with Cell Type (attached versus single cells). However, there is a highly significant difference in the likelihood of forming focal adhesions on protein lines (collagen I versus fibronectin, p = 0.0023). We arrive at the same FN-Collagen difference using Profile Likelihood

Confidence Interval for Parameters on a logit scale and a Wald Confidence Interval (both at the alpha = 0.05 level).

The second model excluded the interaction between protein type and cell type. This reduced the noise in the model as previously mentioned. Using a Wald Chi-square, CellType shows no significant difference in focal adhesion formation (P = 0.2997). We observed a weak interaction with Cell Type. We learn more about this weak interaction by performing an Analysis of Maximum Likelihood Estimates similar to the first model. We find a there is marginally difference (at the P = 0.0851) between the formation of Nascent focal adhesions between attached cells and single cells. The second model confirms the significant difference between the likelihood of focal formation on lines of FN versus Collagen I (P = 0.0031). For robustness we performed the Profile Confidence Likelihood Interval for Adjusted Odds Ratios and Wald's Confidence Interval and they all provided the same conclusions (at the alpha = 0.05 level, estimated odds ratio = 0.295). The odds are reduced by a factor of 29.5% that a focal adhesion would form on a Collagen I line as compared with a FN line.

The third model only evaluated protein type with the same results for protein type / structure combination. Collagen I and Fibronectin are statistically different (Maximum Likelihood estimate, p = 0.0032; Odds Ratio Estimates, alpha = 0.05 level; Adjusted Odds Ratios and Wald's Confidence Interval and they all provided the same conclusions (at the alpha = 0.05 level, estimated odds ratio = 0.296).

Table 3: Summary Results of Logistical Model Procedures (Focal Adhesion Results)

- Generally, Fibroblasts' Focal Adhesion distribution on Protein structures differ significantly (p=0.0004 at the $\alpha = 0.05$ level).
- Generally, Fibroblasts' Focal Adhesion distribution considering Protein structures interaction with Cell Type differ significantly (p=0.0501 at the $\alpha = 0.05$ level).
- Cell Type (Attached/single) is NOT significantly associated with Focal Adhesion (p=0.2072 at the $\alpha = 0.05$ level).
- Fibroblasts' Focal Adhesion Likelihood of frequency count on Collagen I Lines is very significant (p=0.0023 at the $\alpha = 0.05$ level).
- Cell Type (Attached/single) is NOT significantly associated with Focal Adhesion (p=0.2997 at the $\alpha = 0.05$ level).
- Protein (Collagen I) is significantly associated with Focal Adhesion (p=0.0031 at the $\alpha = 0.05$ level).
- Fibroblasts' Focal Adhesion Likelihood of frequency count on Collagen I Lines is significant (at the $\alpha = 0.05$ level).
- The odds are reduced by a factor of 29.5% that a focal adhesion would form on a Collagen I line as compared with a FN line.

4.3.7 Morphometric Response Studies

We looked at the responses between independent variables, “Cell Types” (attached, single, and attached/single data, combined) and “Proteins” (Collagen, Fibronectin and BSA) against the dependent variables logArea and Perimeter. The logarithm of Area data was taken to provide a more homoscedastic area variance.

The Area and Perimeter measurements were made for fibroblasts on Collagen I lines, Fibronectin lines, BSA lines and a BSA monolayer using Metamorph ™ imaging analysis software from Molecular Devices. We measured Area and Perimeter for cells on BSA lines and on BSA monolayer as controls.

To assure repeatability between those who took measurements, we statistically examined the Area and Perimeter data by initially grouping them into “Center” or “Measurer,” “CellType” and “Protein”. “Center” (Measurer” describes which of the two individuals made the measurement which happen to be at different facilities. “Cell Type” includes

cells that are either “Attached” to other cells (implying both cell-cell and cell-matrix interaction) or “Single”, individual cells (cell-matrix interactions).

For the morphology analysis, the different responses such as log(Area), Perimeter, Area/Perimeter^2 were considered as proxies for the cell morphology. This was done to assess which proxy response best correlated to the independent variables. Linear regression models were constructed for each proxy response.

The strategy to evaluate the responses Area (including logAREA), Perimeter, and Area / Perimeter squared (isoperimetric quotient) involves the following tasks: testing the overall model for significance using ANOVA / finding R2 ; evaluating individual predictors; using Tukey’s Studentized Range (HSD) to evaluate any pairwise significance of independent variables (comparing Cell Area on Collagen 1 versus FN for example); and finally, using the Kruskal-Wallis Test which is an alternative to ANOVA in assuring model robustness.

3.7.1 Morphometry Results

In Figure 2, we see Morphometry Results for Fibroblasts are grown on Collagen Type I lines, Fibrinogen lines, BSA lines (as a negative control for biochemical sensing), spaced 10 microns apart. In addition, cells were grown on adsorbed BSA monolayer (as a negative control for topography). Sets of data designed to include three subgroups: areas or perimeters of fibroblasts that are growing on structures both alone and attached to another fibroblast (Left Column); attached to another fibroblast (Center Column); and fibroblasts that are unattached to other cells (Right Column).

The top figure, Fibroblast Area, shows fibroblast areas with respect to cell-cell contact versus no intercellular cell contact, little or no significant difference is found in

the areas for both Collagen and Fibronectin cell groups (i.e., attached versus single areas for each scaffold protein). BSA data only reflects single cell areas due to the fact that no fibroblasts were found in contact with other fibroblasts when grown on BSA monolayer or BSA lines. Areas of fibroblasts grown on Collagen I lines are greater than areas of cells grown on lines of Fibronectin and BSA and a BSA Monolayer. Our statistical analysis determined that each of the Area responses are significantly different from each other. The middle figure, Fibroblast Perimeter , indicates perimeter results for fibroblasts grown on Collagen I seem greater than cell perimeters on Fibronectin, BSA lines and BSA Monolayer. The perimeters of cells on BSA lines and BSA Monolayers appear the same. Our statistical analysis determined that the Perimeters of Fibronectin, BSA and the BSA Monolayer are not different from each other. However, the Perimeter response of cells on Collagen I is significantly different from the Perimeters of each of the other three microenvironments. The bottom figure, Area / Perimeter2 (Isoperimetric Quotient) chart shows very similar fibroblast surface area to perimeter ratios when comparing cells grown on Collagen I and Fibronectin. However, there appears to be a much greater ratio looking at response of cells on the BSA monolayer. This could imply simply variation by itself, or it might imply the lack of focal adhesions result in less control of the cell membrane. Perhaps this speaks to cell migration as a balance between circumferential stress of cell membrane and focal adhesion frequency in the extracellular membrane.

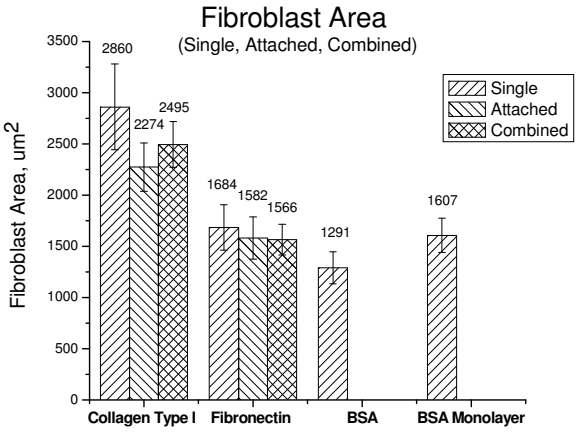

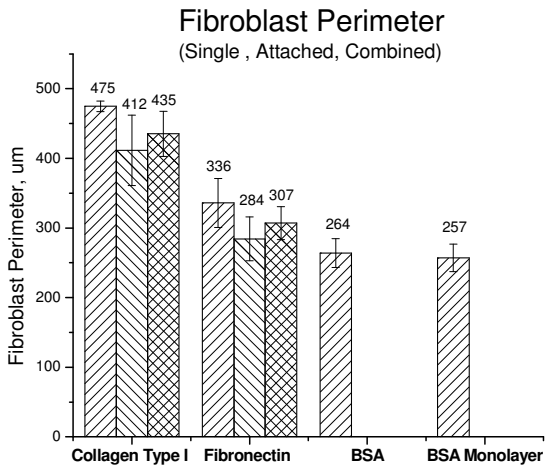

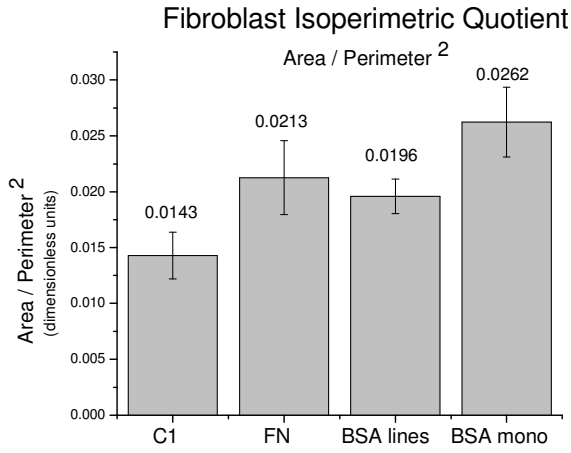

Figure 6, Fibroblast Area, Perimeter and Area / Perimeter^2

4.3.7.1.1 Area / logArea

Using a generalized linear model, we performed a regression on logArea and found a source of variance (ANOVA, $R^2 = 0.183786$). To better understand the variance, the three grouping variables were evaluated further. It was found that the grouping variables Protein ($p = 0.0283$ at the $\alpha = 0.05$ level) and Center, i.e., Measurer, ($p = 0.0349$ at the $\alpha = 0.05$ level) were significant contributors of the variability observed in the collected data. As we are investigating the differences in "Protein", we adjusted the variance between "Measurers." The error was shown to be normally distributed. The significance of any possible differences in the resulting logAreas was evaluated between Cells that were Attached or not Attached (Single). There is no significant difference in logArea when comparing cells that are attached to another cell or if the un-attached (single) cells ($p=0.2669$ at the $\alpha = 0.05$ level).

Using the Tukey's Studentized Range (HSD) Test, we evaluated logArea to localize which level of the grouping variable was actually responsible for the significance of the test having adjusted for the reproducibility between measurers. Having compared all the pair-wise combinations of cells grown on Collagen I lines, Fibronectin lines, BSA lines, or BSA monolayer, we found that the logArea distributions of Collagen I lines and BSA lines differed significantly (at the $\alpha = 0.05$ level) after adjusting for multiplicity. Goodness of fit tests (Kolmogorov-Smirnov, Cramer-von Mises, Anderson-Darling) as well as a quantile-quantile plot all established that the error was normal for logArea. Similar assurances were made for distributions of Perimeter, Area and log ($Area/Perimeter^2$). The results ($p < 0.05$ at the $\alpha = 0.05$ level) for each Perimeter, Area

and log (Area/Perimeter^2) in each case suggests that Normality of the distributions is consistently demonstrated.

Evaluation of Area using the non-parametric Kruskall-Wallis Test showed there is a significant difference in the "Protein" category ($p = 0.0134$ at the $\alpha = 0.05$ level). This non-parametric analysis is used as an alternative analysis if the assumption of normality is not satisfied in the case of "Area", is an additional tool to ANOVA and substantiates the robustness of the model.

Based on the findings in the paragraph above, one would expect that Cells that have attached to Collagen 1 lines would have larger Areas than Cells that attached to BSA lines.

4.3.7.1.2 Perimeter

The linear model of "Perimeter" performed better at describing the variance (ANOVA) ($R^2 = 0.300755$). We found that the 'Center" or "Measurer" was marginally significant ($p=0.0549$ at the $\alpha = 0.05$ level). It was clearly established that the "Protein" groups' Perimeters were highly significantly different ($p < 0.0001$). This supports the other analyses of Protein differences. As with our logArea HSD, we used the Tukey's Studentized Range (HSD) Test to compare all the "Perimeter" pairwise combinations of cells grown on Collagen I lines, Fibronectin lines, BSA lines, or BSA monolayer.

We found that the "Perimeter" distributions of Collagen I and all other combinations differed significantly (at the $\alpha = 0.05$ level) after adjusting for multiplicity. Alternately stated, there is no significant difference in Perimeter between Fibronectin lines, BSA lines and BSA monolayer. Fibroblasts on the collagen structures are likely to

have a greater perimeters compared to fibroblasts on the other two protein structures and the BSA monolayer. These findings are consistent with observations made in Figure 2. When comparing the dependent variable "Perimeter" with independent variables "Cell Type" (attached versus single) and "Protein" (CI, FN or BSA), we find the response of fibroblast Perimeter from Protein structures to be highly significant (F Value = 10.97, p = 0.0002). The evaluation of perimeter from cell-cell contact versus non intracellular contact shows no significant effect (F Value = 2.09, p = 0.1578). In other words, there is no statistical difference in cell perimeter between touching cells or single cells on Fibronectin, Collagen I or BSA which is also consistent with observations made in Figure 2. We were not able to include Perimeters of cells on BSA Monolayer as all cells measured were unattached to other cells.

4.3.7.1.3 Area / Perimeter^2 (Isoperimetric Quotient)

An analysis was performed on the Ratio of Area to Square of the Perimeter ("RatioAPSquared"), so as to investigate this dimensionless relation between area and perimeter (L^2 / L^2). The motivation for this is to assure that the ratios have the numerator and denominator scale properly. An Analysis of Variance was performed for "RatioAPSquared" which was classified by the variable "Protein" (again, Collagen I lines, Fibronectin lines, BSA lines, and BSA monolayer). Note that the mathematical Isoperimetric Quotient is the ratio of the curve area to the area of a circle with same perimeter as the curve. Our biometric, though, being the ratio of area to perimeter-squared, lacks a geometric factor of 4π. For simplicity, we still refer to it as Isoperimetric Quotient (Figure 3). A Kruskal-Wallis Test was performed and showed that there was a significant difference in the variable "RatioAPSquared" for the "Proteins" ($p < 0.0352$).

Therefore, further effort was needed to find out where the differences were. An Analysis of Variance of "RatioAPSquared" gave us a better explanation of what process is involved in the relation between "Proteins" and the ratio of Area / Perimeter^2 (R^2= 0.60). Using the linear model for "RatioAPSquared," it was shown that Cell Type (cell-cell attachment or single) did not have any significant difference. However, "Measurer" and "Protein" were both significant (both $p < 0.0001$). In addition, the "RatioAPSquared" Tukey test showed BSA and Collagen I had significant difference (Alpha = 0.05). The log RatioAPSquared testing demonstrated the same outcome, though the R^2= 0.40 leads us to think the "RatioAPSquared" metric is better for statistical evaluation.

Using the Tukey's Studentized Range (HSD) Test, we evaluated "RatioAPSquared". As with our previous HSD, we compared all the "RatioAPSquared" combinations of cells grown on Collagen I lines, Fibronectin lines, BSA lines, or BSA monolayer. We found that the "RatioAPSquared" (Area / Perimeter^2) distributions of Collagen I lines and BSA lines differed significantly (at $\alpha = 0.05$).

Summary Results of Generalized Linear Models (Morphometry Results)

- The logArea; Perimeter; Area / (Perimeter)^2, and log Area / (Perimeter)^2 Models are statistically robust.
- Overall, Areas of Attached Fibroblasts vs Single Fibroblasts are not significantly different from each other ($p=0.2669$ @ $\alpha = 0.05$).
- Fibroblasts' logArea has significant difference between facilities where measurements were taken (UCHC and WPI; Note WPI only measure BSA and BSA-NL; $p=0.0349$ at the $\alpha = 0.05$ level). Their logAreas are significantly different between Proteins ($p=0.0283$ at the $\alpha = 0.05$ level).
- Fibroblasts on Collagen I & BSA have significantly different logAreas at the $\alpha = 0.05$ level. Fibroblasts on Coll I will have larger areas compared fibroblasts on BSA lines. All other combinations are not significantly different for logArea.
- Fibroblasts' Perimeters have marginally significant differences between the facilities where they were measured ($p=0.0549$ @ $\alpha = 0.05$) Note: WPI only measure BSA and BSA-NL.
- Cell Perimeter has a no significant difference between fibroblasts that are Attached to another fibroblast versus Single cells ($p=0.1291$ @ $\alpha = 0.05$).
- Overall, Perimeters have a significant difference comparing cells grown on BSA lines, CI, FN, and BSA monolayer ($p<0.0001$ @ $\alpha = 0.05$).
- Fibroblasts on Collagen I versus BSA lines have significantly different Perimeters at the $\alpha = 0.05$ level.
- Fibroblasts on Collagen I & BSA monolayer have significantly different Perimeters at the $\alpha = 0.05$ level.
- Fibroblasts on Collagen I & FN have significantly different Fibroblast Perimeters at the $\alpha = 0.05$ level.
    - Fibroblasts' Perimeters on *non-Collagen I, pairwise combinations* are not significantly different. In other words, fibroblasts' perimeters are statistically different when associated with Collagen I.
- Fibroblasts' Perimeters are significantly different in the "Protein" category considering Center UCHC-FN; UCHC-CI; UCHC-BSA; WPI-BSA; WPI BSA monolayer ($p=0.0010$ @ $\alpha = 0.05$).
- Fibroblasts' Areas are significantly different in the "Protein" category considering Center (GroupProtein) UCHC-FN; UCHC-CI; UCHC-BSA; WPI-BSA; WPI BSA monolayer ($p=0.0070$ @ $\alpha = 0.05$).
- Fibroblasts' Area / (Perimeter)^2 , or Isoperimetric Quotients, are significantly different in the "Protein" category considering Center (GroupProtein) UCHC-FN; UCHC-CI; UCHC-BSA; WPI-BSA; WPI BSA monolayer ($p=0.0005$ @ $\alpha = 0.05$).
- Fibroblasts' Areas, Perimeters and Area / (Perimeter)^2 are all significantly different in the "Protein" category . Further investigation revealed that, more specifically, Fibroblasts on Collagen I & BSA lines have significantly different log Area / (Perimeter)^2 and Area / (Perimeter)^2 at the $\alpha = 0.05$ level.

4.4 Discussion

Multiphoton excitation fabrication is important in studying cell response to ECM as it can control topography as well as retaining ECM protein signaling bioactivity after crosslinking. In this study, we utilized cross-linked structures of BSA, FN and Collagen I to assess differences in how these proteins control cell morphology. We found that both topography and ECM protein chemistry play significant roles in extracellular signaling and remodeling by fibroblasts.

We looked at how the cytoskeleton interacts with cross-linked structures to understand the effect the biomimetic ECM has on fibroblast focal adhesion formation, we counted focal adhesions on a per cell basis and categorized according to attachment location. A focal adhesion would be formed on a fabricated protein line, on a stress fiber, simultaneously on a fabricated protein line stress fiber, or on none of the above.
The odds are reduced by a factor of 29.5% that a focal adhesion would form on a Collagen I line as compared with a FN line. Fibers of all observable lengths growing on FN showed different orientations than fibers (with lengths greater than 25 μm) which are associated with Collagen I ($p=0.034$). Stress fiber distributions on Collagen I (all fiber lengths) are significantly different than the distribution of stress fibers of cells on BSA Lines, suggesting contact guidance is the only mechanism only for cells on BSA Lines but a combination of contact guidance and chemical signaling (RGD) with cells on Collagen I Lines. In addition, stress fibers on Collagen I of all length categories have highly, significantly different ($p < 1x10^{-4}$) orientations compared to stress fibers on BSA lines of all length categories perhaps suggesting a fiber stiffness or stronger focal adhesion mechanism involving collagen molecule bonding.

The distributions of fibroblasts' individual stress fibers of all observed lengths on fibronectin and collagen both have distributions that are not significantly different than those on BSA monolayers ($p = 0.206$; $p = 0.222$, respectively). This supports the notion that stress fibers are outwardly migrating and are not encumbered by fibronectin or collagen lines as topographic barriers to migration. This also supports previous overall orientation findings based on fibroblasts' fitted ellipse major axis direction in this chapter for Collagen I and Fibronectin as well as in Chapter 3 (Pins 2006) which studied fibroblast orientation on fabricated lines of Collagens I and II.

Likelihood Focal adhesions' occurrence for given fabricated microenvironments were measured. Stress fiber magnitude and direction were measured with respect to these fabricated microenvironments. For the morphology analysis, a few different responses were considered as proxies for the fibroblast morphology on these microenvironments: log(Area), Perimeter, Isoperimetric Quotient (defined as Area/Perimeter^2) and log(Isoperimetric Quotient). This was done to assess which proxy response best correlated to the independent variables. Linear regression models were constructed for each proxy response.

Based on the morphometric results, one would expect that Cells that have attached to Collagen 1 lines would have larger Areas than Cells that attached to BSA lines. There is no significant difference in Perimeter between Fibronectin lines, BSA lines and BSA monolayer. Fibroblasts on the collagen structures are likely to have a greater perimeters compared to fibroblasts on the other two protein structures and the BSA monolayer (HSD at the $\alpha = 0.05$ level). "Perimeter" distributions of Collagen I and all other combinations differed significantly (at the $\alpha = 0.05$ level) after adjusting for

multiplicity. Alternately stated, there is no significant difference in Perimeter between Fibronectin lines, BSA lines and BSA monolayer. Fibroblasts on the collagen structures are likely to have a greater perimeters compared to fibroblasts on the other two protein structures and the BSA monolayer. We found that the proxy "RatioAPSquared" (Area / Perimeter^2) had distributions of Collagen I lines and BSA lines that differed significantly (at $\alpha = 0.05$). Overall, neither Areas nor Perimeters are significantly different comparing Attached Fibroblasts vs Single Fibroblasts ($p=0.2669$ @ $\alpha = 0.05$; $p=0.1291$ @ $\alpha = 0.05$, respectively). Cell Perimeter has no significant difference between fibroblasts that are Attached to another fibroblast versus Single cells at the $\alpha = 0.05$ level. Fibroblasts' Perimeters on non-Collagen I, pairwise combinations are not significantly different. In other words, fibroblasts' perimeters on Collagen I structures are statistically different when associated with the other proteins. Fibroblasts on Collagen I & BSA lines have significantly different log Area / (Perimeter)^2 and Area / (Perimeter)^2 at the $\alpha = 0.05$ level.

Interestingly, we observed that the stress fiber distribution on BSA Monolayer differed significantly from stress fibers on BSA Lines ($p = .01$). The control BSA monolayer has neither topographic nor chemical signals. These results explicitly underscore the effects of pure contact guidance alone provided by the BSA fibers in comparison to the combined contact guidance and ECM cues provided by the FN, and collagen structures. These results imply that the ECM-integrin binding provides sufficient force (or signal) to migrate over these fabricated RGD-containing protein structures similar size. These also support the premise that RGD-containing proteins can

model and remodel stress fibers that are stiff enough to facilitate migration along these topographical barriers.

These results point to differing roles of integrin signaling between collagen and FN as evidenced by very different response between ECM and integrins. The stronger interactions involving fibroblast response to collagen is consistent with other adhesion data [84, 85]. This is not true for the focal adhesion frequency on BSA lines. The lower frequency may speak to the topographic cues. The fact that BSA lines facilitated few adhesion is not unexpected, but it is adhesive not repulsive such as found previously [7]. Willingham found that when a transformed cell line with poor adhesiveness was treated with a major surface glycoprotein of normal cells which increases adhesiveness to substratum, the cells formed extensive microfilament bundles without any decrease in growth. Willingham concludes that the distribution of microfilament bundles is related to cell adhesiveness to the substratum and cell shape but not to growth properties. We have previously reported a directional response to fibroblasts on BSA lines as a response to micro-environmental topography (Pins 2006). Contact guidance is important for stress fibers.

Collagen evokes a more unique response. Fibroblasts on Collagen I versus BSA lines have significantly different Perimeters. Fibroblasts on Collagen I & BSA monolayer have significantly different Perimeters. Fibroblasts on Collagen I & FN have significantly different Fibroblast Perimeters. In other words, fibroblasts' perimeters are statistically different when associated with Collagen I. Stress fiber bundles on collagen may be stronger and/or stiffer to promote greater morphological response.

These observations underscore Linus Pauling's consideration of Collagen as "a very unusual protein" [86].

ACKNOWLEDGEMENTS

The authors wish to thank the Department of Obstetrics and Gynecology at UMMS (Worcester, MA) for providing us with neonatal foreskins and Kevin Cornwell and Donna Davidson as well as Ved Deshpande, Consulting Services and Doctoral Student, Department of Statistics, University of Connecticut for their technical assistance.

Chapter 5

Freeform multiphoton excited microfabrication
for biological applications using a rapid prototyping CAD-based approach

Freeform multiphoton excited microfabrication for biological applications using a rapid prototyping CAD-based approach

Lawrence P. Cunningham, Matthew P. Veilleux, and Paul J. Campagnola
Center for Cell Analysis and Modeling, Department of Cell Biology, University of Connecticut Health Center, Farmington, CT 06030

Keywords: Optical fabrication; Three-dimensional microscopy; Multiphoton processes; Microstructure fabrication; Laser induced chemistry.

I wish to acknowledge The Optics Society for their permission to reprint (adapt) for the following work (citation below) for this chapter.

Cunningham LP, Veilleux MP, Campagnola PJ., Freeform multiphoton excited microfabrication for biological applications using a rapid prototyping CAD-based approach. Optics Express, 2006 Sep 18;14(19):8613-21.

ABSTRACT

Multiphoton excited polymerization has attracted increasing attention as a powerful 3 dimensional nano/microfabrication tool. The nonlinear excitation confines the fabrication region to the focal volume allowing the potential to achieve freeform fabrication with submicron capabilities. We report the adaptation and use of a computer aided design (CAD) approach, based on rapid prototyping software, which exploits this potential for fabricating with protein and polymers in biologically compatible aqueous environments. 3D structures are drawn in the STL format creating a solid model that can be sliced, where the individual sections are then serially fabricated without overwriting previous layers. The method is shown for potential biological applications including microfluidics, cell entrapment, and tissue engineering.

Keywords: Cell Adhesion, Extracellular Matrix, ECM, Scaffolds, Microfabrication, Tissue Engineering, Integrin, Focal Adhesions, Stress Fibers, Fibroblast

5.1 Introduction

In the last several years, Multiphoton Excited (MPE) fabrication has emerged as a powerful 3D nano/microfabrication technique. The method is analogous to the more common multiphoton excited fluorescence imaging of live cells and tissues where optical sectioning is obtained by confinement of the excitation to the plane of focus. In terms of nano/microfabrication, MPE photochemistry can be used create 3-D objects one plane at a time, without overwriting previous layers. [1-9] Most of this work has centered on microfabrication with polymer resins, with the research being directed at 3-D storage and nanophotonics applications. [10-12]. However, there are also a wide range of potential applications in biology, where these include tissue engineering, cell sorting by microfluidics, and biosensing. MPE can play a unique role here since more traditional methods such as photolithography and microcontact printing do not have freeform capabilities in all 3 dimensions and have somewhat limited biocompatibility. Additionally, solid freeform fabrication cannot provide the submicron feature sizes necessary for current challenges in tissue engineering, nor does it possess the degree of biocompatibility that is achievable by MPE photochemistry in an aqueous environment. To take advantage of these possibilities, several biological applications using MPE polymerization have recently been demonstrated in the areas of cell biology [5] and biomaterials [13-14].

We have primarily directed the MPE fabrication technology towards tissue engineering applications and demonstrated that soluble and structural proteins could be crosslinked, layer by layer, into 3-D protein matrices. Through these efforts we have

shown that we could precisely and reproducibly control materials properties such as the crosslink density, and corresponding diffusion coefficients. [15] In addition, excellent biocompatibility was achieved in all cases to date [16-19] For example, we find high levels of specificity and spreading of cells adhered to MPE patterned surfaces, where the method allows for the systematic investigation of the 3-D topographic and biochemical aspects that are important in cell-matrix interactions. Since the MPE crosslinking process affords 3-D nano/microfabrication capabilities, this is an ideal method to create scaffolds directly from the native extracellular matrix (ECM) proteins since biomaterial surfaces can be modified by the addition of crosslinked bioactive species in virtually any desired topography with the appropriate biochemical signals. In this work, we take steps towards advancing the fabrication technology to achieve this goal. The main advantage in the MPE technique relative to other fabrication methods lies within its potential freeform capabilities and concurrent nano/microscale capabilities. A major challenge in the field has been implementing scanning methods to fully exploit this power. Many reports have used x-y-z stage scanning, as coupled with the appropriate control, allows user-defined fabrication in all 3 dimensions. However, this method is 2-3 orders of magnitude slower than laser-scanning through galvanometer mirrors. The latter is highly preferred for biological applications, where both the starting materials and resulting structure can readily suffer photodamage from prolonged exposure to the high peak powers required for efficient excitation. Additionally, we have previously shown that fabrication rate for proteins is 2-3 orders of magnitude slower than for polymers.[20] However since MPE fabrication is typically a threshold process, simply decreasing the pulse energy with longer pixel dwell times is not a tenable approach to this fabrication task. Thus repetitive

laser galvo scanning with freeform capabilities would be the ideal approach. While laser scanning with galvo mirrors provides great speed, these devices are not designed for complete random access to create user defined patterns. For example, the galvos and control software in laser scanning confocal microscopes are optimized for simple scanning patterns of lines and rectangles. To overcome this limitation, there have been several reports of approaches used to increase the flexibility of laser scanning for MPE fabrication. For example, we constructed an instrument that is capable of variety of geometrical patterns including polygons, ellipses, and circles, in both perimeter and solid patterns.[21] In an alternate approach, Braun [22] and coworkers use modulated raster scanning, where by controlling the power during the scan with an electro-optic modulator, much greater flexibility was obtained. Maruo [23] utilized a combination of stage and circular laser scanning to construct an impressive range of micromachines including gears and actuators. It is of great value for a range of biological applications to extend these ideas and utilize rapid galvo scanning to fabricate user-defined 3D objects directly from soluble proteins. In this article we describe our continuing efforts to achieve this goal, where we link rapid prototyping (RP) stereolithography software into our LabVIEW control code (described in Ref. 21). RP utilizes the STL file format, which creates a triangular mesh of the surface of a solid to be fabricated. This method has been widely used in a variety of industries (e.g. automotive, aerospace, and medical device industries) to create macroscale (mm-cm) physical objects directly from CAD data sources. In this process any desired structure or combination of structures of user-defined complexity and intricacy can be drawn and then rapidly fabricated. Here we adapt this 3D fabrication method to biological applications by crosslinking proteins from a freely

diffusing aqueous environment. The overall approach begins with 3D solid CAD drawing that is sliced into individual files, where these are fed to our laser scanning fabrication microscope. We show several examples of the method, including devices for cell sorting, cell encapsulation, and tissue engineering.

5.2 Experimental methods

5.2.1. Materials and methods

Octadecyltrichlorosilane (Gelest), anhydrous toluene (Aldrich), type I and type II collagen (Sigma), Bovine Serum Albumin (BSA), Rose Bengal (Sigma) were used as received. Water soluble ethoxylated trimethylolpropane triacrylate (TMPTA) was kindly provided by Sartomer.

5.2.2. Photochemistry

We have described the MPE photochemistry for crosslinking proteins and polymers in detail previously.[20] Briefly, we use two-photon excitation of Rose Bengal (1 mM) at 780 nm. Polymerization of the TMPTA requires a co-initiator, where 0.1M of TEA is used. Crosslinking proteins requires only the Rose Bengal photoactivator. BSA was used at a concentration of 10 mg/mL, or ~10-4M. Preparations were created on silanized microscope slides under cover slips that were separated from the slide using glass spacers, such that the enclosed volume was approximately 50 μL.

5.2.3 Fabrication instrument/microscope

The laser- scanning fabrication microscope has been described in detail [21] and is only briefly described here. The multi-photon excitation is achieved through a femtosecond near-infrared titanium-sapphire oscillator (Mira 900-F, Coherent) that is pumped by a 5 W Verdi Nd:YVO4 (Coherent). The laser is coupled to an upright

microscope (Zeiss Axioskop,) that is equipped with both bright field and fluorescence optics, which are used as online diagnostics of the fabrication process. Scanning is achieved by a combination of the laser galvo scanning mirrors as well as a programmable x-y-z motorized stage. Typical pulse energies at the sample were approximately 500 pJ/pulse. A 20X, 0.75 numerical aperture (NA) objective lens was used for the fabrication. The code for operating this instrument for both the scan control and simultaneous data acquisition was written entirely using LabVIEW 7 (National Instruments).

Two-photon fluorescence is used for imaging the fabricated structures, where the contrast arises from either residual Rose Bengal photoactivator or from staining with Rhodamine B or Di-4-ANEPPS. 3D stacks are acquired on an Olympus Fluoview modified for 2-photon imaging. Rendering of the stacks was performed with Imaris Bitplane. 2.4. CAD STL approach. Our overarching scheme to achieve flexible fabrication through laser scanning is to draw a solid 3D model and convert this into a format that is readable by the LabVIEW code that controls the scanning of the galvo mirrors. A flow chart is shown in Fig. 1, which shows the AutoCad (AutoDesk^{TM}) or Pro-E TM In the simplest version, AutoCad can export individual DXF files, which can be processed as described below. Alternatively, RP software can convert a 3D drawing to a solid STL rendering. This model is then sliced into individual DXF files using RP software, where we use Materialise Magics. The resulting slices are then hatched in AutoCAD, where the density of the fill pattern defines the crosslink density. After a hatched DXF file is created, an executable program written in LabVIEW transforms the raw coordinate data from the DXF file into a voltage array that is sent to the

galvanometers. The crosslink density of the structure can be controlled by defining the fill pattern in AutoCAD, where the choosing a tight fill pattern will directly correlate to denser polymerization or crosslinking. This parameter can then be spatially defined over the region of the scan to provide rapid, true 3D fabrication control. Alternatively, the slices can be singly or cross-hatched, depending on the desired structural considerations.

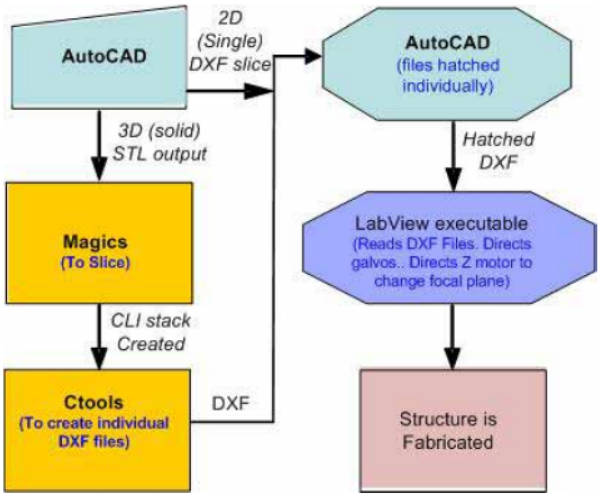

Fig. 1. Flow chart of the possible options to create 2 and 3 dimension structures using STL files and LabVIEW.

5.3 Results

Here we demonstrate our CAD-based MPE fabrication in a microscopic aqueous environment by presenting several examples of biological applications using the STL format to fabricate objects from proteins and polymers. As a demonstrative example, we fabricated a microflow "tunnel" from a water soluble triacrylate. Solid renderings of four of the 20 STL slices are shown in Fig. 2(b). The resulting structure has dimensions of 130 μm (l) by 100 μm (w) by 90 μm (h), with wall thickness 10 μm. Following MPE polymerization, the chamber was washed with water three times to remove un-reacted monomer as well as any entrapped Rose Bengal photoactivator. The structure was

stained with Rhodamine B and imaged by two-photon excited fluorescence (TPEF) at 830 nm. Figure 2 shows two views of the 3D rendered fluorescence image, where (b) and (c) show the two openings as well as the curved interior.

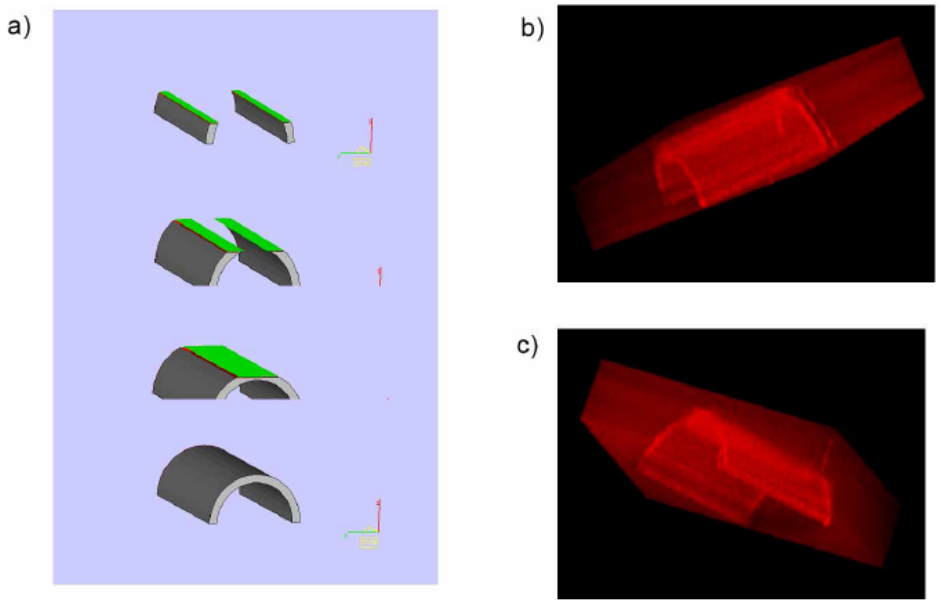

Fig. 2. MPE fabrication of a "tunnel". The four structures in (a) show representative solid renderings of the steps of the process of creating the 3D structure. The images in (b) and (c) are two different projections of the 3D rendering of the Rhodamine B labeled structure.

This type of structure is not possible to create by lithographic methods or by conventional geometric laser scanning. It should be possible to use this fabrication technology to create microflow devices for sorting cells. As a rudimentary example, we have placed L1210 lymphocytes inside a MPE fabricated tunnel (325 x 140 x 172 μm). The structure was washed as described above. The cells were stained with the membrane staining dye Di-4-ANNEPS and introduced into the tunnel by microinjection, such that the cells flowed in a gentle vortex into the tunnel. A 3D TPEF stack was obtained and a one optical section near the bottom of the tunnel, containing the cells is shown in the left panel of Fig. 3, where the arrows point to the cells (diameter ~10 microns). The right panel shows an optical section near the middle region of the structure and cells are seen

near the entrance. This type of structure could further be functionalized with cell attractive molecules such as fibronectin, collagen, or growth factors.

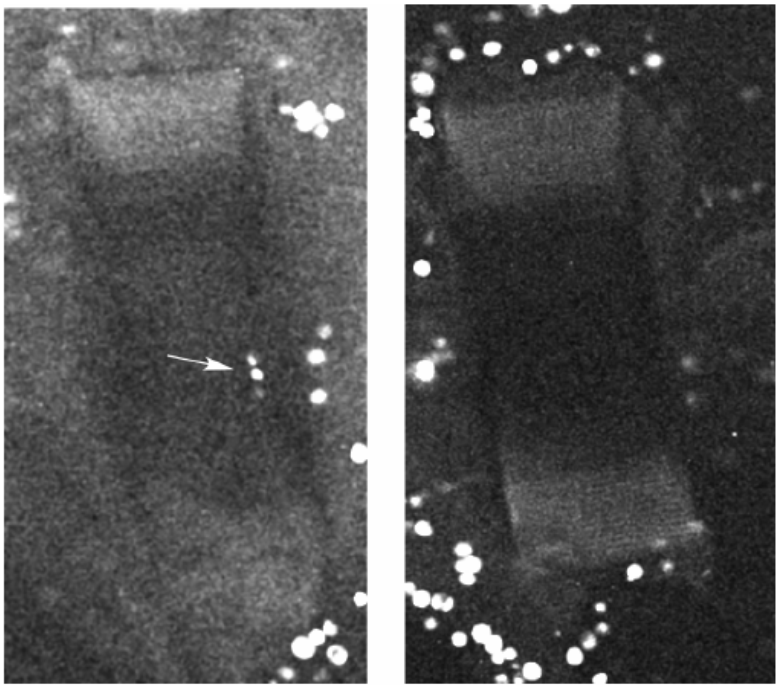

Fig. 3. TPEF optical sections of L1210 cells in the MPE fabricated microflow device, where (a) and (b) are near the bottom and top of the structure, respectively.

5.3.1. MPE crosslinked protein structures

While we demonstrated the CAD based control of the fabrication process with a water soluble acrylate, we ultimately wish to exploit the technology for biological applications where fabricated devices can be created from proteins. Here we show several simple examples to demonstrate the functionality of the approach. Figure 4(a) shows the 3D rendering of the TPEF image of a high aspect ratio cylinder fabricated from MPE crosslinked BSA, where the height is 60 µm, opening of 60 µm, and wall thickness of 1µm. This form of structure can be used to entrap cells to perform motility migration and studies.

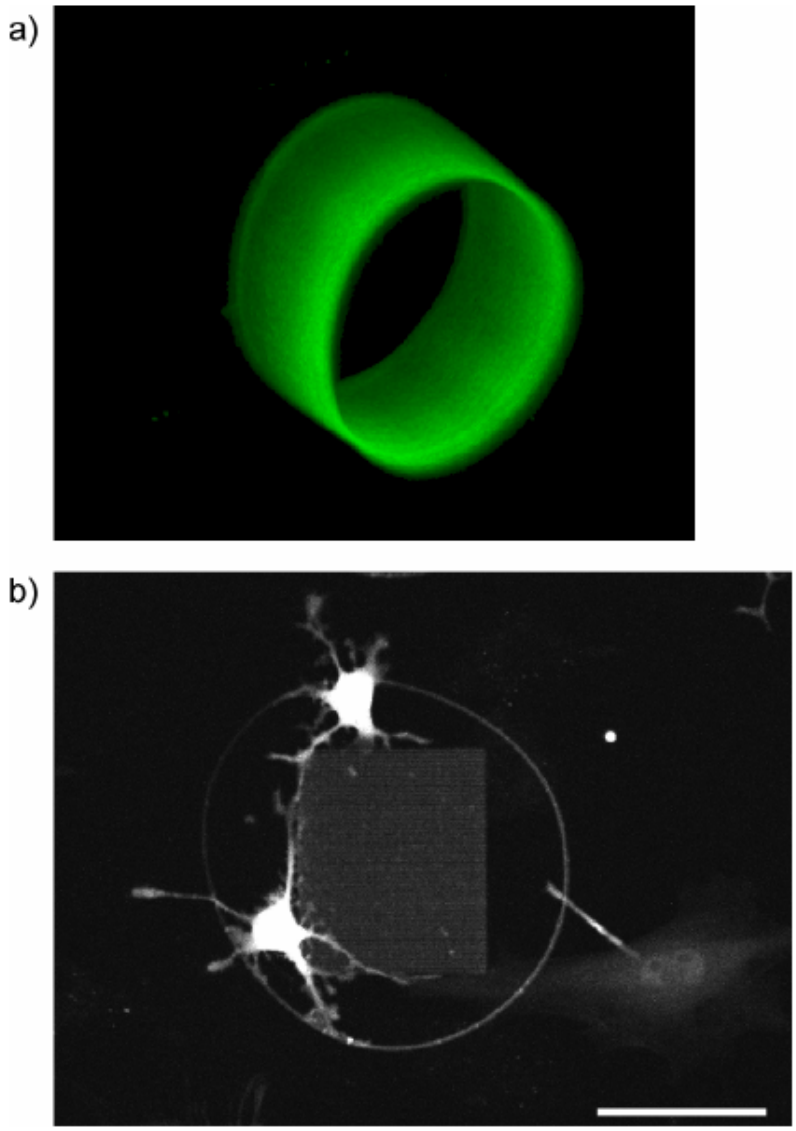

Fig. 4. 3D dimensional cell-containment devices (a) is a high aspect ratio cylinder 60 microns tall with 1 micron thick walls MPE fabricated from BSA (b) Cylinder fabricated from crosslinked fibrinogen/BSA mixture is used to encompass primary neurons and fibroblasts. The inner scaffold is also fabricated from fibrinogen and the cells have migrated to this adhesive structure. Scale bar=50 microns.

To this end as shown in Fig 4(b), we have a fabricated a cylinder from a mixture of crosslinked Texas Red labeled fibrinogen and BSA, where the former provides ECM cues through RGD binding sites,[24] and the latter is used to provide increased mechanical stability. The inner rectangular matrix was fabricated from the same mixture. The image in Fig. 4(b) shows two GFP expressing neurons (isolated from primary culture) that have

migrated into the contained region and have attached to the inner matrix. A fibroblast at the right edge has also migrated towards this region. The general problems of cell motility and migration are not well understood and other work has reported the use of cell entrapment as a means to gain insight into these phenomena.[25]

We suggest that MPE fabricating the entrapment vessel as well functionalizing its interior may be a versatile tool to study motility and migration on attractive surfaces in a well-controlled, spatially confined environment. The CAD based MPE fabrication can also be used to create tissue engineering scaffolds. In previous work, we have studied cell spreading and morphology on simple MPE crosslinked linear patterns, and found that crosslinked ECM proteins effectively direct cell growth.[18-19] We suggested this occurs because these structures provide both topographic and ECM cues that replicate aspects of the native ECM. Here we extend to this to a more complex scaffold. Figure 5(a) shows the 3D rendering of a scaffold created from a 50/50% mixture of Texas Red labeled fibrinogen and BSA, where the mesh size is 10 microns. The image was shadowed to better show the 3D architecture. Figure 5(b) shows a GFP expressing fibroblast adhered to the surface of the scaffold as well as more cells approaching the structure at the 4 hour timepoint. This result shows that the structure possessed its bioactivity in terms of providing ECM cues for cell-binding.

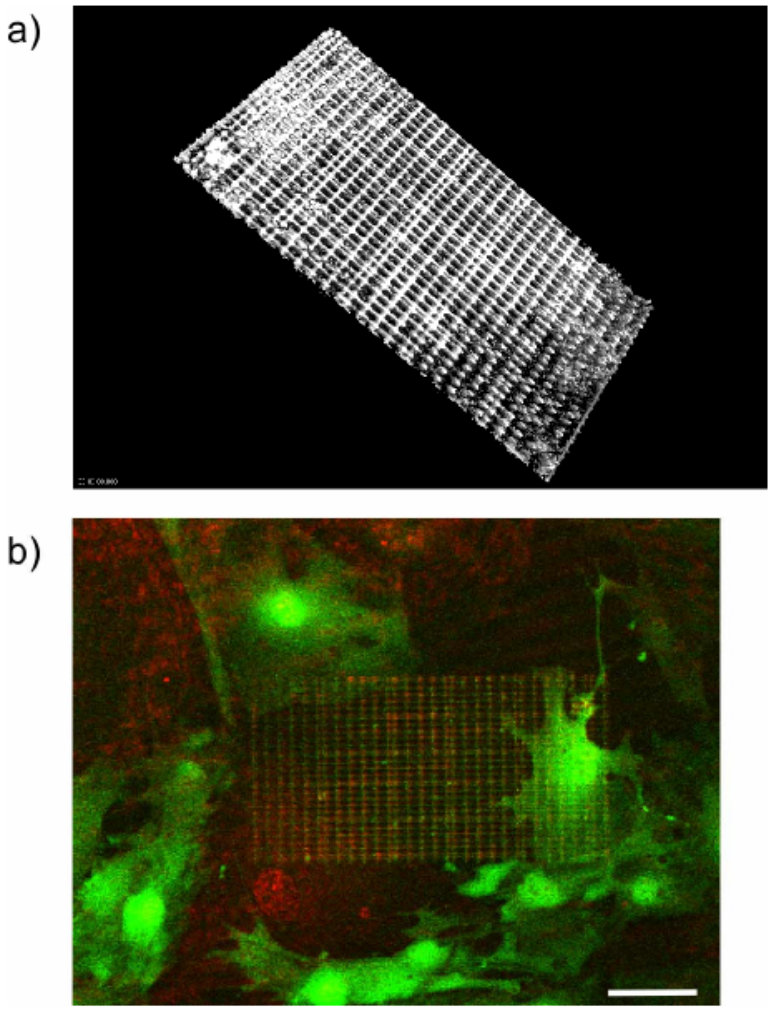

Fig. 5. A tissue engineering scaffolds fabricated from fibrinogen and BSA.,where (a) show a 3D fluorescence rendering of the structure, and (b) shows a GFP expressing fibroblast adhered to the scaffold 4 hours post-plating. Additional fibroblasts are seen to migrate toward the scaffold. Scale bar=25 microns.

While the scaffold shown in Fig. 5 has more 3D structure than we have previously reported, native ECMs have significantly more complex topography. Our long-term goals are to use the freeform capabilities of MPE fabrication to replicate this structure. As a step in this direction, we can use the CAD control approach to fabricate complex, arbitrary 3D structures. As an example, Fig. 6 shows the process for fabricating the

University of Connecticut oak leaf logo. A CAD drawing was created from a JPEG image, processed in AutoCAD and Magics as described above (Fig. 6 left). The logo was then fabricated from BSA, where an optical section of the 3D fluorescence image stack and 3D rendering are shown in the middle and right panels, respectively. The structure is approximately 100 microns in diameter, and faithfully reproduces the original drawing. In the future, we will use this approach to fabricate topographically complex tissue engineering scaffolds.

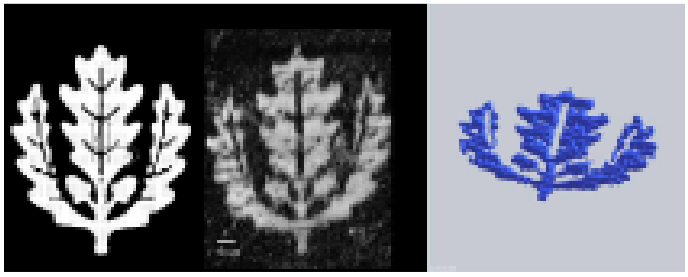

Fig. 6. The fabrication process for the UCONN Oakleaf logo is shown where the CAD drawing, the TPE image, and 3d rendering are shown in the left, middle and right panels, respectively.

5.4 Discussion and conclusions

MPE nano/microfabrication has great potential in biological applications in areas including tissue engineering and biosensing, as well as a tool for probing fundamental questions in cell biology. Given the slow crosslinking rates as well as low damage thresholds relative to polymers, there is a large premium on the speed of fabrication while utilizing the lowest exposure doses possible. The method described here affords 3D capabilities with good speed. For example, the cell-sorting tunnel (Fig. 2) and the UCONN Oak leaf (Fig. 6) required less than a minute of fabrication time. While we specifically used AutoCAD and Materialise to link to our open source LabVIEW code,

we point out that the method would be applicable with any software capable of producing STL output files. There have been other recent reports of using rapid prototyping software for tissue engineering applications.[26, 27] However, these approaches have used either conventional commercially available STL machines, or direct light projection using standard components. Since these approaches are based on the standard methodologies, the resulting minimum feature sizes are in the range of a few hundred microns to several mm. By contrast the technology reported here adapts the powerful CAD based RP approach to the submicron and micron scale and performs the fabrication with biological materials in a biocompatible aqueous environment. This opens up the door to an array of applications in tissue engineering, biosensing, and cell biology.

Acknowledgments: We gratefully acknowledge support under an NIH 1U54-RR022232.

5.5 References

1. W. Lee, S. A. Pruzinsky, and P. V. Braun, "Multi-Photon Polymerization of Waveguide Structures Within Three-Dimensional Photonic Crystals," Adv. Mater. **14**, 271-274 (2002).
2. W. Zhou, S. M. Kuebler, K. L. Braun, T. Yu, J. K. Cammack, C. K. Ober, J. W. Perry, and S. R. Marder, "An Efficient Two-Photon-Generated Photoacid Applied to Positive-Tone 3D Microfabrication," Science **296**, 1106-1109 (2002).
3. S. Kawata, H.-B. Sun, T. Tanaka, and K. Takada, "Microfabrication: Finer features for functional microdevices.," Nature **412**, 697-698 (2001).
4. S. Maruo, O. Nakamura, and S. Kawata, "Three-dimensional microfabrication with two-photon-absorbed photopolymerization," Opt. Lett. **22**, 132-134 (1997).
5. B. Kaehr, R. Allen, D. J. Javier, J. Currie, and J. B. Shear, "Guiding neuronal development with in situ microfabrication," Proc Natl Acad Sci U S A **101**, 16104-16108 (2004).
6. J. H. Strickler and W. W. Webb, "Three-dimensional optical data storage in refractive media by two-photon point excitation.," Opt. Lett. **16**, 1780-1782 (1991).
7. C. N. LaFratta, T. Baldacchini, R. A. Farrer, J. T. Fourkas, M. C. Teich, B. E. A. Saleh, and M. J. Naughton, "Replication of Two-Photon-Polymerized Structures with Extremely High Aspect Ratios and Large Overhangs," J. Phys. Chem. B **108**, 11256 - 11258 (2004).
8. F. J. Qi, Y. Li, H. C. Guo, H. Yang, and Q. H. Gong, "Wavy lines in two-photon photopolymerization microfabrication," Opt. Express **12**, 4725-4730 (2004).
9. T. Baldacchini, A. C. Pons, J. Pons, C. N. LaFratta, J. T. Fourkas, Y. Sun, and M. J. Naughton, "Multiphoton laser direct writing of two-dimensional silver structures," Opt. Express **13**, 1275-1280 (2005).
10. J. Serbin, A. Egbert, A. Ostendorf, B. N. Chichkov, R. Houbertz, G. Domann, J. Schulz, C. Cronauer, L. Frhlich, and M. Popall, "Femtosecond laser-induced two-photon polymerization of inorganic organic hybrid materials for applications in photonics," Opt. Lett. **28**, 301-303 (2003).
11. J. Serbin and M. Gu, "Superprism phenomena in waveguide-coupled woodpile structures fabricated by two-photon polymerization," Opt. Express **14**, 3563-3568 (2006).
12. J. Serbin, A. Ovsianikov, and B. Chichkov, "Fabrication of woodpile structures by two-photon polymerization and investigation of their optical properties," Opt. Express **12**, 5221-5228 (2004).
13. A. Doraiswamy, C. Jin, R. J. Narayan, P. Mageswaran, P. Mente, R. Modi, R. Auyeung, D. B. Chrisey, A. Ovsianikov, and B. Chichkov, "Two photon induced polymerization of organic-inorganic hybrid biomaterials for microstructured medical devices," Acta Biomaterialia **2**, 267-275 (2006).
14. A. Fujita, K. Fujita, O. Nakamura, T. Matsuda, and S. Kawata, "Control of cardiomyocyte orientation on a microscaffold fabricated by photopolymerization with laser beam interference," J Biomed Opt **11**, 021015 (2006).
15. S. Basu, C. W. Wolgemuth, and P. J. Campagnola, "Measurement of Normal and Anomalous Diffusion of Dyes within Protein Structures Fabricated via Multi-photon Excited Crosslinking," Biomacromolecules **5**, 2347-2357 (2004).

16. S. Basu and P. J. Campagnola, "Enzymatic Activity of Alkaline Phosphatase inside Protein and Polymer Structures Fabricated via Multi-photon Excitation," Biomacromolecules **5**, 572-579 (2004).
17. S. Basu and P. J. Campagnola, "Properties of crosslinked protein matrices for tissue engineering applications synthesized by multiphoton excitation," J Biomed Mater Res **71A**, 359-368 (2004).
18. S. Basu, L. P. Cunningham, G. Pins, K. Bush, R. Toboada, A. R. Howell, J. Wang, and P. J. Campagnola, "Multi-photon Excited Fabrication of Collagen Matrices Crosslinked by a Modified Benzophenone Dimer: Bioactivity and Enzymatic Degradation," Biomacromolecules **6**, 1465-1474 (2005).
19. G. D. Pins, K. A. Bush, L. P. Cunningham, and P. J. Campagnola, "Multiphoton Excited Fabricated Nano and MicroPatterned Extracellular Matrix Proteins Direct Cellular Morphology," J. Biomed. Mat. Res. **78A**, 194-204 (2006).
20. J. D. Pitts, P. J. Campagnola, G. A. Epling, and S. L. Goodman, "Reaction efficiencies for sub-micron multi-photon freeform fabrications of proteins and polymers with applications in sustained release," Macromolecules **33**, 1514-1523 (2000).
21. M. Sridhar, S. Basu, V. L. Scranton, and P. J. Campagnola, "Construction of a laser scanning microscope for multiphoton excited optical fabrication," Rev. Sci. Instrum. **74**, 3474-3477 (2003).
22. S. A. Pruzinsky and P. V. Braun, "Fabrication and characterization of two-photon polymerized features in colloidal crystals," Adv. Funct. Mater. **15**, 1995-2004 (2005).
23. S. Maruo, K. Ikuta, and H. Korogi, "Force-controllable, optically driven micromachines fabricated by single-step two-photon micro stereolithography," J. Microelectromech. Syst. **12**, 533-539 (2003).
24. J. Gailit, C. Clarke, D. Newman, M. G. Tonnesen, M. W. Mosesson, and R. A. Clark, "Human fibroblasts bind directly to fibrinogen at RGD sites through integrin alpha(v)beta3," Exp Cell Res **232**, 118-126 (1997).
25. W.-G. Koh, A. Revzin, and M. V. Pishko, "Poly(ethylene glycol) Hydrogel Microstructures Encapsulating Living Cells," Langmuir **18**, 2459-2462 (2002).
26. Y. Lu, G. Mapili, G. Suhali, S. Chen, and K. Roy, "A digital micro-mirror device-based system for the microfabrication of complex, spatially patterned tissue engineering scaffolds," J Biomed Mater Res A **77**, 396-405 (2006).
27. M. N. Cooke, J. P. Fisher, D. Dean, C. Rimnac, and A. G. Mikos, "Use of stereolithography to manufacture critical-sized 3D biodegradable scaffolds for bone ingrowth," J Biomed Mater Res B Appl Biomater **64B**, 65-69 (2003).

Chapter 6

Conclusions and Suggested Future Directions

Conclusions

Aim 1 Conclusions :

Minimum Feature Sizes of MPE Cross-linked Collagen

Theoretical point spread functions (PSF) predict, that at the same wavelength, three-photon excitation will have a smaller 3- dimensional PSF than that of two-photon excitation (Gu and Sheppard [87], Hell SW [88]). To confirm that three-photon excitation with collagen results in a smaller minimum widths of linear structures (type I and II collagen) we compared 780 nm (three-photon) and 850 nm (two-photon) excitation cross-linked collagen/BPD linear structures by SEM. We confirmed that three-photon excitation produces significantly smaller features at comparable excitation wavelengths as a research design consideration to better approach focal adhesion size.

Aim 2(A) Conclusions:

Determination of Bioactivity via Immunofluorescence

A consideration in using this technology for tissue engineering or drug delivery applications is whether these structures retain their biological activity following the intense peak power exposure required for MPE. We crosslinked Type I and type II collagen matrices (60 x40 x5 μm) using BPD photochemistry at both 850 nm (two-photon) and 780 nm (three-photon excitation). A primary antibody was added to cross-linked collagen. After incubation for approximately 30 minutes, the secondary FITC labeled antibody was added. After the secondary incubation, the slide was washed with PBS buffer and a two-photon fluorescence FITC image (830 nm excitation) was acquired. A strong fluorescence was observed from both two and three -photon fabricated

structures establishing that successful binding of the immune-fluorescent probe to the cross-linked structures occurred, suggesting that the collagen is not significantly denatured by the fabrication process. Two negative controls were needed to eliminate the possibility of non-specific binding. First, the primary antibody was replaced with 0.1% BSA. Second, the secondary antibody was added in the absence of the primary. In each case, no increase in fluorescence occurred. Comparable levels of activity between the 850 nm and 780 nm MPE cross-linked structures from both types of Collagen would suggest that significant denaturing is not occurring during the fabrication process. This is important because it is known that multi-photon excitation at 780 nm can damage live cells, and adverse effects have been ascribed to higher order absorption of endogenous proteins [89] and from plasma formation [90].

Aim 2(B) Conclusions:

Cell Adhesion

Continuing the confirmation of cell compatibility with these collagen matrices, we plated primary human dermal fibroblasts on parallel linear structures of MPE cross-linked (three-photon) collagen (type I and type II) on uniform BSA/silanized surfaces and BSA monolayer with BSA fabricated linear structures. As BSA is non-specific, only random cell adhesion is expected on this slide surface. As a control, BSA linear structures were employed to determine if there is a morphological effect on the cell migration without ell signaling. By contrast, if MPE cross-linked collagen has *in vivo* mimicry, then excellent specificity for adhesion of fibroblasts would be expected relative to the background while taking into consideration any effect of structural morphology. We

needed to consider if leaching of BPD out of the cross-linked matrix would have cytotoxic effects on cells adhered to the cross-linked collagen. Since BPD is covalently cross-linked into the protein and unlinked BPD is washed prior to cell plating and culture, this outcome is unlikely. Successful cell survival substantiated cell compatibility.

Aim 2(C) Conclusions:

Enzymatic Degradation of Collagen

Enzymatic degradations of MPE cross-linked structures were used to characterize the chemical and mechanical properties of cross-linked structures. Such measurements provide data on the extent of crosslinking [91] and how this affects the mechanical properties such as compressive modulus [92]. Enzymatic degradation measurements reflect how implanted cross-linked biomaterials might biodegrade. Comparing the relative rates of degradation with different proteases of differing activity have provided an indication of the extent that MPE cross-linked structures mimic the native form. Relative degradation rates of BPD cross-linked collagen matrices were measured using the proteases pepsin, trypsin, and bacterial collagenase. Trypsin and Pepsin are digestive proteases with different target hydrolysis sites. Collagenase is similar to pepsin and is fairly non-specific in its target cleavage sites. We have shown that the relative rates of degradation in these cross-linked matrices are consistent with the known activities of these enzymes. We fabricated matrices from dye-labeled collagen (FITC type II and Oregon Green type IV) with 3-photon excitation of the BPD. The enzymatic degradation of these structures was measured by monitoring the decrease in fluorescence intensity of the labeled collagen over time. The intensity decrease is indicative of the fraction of

cross-linked collagen being digested. The possibility that the decline in fluorescence is due to photo-bleaching of the dye is eliminated by using a control experiment where the cross-linked collagen matrices were imaged in the absence of enzyme under analogous conditions. No appreciable decline in fluorescence intensity was seen in these measurements which supports the validity of the approach.

Enzymatic degradation involves bond cleavage. We therefore expected the structural properties of the matrix, such as the crosslink density and average mesh size, to change following digestion. [92] measured swelling ratios for a Type I collagen chondroitin sulfate matrix and found that collagenase degradation results in increased ability to swell, indicating a decrease in the crosslink density. In prior work [93, 94] on cross-linked BSA, fibrinogen, and fibronectin, the lab approximated the crosslink density or average matrix mesh/pore size by measurement of the swelling ratios of the (hydrated) cross-linked protein matrix to the "dehydrated" (using methanol) matrix in conjunction with a modified Flory-Rehner analysis [95]. The mesh size (cross-link density) is related to the swelling/shrinking ratio.

We used a similar approach to determine whether the cross-linked Type II Collagen matrix undergoes average mesh size changes following enzymatic degradation with pepsin. Since we were most interested in comparing the relative changes under different conditions only the volume changes were measured. Initial structures' heights were measured. The heights of the "dry" structures were measured after repeated methanol washes and air-drying for 15 minutes. Subsequent re-hydrated heights were measured again. Since swelling is taking place in three dimensions, the swelling ratio

was taken as the ratio of the heights. These measurements were repeated after digestion with pepsin. The swelling ratios of pre and post-digested type II collagen were compared. We demonstrated that the least change in heights before and after digestion occur in samples with the matrix having the highest initial crosslink density. Such relatively lower levels in degradation were shown to arise from decreased diffusion of the pepsin due to the decreased average mesh size.

Aim 3 Conclusions:

Topography and biochemistry governing cell adhesion and spreading on ECMs

We used multi-photon excited (MPE) photochemistry to fabricate patterned extracellular matrices (ECM) and to investigate the morphology of human dermal fibroblasts adhered to the resulting photo-cross-linked linear structures of fibronectin (FN), fibrinogen (FG), and bovine serum albumin (BSA). These proteins were chosen in order to systematically investigate the roles of topography and ECM biochemistry on cell spreading as fibroblasts bind directly to both FN and FG at RGD sites through known integrins, whereas BSA provides no comparable ECM cues for cell binding. MPE cross-linked patterns were created from parallel linear structures 700 nm in width, 200 microns in lengths and, spaced by either 10 or 40 microns. Immunofluorescence staining of FN and FG was be used to assay the functionality of cross-linked proteins. The metrics of orientation, elongation, and cell area and perimeter were used to quantitate the resulting cellular response on the cross-linked protein patterns. These parameters reflected statistical differences for cells on BSA, relative to the similar statistical behavior on

fibronectin and fibrinogen. Cells on the BSA patterns were not affected by a cell signaling mechanism but appeared to be constrained by physical guidance and orient between linear structures. By contrast, we confirmed that cells will adhere on FN and FG structures due to inherent cell signaling mechanisms. We showed that the cross-linked, matrix protein structures directed cell adhesion and spreading and that the topography and ECM cues would lead to different forms of guidance. These investigations help us understand the relative roles of topography and biochemistry that govern cell adhesion and spreading on ECMs patterns fabricated directly from cross-linked proteins.

Aim 4 Conclusions:

Morphological and Cytoskeletal dynamics on cross-linked ECM Scaffolds

Having established bioactivity of these structures, and topographic and signaling responses, we investigate the relationship between a focal adhesions and stress fibers with respect to the bioactive, biomimetic extracellular matrix in terms of likelihood of focal adhesion attachment on varied spatial and biochemical microenvironments, stress fiber length and orientation, cell morphology. This is done by fabricating parallel linear structures with extracellular matrices (ECM) proteins fibronectin (FN), and Collagen I and bovine serum albumin (BSA, as a Control) to investigate morphological and the directional response of human dermal fibroblasts grown on the photo-cross-linked linear structures. By plating human dermal fibroblasts on these Collagen, FN and BSA we observe if fibroblasts have a preference for any of these proteins in forming focal adhesions.

Here we extended cytoskeletal dynamics studies to a more in depth morphological analysis, as well examining the cytoskeletal and integrin binding dynamics of dermal fibroblasts on fibers of FN, Type I and II Collagen, and BSA. This approach allows the isolation of purely topographic guidance from that arising from a combination of topographic and biochemical cues. In this regard, we correlated the spatial distribution of focal adhesions and stress fibers for cells adhered to the different protein. We specifically investigated differences for cells adhered to FN and Collagen in spreading and cytoskeletal organization, which arise from differences in their respective roles in promoting migration and new matrix synthesis.

Aim 5 Conclusions:

To advance this multi-photon excited, freeform fabrication technology to 3D

Since the focal volume can be designed to have a sub-micron height, MPE photochemistry is used to create 3-D sub-microfabrication objects one plane at a time, without overwriting previous layers (Lee W [96], Zhou [97], Kawata, Sun [98], Maruo, Nakamura [99], Strickler and Webb [100], LaFratta [101]). Most of this work was centered on micro-fabrication with polymers, with the research being directed at 3-D storage and nano-photonics applications [94]. There are additional potential applications in tissue engineering, cell sorting by microfluidics, and bio-sensing. MPE can play a unique role with these biological applications as more traditional methods such as photolithography and micro-contact printing do not have freeform capabilities in all 3 dimensions. Solid freeform fabrication cannot provide the submicron feature sizes

necessary for current challenges in tissue engineering, nor does it possess the degree of biocompatibility that is achievable by MPE photochemistry in an aqueous environment.

We have advanced the current MPE system such that it can scan in geometrical patterns (polygons, ellipses, and circles, in both perimeter and solid patterns) as well as any stack of slices from a computer aided design (CAD) application. Programs such as ProE ™ and Autocad ™ comply with a data file format (STL). Stacks of slices would comprise of the information required to crosslink a three dimensional solid object with submicron resolution. Pixels that define a two dimensional set of coordinates define a slice. To take advantage of these possibilities, several biological applications using MPE polymerization have recently been demonstrated in the areas of cell biology [102] and biomaterials (Mikos [103], Thomson [104]). We have demonstrated our CAD-based multi-photon excitation fabrication method by fabricating several structures of biological applications in a microscopic aqueous environment. This system included rapid prototyping software that links with Labview™ to drive the laser galvanometers and Z-stage. By utilizing existing CAD file formats (STL format) we developed an improved upon the "left – right" laser scanning of protein "lines" to fabricate 3-D objects from proteins and polymers in solution. To demonstrate freeform MPE fabrication viability we fabricated a microfluidic "tunnel" from a water soluble triacrylate and the University of Connecticut's Oak Leaf logo (at 100 microns in diameter) fabricated from BSA in 30 seconds. Complex structures could not otherwise be created by lithographic methods or by conventional geometric laser scanning. This fabrication technology could be used to create microfluidic devices for sorting cells. Such MPE fabricated structures can be

further functionalized with fibronectin, collagen, or growth factors depending on the desired bioactive response.

MPE nano/microfabrication has great potential in biological applications in areas including tissue engineering and biosensing, as well as a tool for probing fundamental questions in cell biology. Advancing this technology creates new opportunities to an array of applications in tissue engineering, biosensing, and cell biology.

Suggested Future Directions

Soft connective tissues at steady state are dynamic where resident cells continually read environmental cues and respond to them to promote homeostasis, including maintenance of the mechanical properties of the extracellular matrix (ECM) that are fundamental to cellular and tissue health. The mechanosensing process involves assessment of the mechanics of the ECM by the cells through integrins and the actomyosin cytoskeleton, and is followed by a mechanoregulation process, which includes the deposition, rearrangement or removal of the ECM to maintain overall form and function. Progress towards understanding the molecular, cellular and tissue-level effects that promote mechanical homeostasis has helped to identify key questions for future [105].

Advancing the MPE fabrication methods in terms of fabrication accuracy and improved capability for fabricating gradients would be an effective tool for investigating ECM research where 2D and 3D protein concentration gradients can be fabricated. Multiphoton excited 3D fabrication using a blueprint derived directly from high resolution optical microscopy images (e.g. fluorescence and Second Harmonic

Generation) has since been developed [106]. This is accomplished using a modulated raster scanning, where rapid laser shuttering at 10 MHz is used by directly mapping a greyscale image file to the resulting protein concentration in the fabricated scaffold. This has advantages to our STL approach in Chapter 5. Ajeti suggests the method will enable a variety of cell-matrix studies in cancer biology and also provide insight into generating scaffolds for tissue engineering.

Concentration gradients of ECM proteins play active roles in many areas of cell biology including wound healing and metastasis. They may also form the basis of tissue engineering scaffolds, as these can direct cell adhesion and migration and promote new matrix synthesis. To better understand cell-matrix interactions on attractive gradients, multiphoton excited (MPE) photochemistry has recently been done to fabricate by the Campagnola lab to covalently fabricate micro-structured gradients from fibronectin (FN) [107]. The gradient design is comprised of a parallel series of individual linear gradients. A linear dynamic range of nearly 10-fold in concentration was achieved in the gradient. The adhesion dynamics of 3T3 fibroblasts were investigated, where the cell morphology and actin cytoskeleton became increasingly elongated and aligned with the direction of the gradient at increasing protein concentration. Moreover, the cell morphologies are distinct when adhered to regions of differing FN concentration but with similar topography.

These results show that the fabrication approach allows investigating the roles of *contact guidance* and ECM cues on the cell-matrix interactions. This design overcomes some of the limitations with other fabrication methods, especially in terms of 3D

patterning capabilities, and will serve as an improved tool to study cell-matrix interactions.

Integrin-mediated adhesion is regulated by its surface chemical composition, topography, and physical properties. The Geiger lab (Cavalcanti-Adam, 2007) has shown that cell-surface attachment is not sensitive to pattern density, yet the formation of stable focal adhesions and persistent spreading are sensitive to pattern density. Their findings indicate that a critical RGD density is necessary for mature and stable integrin adhesions, which, in turn, induce efficient cell spreading and formation of focal adhesions.

Cellular adhesion to the extracellular matrix plays a key role in physiological and pathological events. Focal adhesions are vital in cell adhesion as they anchor the cytoskeleton to the extracellular matrix, providing signaling pathways that direct cell differentiation and proliferation. As the biochemical and physical mechanisms in the focal adhesion are interrelated, the focal adhesion strength can be strong enough to anchor cells on biological structures that may be observable in terms of cell morphology and stress fiber directionality. Interactions with the extracellular matrix (ECM) provide cells with physical and chemical cues that act in together with growth factors supporting cell survival and proliferation. Xiong (2013) provides a rationale for researching signaling pathways involving integrins as a basis for tumor research. Integrin family transmembrane receptors mediate ECM attachment and play vital roles in sensing and responding to the ECM. Integrin signaling involves large intracellular protein complexes that anchor the cytoskeleton and provide signaling hotspots where enzymes and substrates are concentrated. Many different growth factor signaling cascades are amplified when cells are attached to the ECM. Integrins are involved in many

pathologies. Xiong's efforts focus on their roles in cancer. Though anchorage-independence is a hallmark of cancer cells, genetic studies show that integrins and associated proteins provide essential support for early tumor development and growth. Integrins also provide support during later stages of tumor progression. In some pathologies, however, integrins appear to have the capability to suppress activity though this capability is currently not understood.

Danen (2014) recently reported that gradients of soluble attractants and extracellular matrix (ECM) proteins serve as cues for directional cell movement. Such "chemotaxis" and "haptotaxis" steers migration of cells during embryonic development, wound healing, and immune responses. Chan (2014) shows that the tumor suppressor controls haptotaxis via the microtubule affinity-regulating kinase (MARK) family, which is one of the substrates of the LKB1 master kinase. Without this pathway, melanoma cells migrate irrespective of ECM gradients. This may explain the increased metastatic spread observed in LKB1-deficient tumors. Chan's work highlights a new function for LKB1 as a directional migration sensor of extracellular matrix gradients (haptotaxis response) but not soluble growth factor cues (chemotaxis response).

Our overall work was aimed at advancing multi-photon excited, freeform fabrication technology with nano-scale and sub-micron precision as an enabler for tissue engineers to investigate cellular response to a biomimetic, bio-active extracellular matrix. Such efforts can enable investigations such as the above investigations into understanding metastasis.

4.5 and 6.1 References

1. O'Hara, P.T.B., R. C. , *Contact guidance in vitro. A light, transmission, and scanning electron microscopic study.* . Expl Cell Res. , 1979. **121**: p. 235-249.
2. Clark, P.C., P.; Curtis, A. S. G.; Dow J. A. T.; Wilkinson, C. D. W., *Topographical control of cell behaviour I. Simple step cues.* Development 1987. **99**: p. 439-448
3. Clark, P.C., P.; Curtis, A. S. G.; Dow J. A. T.; Wilkinson, C. D. W., *Topographical control of cell behaviour: II. multiple grooved substrata.* Development 1990. **108**: p. 635-644
4. Ali, I.U. and R.O. Hynes, *Effects of cytochalasin B and colchicine on attachment of a major surface protein of fibroblasts.* Biochim Biophys Acta, 1977. **471**(1): p. 16-24.
5. Hynes, R.O., et al., *LETS glycoprotein: arrangement and function at the cell surface.* Birth Defects Orig Artic Ser, 1978. **14**(2): p. 139-53.
6. Hynes, R.O. and A.T. Destree, *Relationships between fibronectin (LETS protein) and actin.* Cell, 1978. **15**(3): p. 875-86.
7. Willingham, M.C., Yamada, K.M., Yamada, S.S., Pouyssegur, J., Pastan, I., *Microfilament bundles and cell shape are related to adhesiveness to substratum and are dissociable from growth control in cultured fibroblasts.* Cell 1977. **10**: p. 375– 380.
8. Zhang Q, C.W., Peters DM, Albrecht RM, Mosher DF, *Modulation of cell surface fibronectin assembly sites by lysophosphatidic acid.* J Cell Biol 1994. **127**: p. 1447-1459.
9. Zhang Q, M.K., Mosher DF, *Lysophosphatidic acid and microtubule-destabilizing agents stimulate fibronectin matrix assembly through rho-dependent actin stress fiber formation and cell contraction.* Mol Biol Cell 1997. **8**: p. 1415-1425.
10. Zhong CL, C.M., Brown J, Shaub A, Belkin AM, Burridge K, *Rho-mediated contractility exposes a cryptic site in fibronectin and induces fibronectin matrix assembly.* J Cell Biol, 1998. **141**: p. 539-551.
11. Christopher RA, K.A., McKeown-Longo PJ, *Localization of fibronectin matrix assembly sites on fibroblasts and endothelial cells.* J Cell Sci 1997. **110**: p. 569-581.
12. Hocking DC, S.J., McKeown-Longo PJ, *Fibronectin's III-1 module contains a conformation-dependent binding site for the amino-terminal region of fibronectin.* J Biol Chem 1994. **269**: p. 19183-19187.
13. Ingham KC, B.S., Huff S, Litvinovich SV, *Cryptic self-association sites in type III modules of fibronectin.* J Biol Chem 1997. **272**: p. 1718-1724.
14. Ohashi T, K.D., Erickson HP, *Dynamics and elasticity of the fibronectin matrix in living cell culture visualized by fibronectin-green fluorescent protein.* Proc Natl Acad Sci USA, 1999. **96**: p. 2153-2158.
15. Sechler JL, S.J., *Control of cell cycle progression by fibronectin matrix architecture.* J Biol Chem 1998. **273**: p. 25533-25536.
16. Mercurius KO, M.A., *Inhibition of vascular smooth muscle cell growth by inhibition of fibronectin matrix assembly.* Circ Res, 1998. **82** p. 548-556.

17. Dalby, M.R., MO; Sutherland, DS; Agheli,H; Curtis, ASG, *Morphological And Microarray Analysis Of Human Fibroblasts Cultured On Nanocolumns Produced By Colloidal Lithography.* European Cells and Materials, 2005. **9**: p. 1-8.
18. Bunting, M., Harris,E.S., McIntyre,T.M., Prescott,S.M., and Zimmerman,G.A. , *Leukocyte adhesion deficiency syndromes: adhesion and tethering defects involving beta 2 integrins and selectin ligands.* Curr.Opin.Hematol. , 2002. **9**: p. 30-35.
19. McEver, R.P., *Adhesive interactions of leukocytes, platelets, and the vessel wall during hemostasis and inflammation.* Thromb.Haemost, 2001. **86**: p. 746-756.
20. Brakebusch, C., Bouvard,D., Stanchi,F., Sakai,T., and Fassler,R. , *Integrins in invasive growth.* J Clin.Invest 2002. **109**: p. 999-1006.
21. Anderson, J.M., Bonfield,T.L., Ziats,N.P, *Protein adsorption and cellular adhesion and activation on biomedical polymers.* Int J Artif Organs 1990. **13**: p. 375-382.
22. Shen, M.H., T.A, *The effects of surface chemistry and adsorbed proteins on monocyte/macrophage adhesion to chemically modified polystyrene surfaces.* J Biomed Mater Res 2001. **57**: p. 336-345.
23. Lom, B.H., KE; Hockberger, PE, *A versatile technique for patterning biomolecules onto glass coverslips.* J Neurosci Methods 1993. **50**(3): p. 385-397
24. Ito, Y., *Surface micropatterning to regulate cell functions.* Biomaterials 1999. **20**: p. 2333-2342
25. Mrksich, M.D., LE; Tien, J; Ingber, DE; Whitesides, GM, *Using microcontact printing to pattern the attachment of mammalian cells to self-assembled monolayers of alkanethiolates on transparent films of gold and silver.* Exp Cell Res 1997. **235**(2): p. 305-313
26. Xia, Y.W., GM, *Extending microcontact printing as a microlithographic technique.* Langmuir 1997. **13**: p. 2059-2067
27. Kung, L.K., L; Hovis, JS; Boxer, SG, *Patterning Hybrid Surfaces of Proteins and Supported Lipid Bilayers.* Langmuir 2000. **16**: p. 6773 - 6776
28. James, C.D., RC; Kam, L; Craighead, HG; Isaacson, M; Turner, JN; Shain W, *Patterned protein layers on solid substrates by thin stamp microcontact printing.* Langmuir 1998. **14**: p. 741-744
29. Boateng, S.L., SS; Crot,C.; Motlagh, T; Desa, T; Samare, A.M.; Russell, B.; Hanley, L, *Peptides Bound to Silicone Membr anes and 3D Microfabrication for Cardiac Cell Culture.* Adv. Mater, 2002. **14**: p. 461-463
30. Demers, L.G., DS; Park, SJ; Li, Z; Chung,SW; Mirkin,CA, *Direct patterning of modified oligonucleotides on metals and insulators by dip-pen nanolithography.* Science, 2002. **Jun 7;296**(5574): p. 1836-8.
31. Göppert-Mayer, M., *Über Elementarakte mit zwei Quantensprüngen.* Annals of Physics (Leipzig), 1931. **9** (3): p. 273–295.
32. Eaton, D., *Dye sensitized photopolymerization.* Advances in photochemistry, 1986. **13**: p. 427-487.
33. Denk, W.P., D. W.; Webb, W. W. , ed. *Handbook of Biological Confocal Microscopy*. ed. J.B. Pawley, Ed. Vol. New York, 1995; pp 445-458. 1995 Plenum Press: New York. 445-458.

34. Bhatia, N.C., C. S., *Tissue engineering at the micro-scale.* Biomed. Microdev. , 1999. **2**: p. 131-144.
35. Desai, T.A., *Micro- and nanoscale structures for tissue engineering constructs.* Med Eng Phys, 2000. **22**(9): p. 595-606.
36. Lickorish, D.R.J.W., JA; Glattauer, V; Howlett, VR, *Collagen-hydroxyapatite composite prepared by biomimetic process.* J Biomed Mater Res A., 2004. **68**(1): p. 19-27.
37. Chen, G.S., T; Ushida,T; Hirochika, R; Shirasaki,Y; Ochiai, N; Tateishi, T, *The use of a novel PLGA fiber/collagen composite web as a scaffold for engineering of articular cartilage tissue with adjustable thickness.* J Biomed Mater Res A, 2003 **67 Dec 15**(4): p. 1170-80.
38. Pitts, J.D., et al., *New photoactivators for multiphoton excited three-dimensional submicron cross-linking of proteins: bovine serum albumin and type 1 collagen.* Photochem Photobiol, 2002. **76**(2): p. 135-44.
39. Pitts JD, C.P., Epling GA, Goodman SL. , *Reaction efficiencies for sub-micron multi-photon freeform fabrications of proteins and polymers with applications in sustained release.* Macromolecules 2000. **33**: p. 1514-1523.
40. Ratner, B.D., *Reducing capsular thickness and enhancing angiogenesis around implant drug release systems.* J Control Release, 2002. **78**(1-3): p. 211-8.
41. Bhatia, S.N. and C.S. Chen, *Tissue engineering at the micro-scale.* Biomed. Microdev., 1999. **2**: p. 131-144.
42. Desai, T., *Micro- and nanoscale structures for tissue engineering constructs.* Medical Engineering and Physics, 2000. **22**: p. 595-606.
43. Goodman, S.L., P.A. Sims, and R.M. Albrecht, *Three-dimensional extracellular matrix textured biomaterials.* Biomaterials, 1996. **17**(21): p. 2087-2095.
44. Abrams, G.A., S. Goodman, and C.J. Murphy, *Nanoscale Topography of the Extracellular Matrix Underlying the Corneal Epithelium of the Primate.* Invest Ophthal Visual Sci, 1997. **38**: p. S505.
45. Burgeson, R.E., *Basement Membranes*, in *Dermatology in General Medicine*, T.B. Fitzpatrick, et al., Editors. 1987, McGraw-Hill: New York, NY. p. 288-303.
46. Abrams, G.A., et al., *Nanoscale topography of the basement membrane underlying the corneal epithelium of the rhesus macaque.* Cell Tissue Res, 2000. **299**(1): p. 39-46.
47. Grinnell, F., K.-I. Toda, and C. Lamke-Seymour, *Reconstitution of human epidermis in vitro is accompanied by transient activation of basal keratinocyte spreading.* Exp. Cell Res., 1987. **172**: p. 439-449.
48. Carter, W.G., et al., *Distinct functions for integrins $\alpha 3\beta 1$ in focal adhesions and $\alpha 6\beta 4$/bullous perphigoid antigen in a new stable anchoring contact (SAC) of keratinocytes: relation to hemidesmosomes.* J. Cell Biol, 1990. **111**: p. 3141-3154.
49. Carter, W.G., B.E. Symington, and P. Kaur, *Cell adhesion and the basement membrane in early epidermal morphogenesis*, in *Epithelial Organization and Development*, T.P. Fleming, Editor. 1992, Chapman and Hall: London. p. 299-327.
50. Ekblom, P., *Basement membranes in development*, in *Molecular and Cellular Aspects of Basement Membranes*, D.H. Rohrbach and R. Timpl, Editors. 1993, Academic Press: New York, New York. p. 359-383.

51. Uitto, J., A. Mauviel, and J. McGrath, *The Dermal-Epidermal Basement Membrane Zone in Cutaneous Wound Healing*, in *The Molecular and Cellular Biology of Wound Healing*, R.A.F. Clark, Editor. 1996, Plenum Press: New York, NY. p. 513-560.
52. Fleischmajer, R., et al., *Initiation of skin basement membrane formation at the epidermo-dermal interface involves assembly of laminins through binding to cell membrane receptors.* J. Cell Sci., 1998. **111**: p. 1929-1940.
53. Flemming, R.G., et al., *Effects of synthetic micro- and nano-structured surfaces on cell behavior.* Biomaterials, 1999. **20**: p. 573-588.
54. Curtis, A. and C. Wilkinson, *Topographical control of cells.* Biomaterials, 1997. **18**: p. 1573-1583.
55. Dalby, M.J., et al., *Changes in fibroblast morphology in response to nano-columns produced by colloidal lithography.* Biomaterials, 2004. **25**(23): p. 5415-22.
56. Dalby, M.J., et al., *Increasing fibroblast response to materials using nanotopography: morphological and genetic measurements of cell response to 13-nm-high polymer demixed islands.* Exp Cell Res, 2002. **276**(1): p. 1-9.
57. Uttayarat, P., et al., *Topographic guidance of endothelial cells on silicone surfaces with micro- to nanogrooves: Orientation of actin filaments and focal adhesions.* J Biomed Mater Res A, 2005. **75**(3): p. 668-80.
58. den Braber, E.T., et al., *Quantitative analysis of fibroblast morphology on microgrooved surfaces with various grove and ridge dimensions.* Biomaterials, 1996. **17**: p. 2037-2044.
59. den Braber, E.T., et al., *Orientation of ECM protein deposition, fibroblast cytoskeleton, and attachment complex components on silicone microgrooved surfaces.* J Biomed Mater. Res, 1998. **40**: p. 291-300.
60. Thapa, A., T.J. Webster, and K.M. Haberstroh, *Polymers with nano-dimensional surface features enhance bladder smooth muscle cell adhesion.* J Biomed Mater Res A, 2003. **67**(4): p. 1374-83.
61. Miller, D.C., et al., *Endothelial and vascular smooth muscle cell function on poly(lactic-co-glycolic acid) with nano-structured surface features.* Biomaterials, 2004. **25**(1): p. 53-61.
62. Campagnola, P.J., et al., *3-Dimensional sub-micron polymerization of acrylamide by multi-photon excitation of xanthene dyes.* Macromolecules, 2000. **33**: p. 1511-1513.
63. Pitts, J.D., et al., *Reaction efficiencies for sub-micron multi-photon freeform fabrications of proteins and polymers with applications in sustained release.* Macromolecules, 2000. **33**: p. 1514-1523.
64. Lee, W., S.A. Pruzinsky, and P.V. Braun, *Multi-Photon Polymerization of Waveguide Structures Within Three-Dimensional Photonic Crystals.* Adv. Mater., 2002. **14**: p. 271-274.
65. Zhou, W., et al., *An Efficient Two-Photon-Generated Photoacid Applied to Positive-Tone 3D Microfabrication.* Science, 2002. **296**: p. 1106-1109.
66. Olson, C.E., M.J. Previte, and J.T. Fourkas, *Efficient and robust multiphoton data storage in molecular glasses and highly crosslinked polymers.* Nat Mater, 2002. **1**(4): p. 225-8.

67. Witzgall, G., et al., *Single-shot two-photon exposure of commercial photoresist for the production of three-dimensional structures.* Optics Letters, 1998. **23**: p. 1745-1747.
68. Kawata, S., et al., *Microfabrication: Finer features for functional microdevices.* Nature, 2001. **412**: p. 697-698.
69. Maruo, S., O. Nakamura, and S. Kawata, *Three-dimensional microfabrication with two-photon-absorbed photopolymerization.* Optics Letters, 1997. **22**: p. 132-134.
70. Kawata, Y., H. Ishitobi, and S. Kawata, *Use of two-photon absorption in a photorefractive crystal for three-dimensional optical memory.* Opt. Lett., 1998. **23**: p. 756-758.
71. Basu, S. and P.J. Campagnola, *Enzymatic Activity of Alkaline Phosphatase inside Protein and Polymer Structures Fabricated via Multi-photon Excitation.* Biomacromolecules, 2004. **5**: p. 572-579.
72. Basu, S. and P.J. Campagnola, *Properties of crosslinked protein matrices for tissue engineering applications synthesized by multiphoton excitation.* J Biomed Mater Res, 2004. **71A**(2): p. 359-68.
73. Basu, S., C.W. Wolgemuth, and P.J. Campagnola, *Measurement of Normal and Anomalous Diffusion of Dyes within Protein Structures Fabricated via Multi-photon Excited Crosslinking.* Biomacromolecules, 2004. **5**: p. 2347-2357.
74. Sridhar, M., et al., *Construction of a laser scanning microscope for multiphoton excited optical fabrication.* Rev. Sci. Instrum., 2003. **74**(7): p. 3474-3477.
75. Eaton, D.F., *Dye sensitized photopolymerization.* Advances in photochemistry, 1986. **13**: p. 427-487.
76. Balasubramanian, D., X. Du, and J.S.J. Zigler, *The reaction of singlet oxygen with proteins, with special reference to crystallins.* Photochem. Photobiol., 1990. **52**: p. 761-768.
77. Pins, G.D., et al., *Plasmin triggers rapid contraction and degradation of fibroblast-populated collagen lattices.* J. Invest. Dermatol., 2000. **114**: p. 647-653.
78. Keselowsky, B.G. and A.J. Garcia, *Quantitative methods for analysis of integrin binding and focal adhesion formation on biomaterial surfaces.* Biomaterials, 2005. **26**(4): p. 413-8.
79. Kaunas, R., et al., *Cooperative effects of Rho and mechanical stretch on stress fiber organization.* Proc Natl Acad Sci U S A, 2005. **102**(44): p. 15895-900.
80. Pins, G.B., KA; Cunningham, LP; Campagnola, PJ *Multiphoton Excited Fabricated Nano and MicroPatterned Extracellular Matrix Proteins Direct Cellular Morphology.* J. Biomed. Mat. Res. , 2006. **78A**: p. 194-204
81. Fisher, N., *Statistical Analysis of Circular Data.* Cambridge, U.K: Cambridge University Press, 1993.
82. Batschelet, E., *Circular statistics in biology.* London: Academic Press, 1981.
83. Zar, J., *Biostatistical Analysis.* Englewood Cliffs, NJ: Prentice-Hall, 1996.
84. Bouafsoun, A., et al., *Evaluation of endothelial cell adherence onto collagen and fibronectin: A comparison between jet impingement and flow chamber techniques.* Materials Science & Engineering C-Biomimetic and Supramolecular Systems, 2006. **26**(2-3): p. 260-266.

85. Yamamoto, A., et al., *Quantitative evaluation of cell attachment to glass, polystyrene, and fibronectin- or collagen-coated polystyrene by measurement of cell adhesive shear force and cell detachment energy.* Journal of Biomedical Materials Research, 2000. **50**(2): p. 114-124.
86. Pauling, L. and R.B. Corey, *The structure of fibrous proteins of the collagen-gelatin group.* Proc Natl Acad Sci U S A, 1951. **37**(5): p. 272-81.
87. Gu, M. and C.J. Sheppard, *Effects of defocus and primary spherical aberration on three-dimensional coherent transfer functions in confocal microscopes.* Appl Opt, 1992. **31**(14): p. 2541-9.
88. Hell SW, S.E., *Fundamental improvement of resolution with a 4pi-confocal fluorescence microscope using two-photon excitation.* Optics Comm. , 1992. **93**: p. 277-282.
89. Hopt, A. and E. Neher, *Highly nonlinear photodamage in two-photon fluorescence microscopy.* Biophys J, 2001. **80**(4): p. 2029-36.
90. Konig, K., et al., *Cellular response to near-infrared femtosecond laser pulses in two-photon microscopes.* Opt Lett, 1997. **22**(2): p. 135-6.
91. Burdick, J.A., et al., *Controlled degradation and mechanical behavior of photopolymerized hyaluronic acid networks.* Biomacromolecules, 2005. **6**(1): p. 386-91.
92. Pek, Y.S., et al., *Degradation of a collagen-chondroitin-6-sulfate matrix by collagenase and by chondroitinase.* Biomaterials, 2004. **25**(3): p. 473-82.
93. Basu, S. and P.J. Campagnola, *Enzymatic activity of alkaline phosphatase inside protein and polymer structures fabricated via multiphoton excitation.* Biomacromolecules, 2004. **5**(2): p. 572-9.
94. Basu, S. and P.J. Campagnola, *Properties of crosslinked protein matrices for tissue engineering applications synthesized by multiphoton excitation.* J Biomed Mater Res A, 2004. **71**(2): p. 359-68.
95. Baier Leach, J., et al., *Photocrosslinked hyaluronic acid hydrogels: natural, biodegradable tissue engineering scaffolds.* Biotechnol Bioeng, 2003. **82**(5): p. 578-89.
96. Lee W, P.S., Braun PV, *Multi-Photon Polymerization of Waveguide Structures Within Three-Dimensional Photonic Crystals..* Adv. Mater, 2002. **14**: p. 271-274.
97. Zhou, W.K., SM; Braun, KL; Yu, T; Cammack, YK; Ober, CK; Perry, JW; Marder, SR, *An Efficient Two-Photon-Generated Photoacid Applied to Positive-Tone 3D Microfabrication.* Science 2002. **296**: p. 1106-1109
98. Kawata, S., et al., *Finer features for functional microdevices.* Nature, 2001. **412**(6848): p. 697-8.
99. Maruo, S., O. Nakamura, and S. Kawata, *Three-dimensional microfabrication with two-photon-absorbed photopolymerization.* Opt Lett, 1997. **22**(2): p. 132-4.
100. Strickler, J.H. and W.W. Webb, *Three-dimensional optical data storage in refractive media by two-photon point excitation.* Opt Lett, 1991. **16**(22): p. 1780-2.
101. LaFratta, C.B., T; Farrer, RA; Fourkas, JT; Teich, MC; Saleh, BEA; Naughton, MJ, *Replication of Two-Photon-Polymerized Structures with Extremely High Aspect Ratios and Large Overhangs.* J. Phys. Chem. B 2004. **108**: p. 11256 - 11258

102. Kaehr, B., et al., *Guiding neuronal development with in situ microfabrication.* Proc Natl Acad Sci U S A, 2004. **101**(46): p. 16104-8.
103. Mikos, A.S., G; Leite, SM; Vacanti, JP; Langer R, *Laminated three-dimensional biodegradable foams for use in tissue engineering.* Biomaterials 1993. **14**(5): p. 323-330
104. Thomson, R.Y., MJ; Powers, JM; Mikos, AG, *Fabrication of biodegradable polymer scaffolds to engineer trabecular bone.* J Biomater Sci Polym Ed 1995. **7**(1): p. 97-106
105. Humphrey, J.D., E.R. Dufresne, and M.A. Schwartz, *Mechanotransduction and extracellular matrix homeostasis.* Nat Rev Mol Cell Biol, 2014. **15**(12): p. 802-12.
106. Ajeti, V., et al., *Image-inspired 3D multiphoton excited fabrication of extracellular matrix structures by modulated raster scanning.* Opt Express, 2013. **21**(21): p. 25346-55.
107. Chen, X., et al., *Cell Adhesion on Micro-Structured Fibronectin Gradients Fabricated by Multiphoton Excited Photochemistry.* Cell Mol Bioeng, 2012. **5**(3): p. 307-319.

Supplemental Tables and Appendix A

Supplemental Table 1: Tabular Results of Logistical Model Procedures in Appendix A

Supplemental Table 2: Tabular Results of Generalized Linear Model Procedures in Appendix A

Supplemental Table 3: Stress Fiber Magnitude Statistics (top) and Angular Statistics (bottom)

Appendix A: Three Logistic Procedures

Supplemental Table 1:
Tabular Results of Logistical Model Procedures in Appendix A

Model / Canonical Function:
Logistic Procedure / generalized logit
(refer to Appendix A, First to Third Logistic Procedure: The Generalized Linear Model)

Model Page	Response Variable / Order	Frequency Varial	Class1	Class2
1	FAStructure (FA on Line, on SF, Both Line & SF, NotB/naiscent)	FACounts	Cell type (Attached vs Single)	Protein (Collagen I, Fibronectin)
2	Protein	Type 3 Analysis of Effects Wald Chi-Sq	Generally, Fibroblasts' Focal Adhesion distribution on Protein structures differ significantly (p=0.0004 at the $\alpha = 0.05$ level).	
2	CellType*Protein	Type 3 Analysis of Effects Wald Chi-Sq	Generally,Fibroblasts' Focal Adhesion distribution considering Protein structures interaction with Cell Type differ significantly (p=0.0501 at the $\alpha = 0.05$ level).	
2	CellType	Type 3 Analysis of Effects Wald Chi-Sq	Cell Type (Attached/single) is NOT significantly associated with Focal Adhesion (p=0.2072 at the $\alpha = 0.05$ level).	
2	CollagenI * Line	Maximum Likelihood	Fibroblasts' Focal Adhesion Likelihood of frequency count on Collagen I Lines is very significant (p=0.0023 at the $\alpha = 0.05$ level).	
3	CollagenI * Line	Profile Likelihood C.I. for Parameters	Fibroblasts' Focal Adhesion Likelihood of frequency count on Collagen I Lines is significant (at the $\alpha = 0.05$ level).	
3	CollagenI * Line	Wald C.I. for Parameters	Fibroblasts' Focal Adhesion Likelihood of frequency count on Collagen I Lines is significant (at the $\alpha = 0.05$ level).	
6	CellType	Type 3 Analysis of Effects Wald Chi-Sq	Cell Type (Attached/single) is NOT significantly associated with Focal Adhesion (p=0.2997 at the $\alpha = 0.05$ level).	
6	Protein	Type 3 Analysis of Effects Wald Chi-Sq	Protein (Collagen I) is significantly associated with Focal Adhesion (p=0.0031 at the $\alpha = 0.05$ level).	
7	Protein*CellType*Line	Profile Likelihood C.I. for Parameters	Fibroblasts' Focal Adhesion Likelihood of frequency count on Collagen I Lines is significant (at the $\alpha = 0.05$ level).	
7	Protein*CellType*Line	Wald C.I. for Parameters	Fibroblasts' Focal Adhesion Likelihood of frequency count on Collagen I Lines is significant (at the $\alpha = 0.05$ level).	
7	CollagenI * FN	Odds Ratio	The odds are reduced by a factor of 29.5% that a focal adhesion would form on a Collagen I line as compared with a FN line.	
7	CollagenI * FN	Wald C.I. for Adjusted Odds Ratios	The odds are reduced by a factor of 29.5% that a focal adhesion would form on a Collagen I line as compared with a FN line.	

Supplemental Table 2:
Tabular Results of Generalized Linear Model Procedures in Appendix A

Model / Canonical Function:
Generalized Linear Model (GLM) / Poisson distribution
(refer to Appendix A, Fourth Procedure: The Generalized Linear Model)

Model Page	Dependent Variable		Class1 (Levels) Center/Measurer (UCHC/WPI)CellType (Single Attached)	Class2 (Levels) CellType (Attached / Single)	Class3 (Levels) Protein (BSA lines, CI, FN, BSA no lines)
1	logArea	$R^2 = 0.18$	**p=0.0349 @ α = 0.05**	p=0.2669 @ α = 0.05	**p=0.0283 @ α = 0.05**
		robust model	Fibroblasts' logArea has significant difference between UCHC and WPI. Note WPI only measure BSA and BSA-NL.	**Overall, Attached vs Single Fibroblast are not significantly different at alpha = 0.05**	Fibroblasts' logArea is significantly diff betw Proteins.
2	logArea	Tukey's HSD	Fibroblasts on Collagen I & BSA have significantly different logAreas at the α = 0.05 level. Fibroblasts on Coll I will have larger areas compared fibroblasts on BSA lines. All other combinations are not significantly different for logArea.		
11	Perimeter	$R^2 = 0.30$	**p=0.0549 @ α = 0.05**	p=0.1291 @ α = 0.05	**p<0.0001 @ α = 0.05**
		robust model	Fibroblasts' Perimeter has a marginally significant difference between UCHC and WPI. Note WPI only measure BSA and BSA-NL.	Perimeter has a no significant difference between fibroblasts that are Attached to versus Single	Fibroblast Perimeter has a significant difference growing on BSA lines, CI, FN, and BSA monolayer
		Class3 (Levels)			
12	Perimeter	Tukey's HSD	Fibroblasts on Collagen I & BSA lines have significantly different Fibroblast Perimeters at the α = 0.05 level. Fibroblasts on Collagen I & BSA monolayer have significantly different Perimeters at the α = 0.05 level. Fibroblasts on Collagen I & FN have significantly different Fibroblast Perimeters at the α = 0.05 level. Fibroblasts' Perimeters on non-Collagen I pairwise combinations are not significantly different.		
21	Area	Kruskall-Wallis	**p=0.0134 @ α = 0.05** Fibroblast Areas are significantly different in the "Protein" category FN, CI, BSA, BSA monolayer		
23	Perimeter	Kruskall-Wallis	**p=0.0015 @ α = 0.05** Fibroblast Perimeters are significantly different in the "Protein" category		
28	Area / (Perimeter)^2 (APS)	Kruskall-Wallis	**p=0.0352 @ α = 0.05** Fibroblasts' Area / (Perimeter)2 are significant different in the "Protein" category Validates scaling L^2/L^2		
31	Area	Kruskall-Wallis	**p=0.0070 @ α = 0.05** Fibroblasts' Areas are significantly different in the "Protein" category considering Center (GroupProtein) UCHC-FN; UCHC-CI; UCHC-BSA; WPI-BSA; WPI BSA monolayer		
33	Perimeter	Kruskall-Wallis	**p=0.0010 @ α = 0.05** Fibroblasts' Perimeters are significantly different in the "Protein" category considering Center UCHC-FN; UCHC-CI; UCHC-BSA; WPI-BSA; WPI BSA monolayer		
39	Area / (Perimeter)^2 (APS)	Kruskall-Wallis	**p=0.0005 @ α = 0.05** Fibroblasts' Area / (Perimeter)^2 are significantly different in the "Protein" category considering Center (GroupProtein) UCHC-FN; UCHC-CI; UCHC-BSA; WPI-BSA; WPI BSA monolayer		
51	Area / (Perimeter)^2 (APS)	$R^2 = 0.602$ robust model			
52	Area / (Perimeter)^2 (APS)	Tukey's HSD	Fibroblasts on Collagen I & BSA lines have significantly different Area / (Perimeter)^2 at the α = 0.05 level.		
61	log Area / (Perimeter)^2 log(APS)	$R^2 = 0.403$ robust model			
62	log Area / (Perimeter)^2 log(APS)	Tukey's HSD	Fibroblasts on Collagen I & BSA lines have significantly different log Area / (Perimeter)^2 at the α = 0.05 level.		

Supplemental Table 3:
Stress Fiber Magnitude Statistics (top) and Angular Statistics (bottom)

CIRCULAR STATISTICS							
Variable	Angle of Single Cells on FN Lines	Angle of Attached Cells on FN Lines	FN Combined	Angle of Single Cells on Collagen I Lines	Angle of Attached Cells on Collagen I Lines	Collagen combined	Angle of Single Cells on BSA Lines
Data Type	Angles	Angles	Angles	Angles	Angles	Angles	Angles
N	38	60	52	26	43	69	12
Data Grouped?	No	No	No	No	No	No	No
Group Width (& Number of Groups)							
Mean Vector (μ)	1.314°	0.686°	352.643°	213.589°	236.597°	232.173°	53.926°
Length of Mean Vector (r)	0.164	0.142	0.192	0.078	0.195	0.149	0.207
Concentration	0.333	0.286	0.391	0.157	0.399	0.302	0.028
Circular Variance	0.836	0.858	0.808	0.922	0.805	0.851	0.793
Circular Standard Deviation	108.874°	113.27°	104.122°	129.335°	103.52°	111.719°	101.732°
Rao's Spacing Test (U)	241.784	225.848	225.704	181.596	243.424	211.271	218.951
Rao's Spacing Test (p)	< 0.01	< 0.01	< 0.01	< 0.01	< 0.01	< 0.01	< 0.01
Watson's U^2 Test (von Mises, U^2)	0.201	0.211	0.225	0.135	0.154	0.208	0.111
Watson's U^2 Test (p)	< 0.005	< 0.005	< 0.005	< 0.005	< 0.005	< 0.005	< 0.005
Kuiper's Test (von Mises, V)	2.024	2.341	2.381	1.611	1.937	2.335	1.447
Kuiper's Test (p)	< 0.01	< 0.01	< 0.01	0.15 > p > 0.10	< 0.025	< 0.01	> 0.15
V Test (V; expected mean 0.00°)	0.164	0.142	0.19	-0.065	-0.108	-0.092	0.122
V Test (u)	1.433	1.552	1.94	-0.47	-0.998	-1.076	0.596
V Test (p)	0.076	0.06	0.026	0.68	0.84	0.859	0.278

	MARDIA-WATSON-WHEELER TESTS														
Angle distributions compared for various SF Lengths combinations (and reported Probabilities)	Coll 1 0-max	FN 0-max	BSAMonoAngle 0-max	BSAMagn 0-max	Coll 1 0-25	FN 0-25	BSAMonoAngle 0-25	BSAMagn 0-25	Coll 1 >25	FN >25	BSAMonoAngle >25	BSAMagn >25	Coll 1 >50	FN >50	BSAMonoAngle >50	BSAMagn >50
Coll 1 0-max	-----	0.088	0.222	**1.83E-04**	0.365	*****	0.211	*****	0.808	0.082	*****	**2.96E-04**	0.561	0.135	*****	*****
FN 0-max		-----	0.206	0.135	0.521	*****	0.24	*****	**0.034**	0.956	*****	0.082	0.055	0.976	*****	*****
BSAMonoAngle 0-max			-----	**0.01**	0.124	*****	0.983	*****	0.229	0.187	*****	**0.011**	0.109	0.185	*****	*****
BSAMagn 0-max				-----	**0.027**	*****	**0.023**	*****	**6.20E-05**	0.233	*****	0.937	**4.57E-05**	0.239	*****	*****
Coll 1 0-25					-----	*****	0.143	*****	0.206	0.457	*****	**0.032**	0.175	0.487	*****	*****
FN 0-25						-----	*****	*****	*****	*****	*****	*****	*****	*****	*****	*****
BSAMonoAngle 0-25							-----	*****	0.248	0.226	*****	**0.04**	0.124	0.197	*****	*****
BSAMagn 0-25								-----	*****	*****	*****	*****	*****	*****	*****	*****
Coll 1 >25									-----	**0.034**	*****	**9.28E-05**	0.8	0.056	*****	*****
FN >25										-----	*****	0.129	0.063	0.988	*****	*****
BSAMonoAngle >25											-----	*****	*****	*****	*****	*****
BSAMagn >25												-----	**6.49E-05**	0.123	*****	*****
Coll 1 >50													-----	0.095	*****	*****
FN >50														-----	*****	*****
BSAMonoAngle >50															-----	*****
BSAMagn >50																-----

Appendix A:

Three Logistic Procedures using a generalized logit as the model are provided. The Response Variable name is "FAStructure." Frequency Variable name is "FACounts." Focal Adhesion Structures (FA) has four levels (FAStructure), namely, the number of fibroblasts' Focal Adhesions on fabricated lines (Line), on a stress fiber only (SFOn), on both a fabricated line and another stress fiber (Both), and Nascent focal adhesions that are neither on a line nor stress fiber (NotB).

A Fourth Procedure, a Generalized Linear Model, using a Poisson distribution is provided. The Dependent Variables include fibroblast logArea, Perimeter, Perimeter/Area ratio, Area, and Area/Perimeter^2. These variables are classified by Cell Type (attached fibroblasts or single fibroblasts); Protein structures (BSA, Collagen I, Fibronectin or BSA monolayer); and Center / Measurer (UCHC or WPI).

First Logistic Procedure

10:15 Thursday, December 04, 2014 **1**

The SAS System

The LOGISTIC Procedure

Model Information	
Data Set	WORK.CELLDATALOGISTIC
Response Variable	FAStructure
Number of Response Levels	4
Frequency Variable	FACounts
Model	generalized logit
Optimization Technique	Fisher's scoring

Number of Observations Read	132
Number of Observations Used	69
Sum of Frequencies Read	355
Sum of Frequencies Used	355

Response Profile		
Ordered Value	**FAStructure**	**Total Frequency**
1	Both	156
2	Line	62
3	NotB	82
4	SFOn	55

Logits modeled use FAStructure='SFOn' as the reference category.

Note: 63 observations having nonpositive frequencies or weights were excluded since they do not contribute to the analysis.

Class Level Information		
Class	**Value**	**Design Variables**
CellType	**attached**	1
	single	-1
Protein	**Coll1**	1
	FN	-1

Model Convergence Status
Convergence criterion (GCONV=1E-8) satisfied.

The SAS System

The LOGISTIC Procedure

Model Fit Statistics		
Criterion	Intercept Only	Intercept and Covariates
AIC	924.375	911.279
SC	935.992	957.745
-2 Log L	918.375	887.279

R-Square	0.0839	Max-rescaled R-Square	0.0907

Testing Global Null Hypothesis: BETA=0			
Test	Chi-Square	DF	Pr > ChiSq
Likelihood Ratio	31.0959	9	0.0003
Score	29.7172	9	0.0005
Wald	25.5873	9	0.0024

Type 3 Analysis of Effects			
Effect	DF	Wald Chi-Square	Pr > ChiSq
CellType	3	4.5582	0.2072
Protein	**3**	**18.0140**	**0.0004**
CellType*Protein	**3**	**7.8117**	**0.0501**

Analysis of Maximum Likelihood Estimates								
Parameter			FAStructure	DF	Estimate	Standard Error	Wald Chi-Square	Pr > ChiSq
Intercept			Both	1	1.0939	0.1707	41.0707	<.0001
Intercept			Line	1	-0.1643	0.2537	0.4191	0.5174
Intercept			NotB	1	0.4442	0.1892	5.5141	0.0189
CellType	attached		Both	1	-0.2389	0.1707	1.9584	0.1617
CellType	attached		Line	1	0.0964	0.2537	0.1442	0.7041
CellType	attached		NotB	1	-0.2847	0.1892	2.2657	0.1323
Protein	Coll1		Both	1	-0.1922	0.1707	1.2685	0.2600
Protein	**Coll1**		**Line**	**1**	**-0.7751**	**0.2537**	**9.3322**	**0.0023**

The SAS System

The LOGISTIC Procedure

Analysis of Maximum Likelihood Estimates								
Parameter			FAStructure	DF	Estimate	Standard Error	Wald Chi-Square	Pr > ChiSq
Protein	Coll1		NotB	1	0.1782	0.1892	0.8873	0.3462
CellType*Protein	attached	Coll1	Both	1	0.0844	0.1707	0.2448	0.6208
CellType*Protein	attached	Coll1	Line	1	0.3505	0.2537	1.9085	0.1671
CellType*Protein	attached	Coll1	NotB	1	-0.2323	0.1892	1.5080	0.2194

Profile Likelihood Confidence Interval for Parameters						
Parameter			FAStructure	Estimate	95% Confidence Limits	
Intercept			Both	1.0939	0.7694	1.4412
Intercept			Line	-0.1643	-0.7162	0.3095
Intercept			NotB	0.4442	0.0782	0.8231
CellType	attached		Both	-0.2389	-0.5836	0.0889
CellType	attached		Line	0.0964	-0.3789	0.6475
CellType	attached		NotB	-0.2847	-0.6629	0.0821
Protein	Coll1		Both	-0.1922	-0.5292	0.1442
Protein	Coll1		Line	-0.7751	-1.3298	-0.3067
Protein	Coll1		NotB	0.1782	-0.1927	0.5526
CellType*Protein	attached	Coll1	Both	0.0844	-0.2517	0.4217
CellType*Protein	attached	Coll1	Line	0.3505	-0.1203	0.9040
CellType*Protein	attached	Coll1	NotB	-0.2323	-0.6068	0.1384

Wald Confidence Interval for Parameters						
Parameter			FAStructure	Estimate	95% Confidence Limits	
Intercept			Both	1.0939	0.7593	1.4284
Intercept			Line	-0.1643	-0.6615	0.3330
Intercept			NotB	0.4442	0.0734	0.8150
CellType	attached		Both	-0.2389	-0.5734	0.0957
CellType	attached		Line	0.0964	-0.4009	0.5936
CellType	attached		NotB	-0.2847	-0.6555	0.0860
Protein	Coll1		Both	-0.1922	-0.5268	0.1423
Protein	Coll1		Line	-0.7751	-1.2724	-0.2778

The SAS System

The LOGISTIC Procedure

Wald Confidence Interval for Parameters						
Parameter			**FAStructure**	**Estimate**	**95% Confidence Limits**	
Protein	**Coll1**		**NotB**	0.1782	-0.1926	0.5490
CellType*Protein	**attached**	**Coll1**	**Both**	0.0844	-0.2501	0.4190
CellType*Protein	**attached**	**Coll1**	**Line**	0.3505	-0.1468	0.8478
CellType*Protein	**attached**	**Coll1**	**NotB**	-0.2323	-0.6031	0.1385

Second Logistic Procedure

10:15 Thursday, December 04, 2014 **5**

The SAS System

The LOGISTIC Procedure

Model Information	
Data Set	WORK.CELLDATALOGISTIC
Response Variable	FAStructure
Number of Response Levels	4
Frequency Variable	FACounts
Model	generalized logit
Optimization Technique	Fisher's scoring

Number of Observations Read	132
Number of Observations Used	69
Sum of Frequencies Read	355
Sum of Frequencies Used	355

Response Profile		
Ordered Value	**FAStructure**	**Total Frequency**
1	Both	156
2	Line	62
3	NotB	82
4	SFOn	55

Logits modeled use FAStructure='SFOn' as the reference category.

Note: 63 observations having nonpositive frequencies or weights were excluded since they do not contribute to the analysis.

Class Level Information		
Class	**Value**	**Design Variables**
CellType	**attached**	1
	single	-1
Protein	**Coll1**	1
	FN	-1

Model Convergence Status
Convergence criterion (GCONV=1E-8) satisfied.

The SAS System

The LOGISTIC Procedure

Model Fit Statistics		
Criterion	Intercept Only	Intercept and Covariates
AIC	924.375	913.880
SC	935.992	948.729
-2 Log L	918.375	895.880

R-Square	0.0614	Max-rescaled R-Square	0.0664

Testing Global Null Hypothesis: BETA=0			
Test	Chi-Square	DF	Pr > ChiSq
Likelihood Ratio	22.4949	6	0.0010
Score	21.6450	6	0.0014
Wald	20.5679	6	0.0022

Type 3 Analysis of Effects			
Effect	DF	Wald Chi-Square	Pr > ChiSq
CellType	3	3.6672	0.2997
Protein	**3**	**16.8346**	**0.0008**

Analysis of Maximum Likelihood Estimates							
Parameter		FAStructure	DF	Estimate	Standard Error	Wald Chi-Square	Pr > ChiSq
Intercept		Both	1	1.0974	0.1704	41.4693	<.0001
Intercept		Line	1	-0.0396	0.2196	0.0325	0.8568
Intercept		NotB	1	0.4840	0.1860	6.7745	0.0092
CellType	attached	Both	1	-0.2544	0.1697	2.2467	0.1339
CellType	attached	Line	1	-0.1224	0.2025	0.3653	0.5456
CellType	**attached**	**NotB**	**1**	**-0.3198**	**0.1857**	**2.9649**	**0.0851**
Protein	Coll1	Both	1	-0.1718	0.1586	1.1739	0.2786
Protein	**Coll1**	**Line**	**1**	**-0.6111**	**0.2065**	**8.7607**	**0.0031**
Protein	Coll1	NotB	1	0.1462	0.1756	0.6929	0.4052

The SAS System

The LOGISTIC Procedure

Odds Ratio Estimates				
Effect	FAStructure	Point Estimate	95% Wald Confidence Limits	
CellType attached vs single	Both	0.601	0.309	1.169
CellType attached vs single	Line	0.783	0.354	1.731
CellType attached vs single	NotB	0.528	0.255	1.092
Protein Coll1 vs FN	Both	0.709	0.381	1.321
Protein Coll1 vs FN	Line	0.295	0.131	0.662
Protein Coll1 vs FN	NotB	1.340	0.673	2.666

Profile Likelihood Confidence Interval for Parameters					
Parameter		FAStructure	Estimate	95% Confidence Limits	
Intercept		Both	1.0974	0.7736	1.4443
Intercept		Line	-0.0396	-0.4773	0.3893
Intercept		NotB	0.4840	0.1258	0.8577
CellType	attached	Both	-0.2544	-0.5975	0.0711
CellType	attached	Line	-0.1224	-0.5243	0.2729
CellType	attached	NotB	-0.3198	-0.6923	0.0388
Protein	Coll1	Both	-0.1718	-0.4833	0.1404
Protein	Coll1	Line	-0.6111	-1.0277	-0.2143
Protein	Coll1	NotB	0.1462	-0.1976	0.4926

Wald Confidence Interval for Parameters					
Parameter		FAStructure	Estimate	95% Confidence Limits	
Intercept		Both	1.0974	0.7634	1.4314
Intercept		Line	-0.0396	-0.4701	0.3908
Intercept		NotB	0.4840	0.1195	0.8485
CellType	attached	Both	-0.2544	-0.5870	0.0782
CellType	attached	Line	-0.1224	-0.5192	0.2744
CellType	attached	NotB	-0.3198	-0.6838	0.0442
Protein	Coll1	Both	-0.1718	-0.4827	0.1390
Protein	Coll1	Line	-0.6111	-1.0158	-0.2064
Protein	Coll1	NotB	0.1462	-0.1980	0.4903

The SAS System

The LOGISTIC Procedure

Profile Likelihood Confidence Interval for Adjusted Odds Ratios					
Effect	**FAStructure**	**Unit**	**Estimate**	**95% Confidence Limits**	
CellType attached vs single	**Both**	1.0000	0.601	0.303	1.153
CellType attached vs single	**Line**	1.0000	0.783	0.592	1.314
CellType attached vs single	**NotB**	1.0000	0.528	0.500	1.040
Protein Coll1 vs FN	**Both**	1.0000	0.709	0.617	1.151
Protein Coll1 vs FN	**Line**	**1.0000**	**0.295**	**0.358**	**0.807**
Protein Coll1 vs FN	**NotB**	1.0000	1.340	0.821	1.637

Wald Confidence Interval for Adjusted Odds Ratios					
Effect	**FAStructure**	**Unit**	**Estimate**	**95% Confidence Limits**	
CellType attached vs single	**Both**	1.0000	0.601	0.309	1.169
CellType attached vs single	**Line**	1.0000	0.783	0.354	1.731
CellType attached vs single	**NotB**	1.0000	0.528	0.255	1.092
Protein Coll1 vs FN	**Both**	1.0000	0.709	0.381	1.321
Protein Coll1 vs FN	**Line**	**1.0000**	**0.295**	**0.131**	**0.662**
Protein Coll1 vs FN	**NotB**	1.0000	1.340	0.673	2.666

The SAS System

The LOGISTIC Procedure

Model Information	
Data Set	WORK.CELLDATALOGISTIC
Response Variable	FAStructure
Number of Response Levels	4
Frequency Variable	FACounts
Model	generalized logit
Optimization Technique	Fisher's scoring

Number of Observations Read	132
Number of Observations Used	69
Sum of Frequencies Read	355
Sum of Frequencies Used	355

Response Profile		
Ordered Value	**FAStructure**	**Total Frequency**
1	Both	156
2	Line	62
3	NotB	82
4	SFOn	55

Logits modeled use FAStructure='SFOn' as the reference category.

Note: 63 observations having nonpositive frequencies or weights were excluded since they do not contribute to the analysis.

Class Level Information		
Class	**Value**	**Design Variables**
Protein	**Coll1**	1
	FN	-1

Model Convergence Status
Convergence criterion (GCONV=1E-8) satisfied.

Third Logistic Procedure

10:15 Thursday, December 04, 2014 **10**

The SAS System

The LOGISTIC Procedure

Model Fit Statistics		
Criterion	Intercept Only	Intercept and Covariates
AIC	924.375	911.656
SC	935.992	934.889
-2 Log L	918.375	899.656

R-Square	0.0514	Max-rescaled R-Square	0.0555

Testing Global Null Hypothesis: BETA=0			
Test	Chi-Square	DF	Pr > ChiSq
Likelihood Ratio	18.7194	3	0.0003
Score	17.9582	3	0.0004
Wald	16.9579	3	0.0007

Type 3 Analysis of Effects			
Effect	DF	Wald Chi-Square	Pr > ChiSq
Protein	**3**	**16.9579**	**0.0007**

Analysis of Maximum Likelihood Estimates							
Parameter		FAStructure	DF	Estimate	Standard Error	Wald Chi-Square	Pr > ChiSq
Intercept		Both	1	1.0197	0.1580	41.6464	<.0001
Intercept		Line	1	-0.0843	0.2063	0.1669	0.6829
Intercept		NotB	1	0.3961	0.1748	5.1358	0.0234
Protein	Coll1	Both	1	-0.1669	0.1580	1.1158	0.2908
Protein	**Coll1**	**Line**	**1**	**-0.6088**	**0.2063**	**8.7074**	**0.0032**
Protein	Coll1	NotB	1	0.1525	0.1748	0.7610	0.3830

The SAS System

The LOGISTIC Procedure

Odds Ratio Estimates				
Effect	FAStructure	Point Estimate	95% Wald Confidence Limits	
Protein Coll1 vs FN	Both	0.716	0.386	1.331
Protein Coll1 vs FN	Line	0.296	0.132	0.664
Protein Coll1 vs FN	NotB	1.357	0.684	2.691

Profile Likelihood Confidence Interval for Parameters					
Parameter		FAStructure	Estimate	95% Confidence Limits	
Intercept		Both	1.0197	0.7167	1.3374
Intercept		Line	-0.0843	-0.4980	0.3153
Intercept		NotB	0.3961	0.0565	0.7433
Protein	Coll1	Both	-0.1669	-0.4772	0.1443
Protein	Coll1	Line	-0.6088	-1.0252	-0.2123
Protein	Coll1	NotB	0.1525	-0.1896	0.4974

Wald Confidence Interval for Parameters					
Parameter		FAStructure	Estimate	95% Confidence Limits	
Intercept		Both	1.0197	0.7100	1.3294
Intercept		Line	-0.0843	-0.4887	0.3201
Intercept		NotB	0.3961	0.0535	0.7387
Protein	Coll1	Both	-0.1669	-0.4766	0.1428
Protein	Coll1	Line	-0.6088	-1.0132	-0.2044
Protein	Coll1	NotB	0.1525	-0.1901	0.4950

Profile Likelihood Confidence Interval for Adjusted Odds Ratios					
Effect	FAStructure	Unit	Estimate	95% Confidence Limits	
Protein Coll1 vs FN	Both	1.0000	0.716	0.385	1.334
Protein Coll1 vs FN	Line	1.0000	0.296	0.359	0.809
Protein Coll1 vs FN	NotB	1.0000	1.357	0.827	1.644

The SAS System

The LOGISTIC Procedure

Wald Confidence Interval for Adjusted Odds Ratios					
Effect	**FAStructure**	**Unit**	**Estimate**	**95% Confidence Limits**	
Protein Coll1 vs FN	**Both**	1.0000	0.716	0.386	1.331
Protein Coll1 vs FN	**Line**	**1.0000**	**0.296**	**0.132**	**0.664**
Protein Coll1 vs FN	**NotB**	1.0000	1.357	0.684	2.691

Fourth Procedure: The Generalized Linear Model

10:16 Thursday, December 04, 2014 **1**

The GLM Procedure

Dependent Variable: logArea

Class Level Information		
Class	**Levels**	**Values**
Center	2	UCHC WPI
CellType	2	attached single
Protein	4	BSA Coll1 FN NLBSA

Number of Observations Read	77
Number of Observations Used	77

Source	DF	Sum of Squares	Mean Square	F Value	Pr > F
Model	5	5.01210233	1.00242047	3.20	0.0116
Error	71	22.25929124	0.31351114		
Corrected Total	76	27.27139357			

R-Square	Coeff Var	Root MSE	logArea Mean
0.183786	7.730431	0.559921	7.243071

Source	DF	Type III SS	Mean Square	F Value	Pr > F
Center	1	1.45085050	1.45085050	4.63	**0.0349**
CellType	1	0.39259657	0.39259657	1.25	0.2669
Protein	3	3.01287090	1.00429030	3.20	**0.0283**

The GLM Procedure

Tukey's Studentized Range (HSD) Test for logArea

Note: This test controls the Type I experimentwise error rate.

Alpha	0.05
Error Degrees of Freedom	71
Error Mean Square	0.313511
Critical Value of Studentized Range	3.72071

Comparisons significant at the 0.05 level are indicated by *.**				
Protein Comparison	**Difference Between Means**	**Simultaneous 95% Confidence Limits**		
Coll1 - NLBSA	0.4911	-0.1618	1.1440	
Coll1 - FN	0.5767	-0.0217	1.1751	
Coll1 - BSA	0.7008	0.1146	1.2870	***
NLBSA - Coll1	-0.4911	-1.1440	0.1618	
NLBSA - FN	0.0856	-0.4061	0.5774	
NLBSA - BSA	0.2097	-0.2671	0.6865	
FN - Coll1	-0.5767	-1.1751	0.0217	
FN - NLBSA	-0.0856	-0.5774	0.4061	
FN - BSA	0.1241	-0.2748	0.5230	
BSA - Coll1	-0.7008	-1.2870	-0.1146	***
BSA - NLBSA	-0.2097	-0.6865	0.2671	
BSA - FN	-0.1241	-0.5230	0.2748	

Model Fit

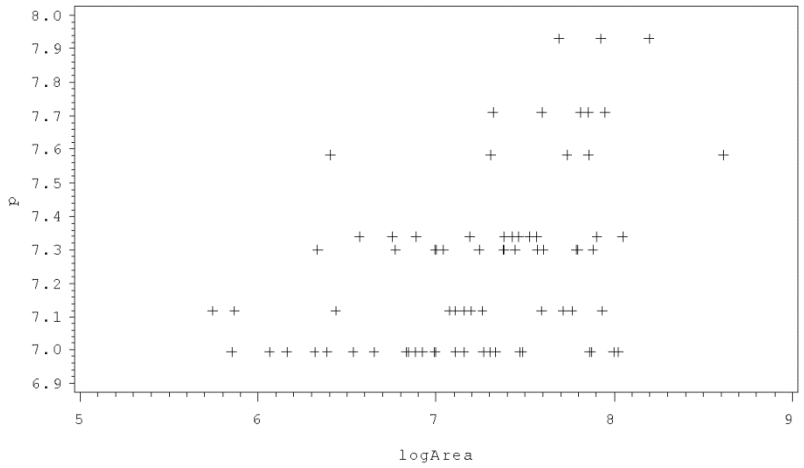

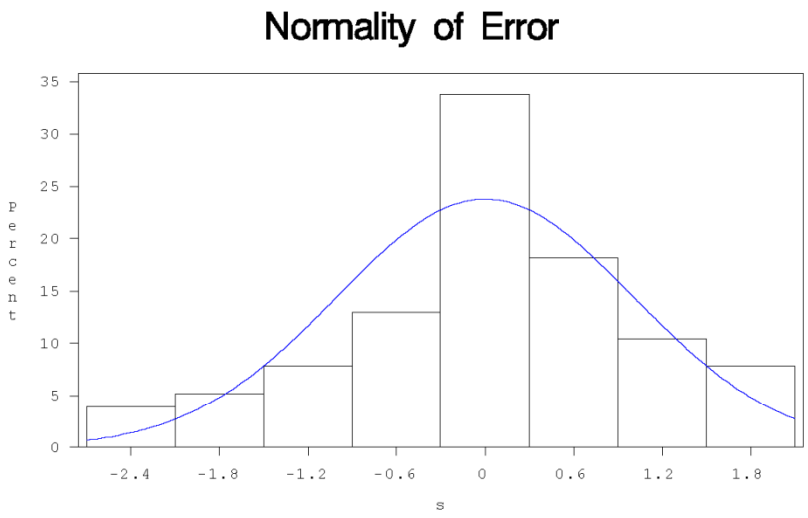
Normality of Error
35
30
25
20
15
10
5
0
percent
-2.4
-1.8
-1.2
-0.6
0
0.6
1.2
1.8
s

Normality of Error

The UNIVARIATE Procedure
Fitted Distribution for s

Parameters for Normal Distribution		
Parameter	**Symbol**	**Estimate**
Mean	Mu	5.809E-6
Std Dev	Sigma	1.006276

Goodness-of-Fit Tests for Normal Distribution				
Test	**Statistic**		**p Value**	
Kolmogorov-Smirnov	**D**	0.08639066	**Pr > D**	>0.150
Cramer-von Mises	**W-Sq**	0.09381269	**Pr > W-Sq**	0.137
Anderson-Darling	**A-Sq**	0.52307123	**Pr > A-Sq**	0.186

Quantiles for Normal Distribution		
	Quantile	
Percent	**Observed**	**Estimated**
1.0	-2.53688	-2.34094
5.0	-2.07806	-1.65517
10.0	-1.43313	-1.28959
25.0	-0.55679	-0.67872
50.0	0.14105	0.00001
75.0	0.55798	0.67873
90.0	1.19167	1.28960
95.0	1.59971	1.65518
99.0	2.05726	2.34095

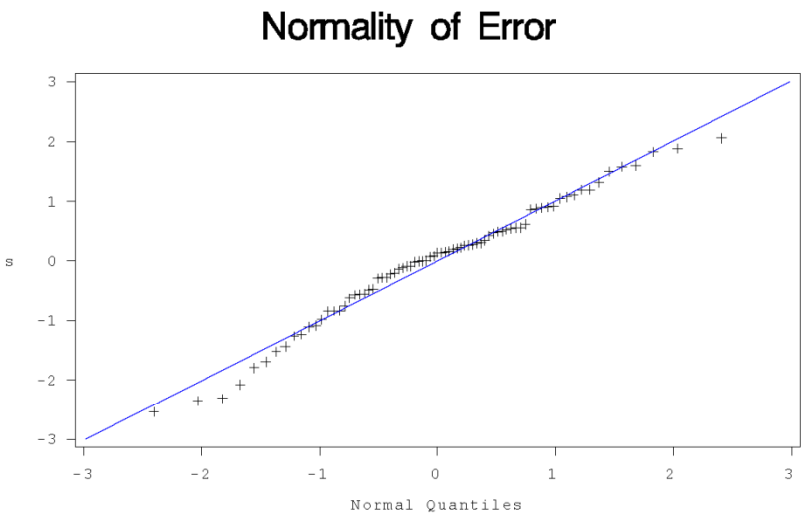

Normality of data for Tukey's HSD (T test) page 2 and 3

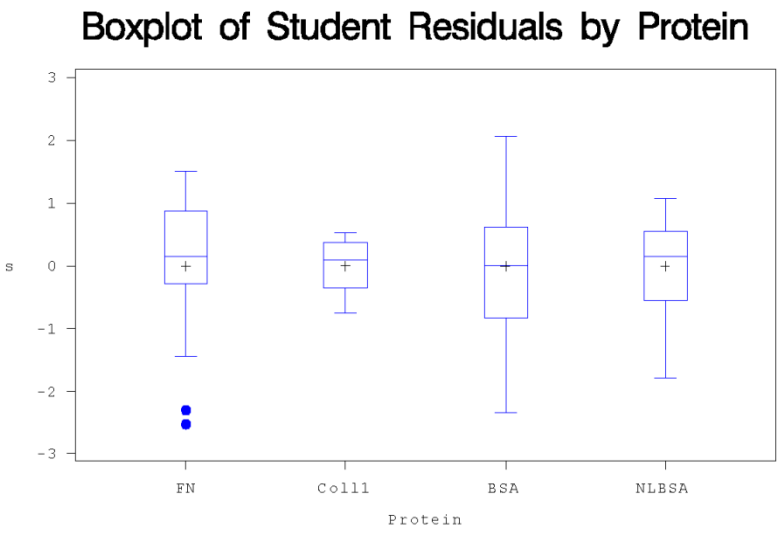
Boxplot of Student Residuals by Protein
s
3
2
1
0
-1
-2
-3
FN
Coll1
BSA
NLBSA
Protein

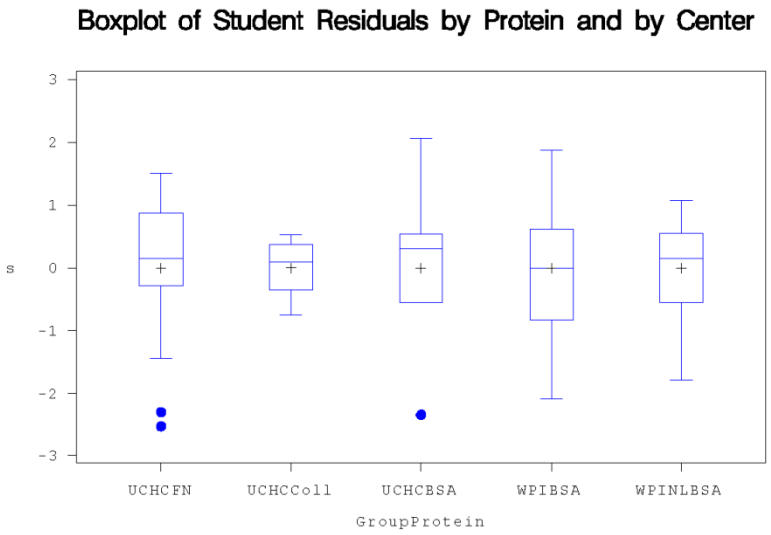
Boxplot of Student Residuals by Protein and by Center
s
3
2
1
0
-1
-2
-3
UCHCFN
UCHCColl
UCHCBSA
WPIBSA
WPINLBSA
GroupProtein

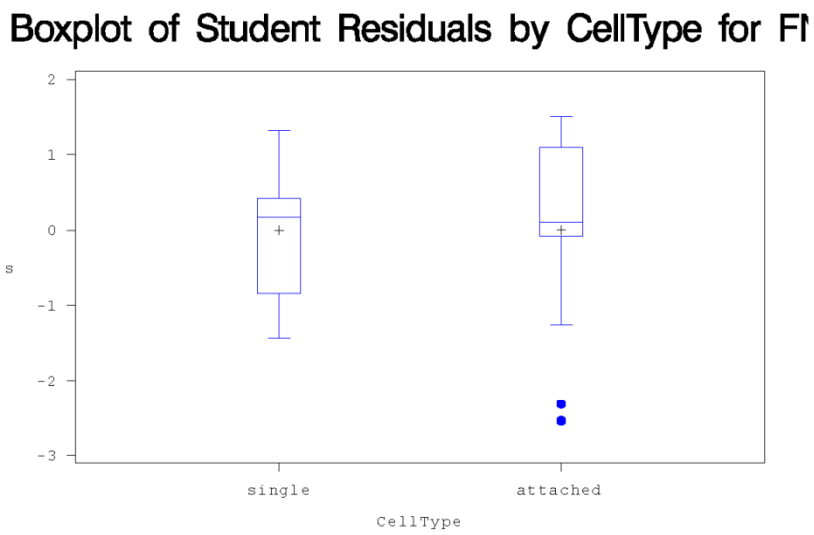
Boxplot of Student Residuals by CellType for Fl
2
1
0
-1
-2
-3
s
single
attached
CellType

The GLM Procedure

Class Level Information		
Class	**Levels**	**Values**
Center	2	UCHC WPI
CellType	2	attached single
Protein	4	BSA Coll1 FN NLBSA

Number of Observations Read	77
Number of Observations Used	77

---

perimeter

10:16 Thursday, December 04, 2014 **11**

The GLM Procedure

Dependent Variable: Perimeter

Source	DF	Sum of Squares	Mean Square	F Value	Pr > F
Model	5	305606.437	61121.287	6.11	<.0001
Error	71	710523.831	10007.378		
Corrected Total	76	1016130.269			

R-Square	Coeff Var	Root MSE	Perimeter Mean
0.300755	34.70209	100.0369	288.2734

Source	DF	Type III SS	Mean Square	F Value	Pr > F
Center	1	38135.8239	38135.8239	3.81	**0.0549**
CellType	1	23600.9266	23600.9266	2.36	0.1291
Protein	3	248620.8101	82873.6034	8.28	**<.0001**

Here Center (i.e., Measurer) is marginally significant.

The GLM Procedure

Tukey's Studentized Range (HSD) Test for Perimeter

Note: This test controls the Type I experimentwise error rate.

Alpha	0.05
Error Degrees of Freedom	71
Error Mean Square	10007.38
Critical Value of Studentized Range	3.72071

Comparisons significant at the 0.05 level are indicated by *.**

Protein Comparison	Difference Between Means	Simultaneous 95% Confidence Limits		
Coll1 - FN	128.10	21.19	235.01	***
Coll1 - NLBSA	178.17	61.52	294.81	***
Coll1 - BSA	187.20	82.47	291.92	***
FN - Coll1	-128.10	-235.01	-21.19	***
FN - NLBSA	50.06	-37.79	137.92	
FN - BSA	59.09	-12.18	130.37	
NLBSA - Coll1	-178.17	-294.81	-61.52	***
NLBSA - FN	-50.06	-137.92	37.79	
NLBSA - BSA	9.03	-76.16	94.22	
BSA - Coll1	-187.20	-291.92	-82.47	***
BSA - FN	-59.09	-130.37	12.18	
BSA - NLBSA	-9.03	-94.22	76.16	

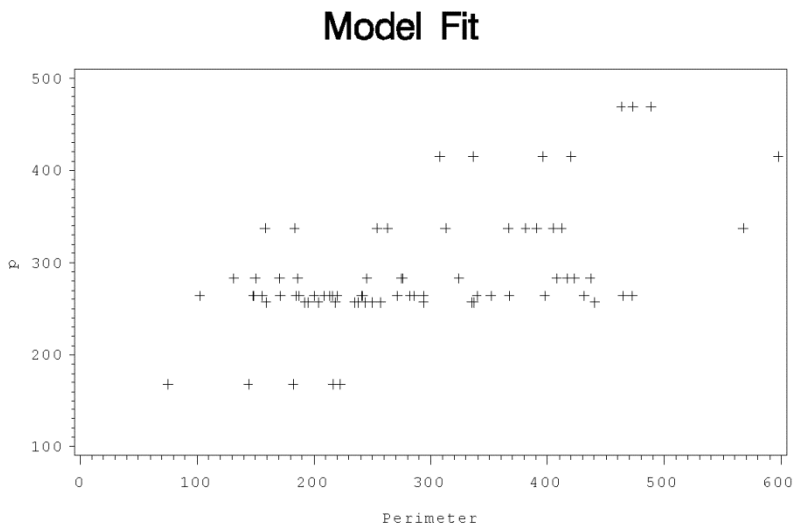
Model Fit
500
400
300
200
100
p
0
100
200
300
400
500
600
Perimeter

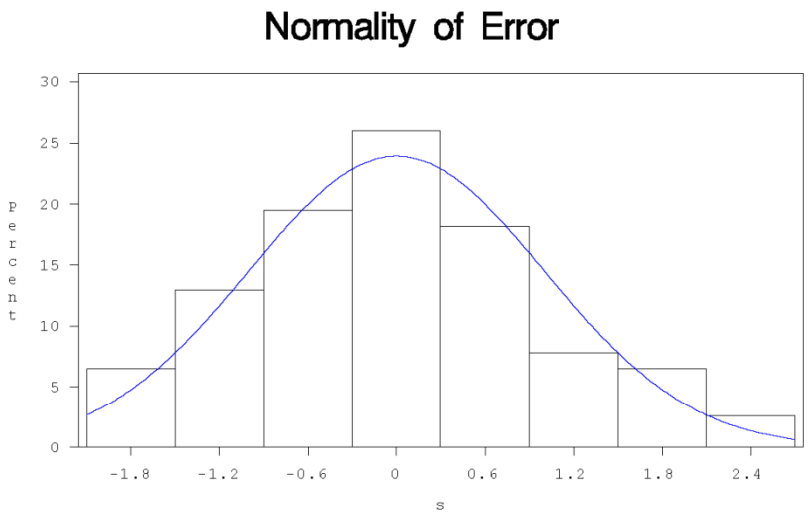
Normality of Error
30
25
20
15
10
5
0
percent
-1.8
-1.2
-0.6
0
0.6
1.2
1.8
2.4
s

Normality of Error

The UNIVARIATE Procedure
Fitted Distribution for s

Parameters for Normal Distribution		
Parameter	**Symbol**	**Estimate**
Mean	Mu	0.000026
Std Dev	Sigma	1.001636

Goodness-of-Fit Tests for Normal Distribution				
Test	**Statistic**		**p Value**	
Kolmogorov-Smirnov	**D**	0.07338248	**Pr > D**	>0.150
Cramer-von Mises	**W-Sq**	0.07298047	**Pr > W-Sq**	>0.250
Anderson-Darling	**A-Sq**	0.49987081	**Pr > A-Sq**	0.212

Quantiles for Normal Distribution		
	Quantile	
Percent	**Observed**	**Estimated**
1.0	-1.86549	-2.33013
5.0	-1.56836	-1.64752
10.0	-1.17790	-1.28362
25.0	-0.77108	-0.67557
50.0	-0.08826	0.00003
75.0	0.61099	0.67562
90.0	1.44327	1.28367
95.0	1.96836	1.64757
99.0	2.39509	2.33018

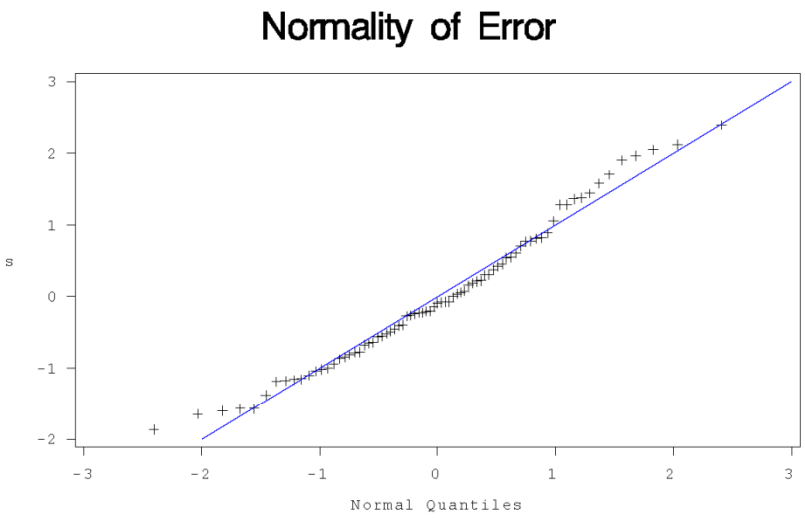
Normality of Error
3
2
1
0
-1
-2
S
-3
-2
-1
0
1
2
3
Normal Quantiles

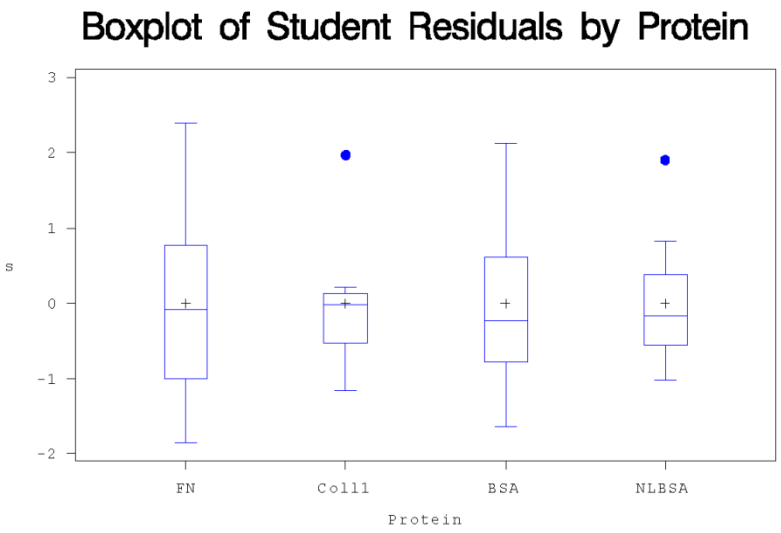
Boxplot of Student Residuals by Protein
3
2
1
0
-1
-2
s
FN
Coll1
BSA
NLBSA
Protein

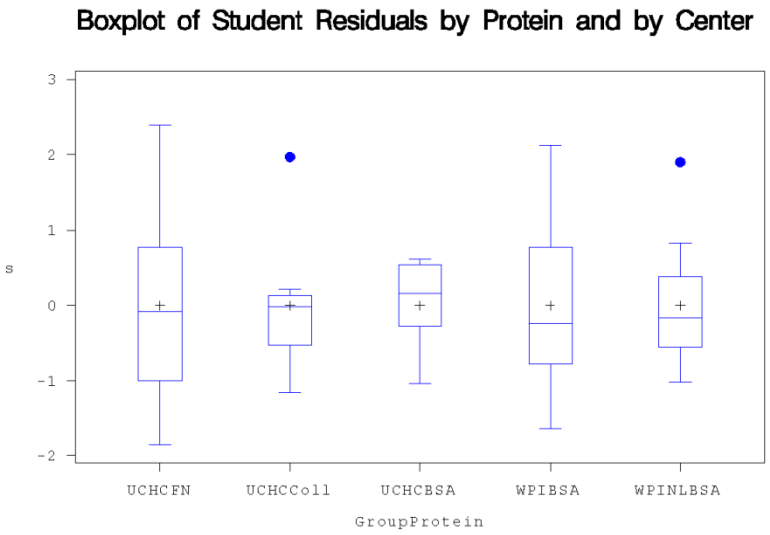
Boxplot of Student Residuals by Protein and by Center
s
3
2
1
0
-1
-2
UCHCFN
UCHCColl
UCHCBSA
WPIBSA
WPINLBSA
GroupProtein

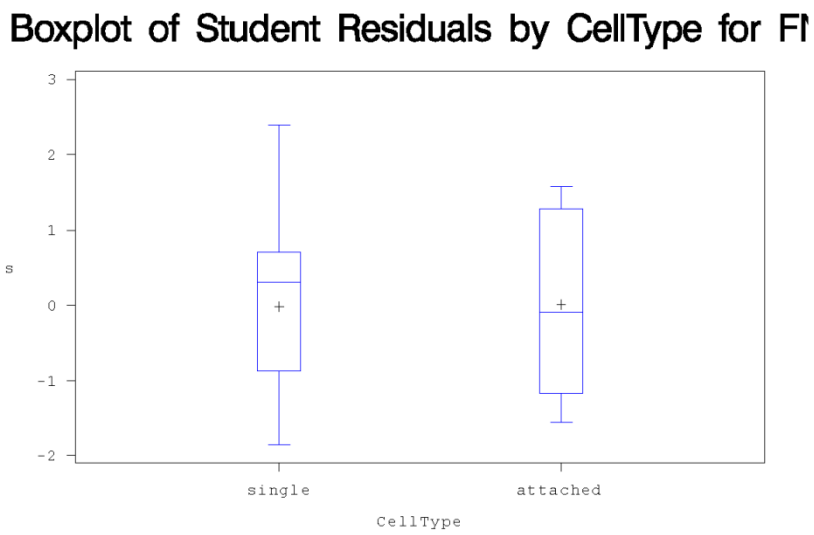
Boxplot of Student Residuals by CellType for Fl
3
2
1
0
-1
-2
s
single
attached
CellType

The NPAR1WAY Procedure

Analysis of Variance for Variable Area Classified by Variable Protein		
Protein	**N**	**Mean**
FN	25	1565.91264
Coll1	8	2494.81800
BSA	30	1492.25330
NLBSA	14	1607.49793

Source	DF	Sum of Squares	Mean Square	F Value	Pr > F
Among	3	6652468.82790	2217489.609	2.8963	0.0408
Within	73	55891086.34097	765631.320		
Average scores were used for ties.					

The NPAR1WAY Procedure

Wilcoxon Scores (Rank Sums) for Variable Area Classified by Variable Protein					
Protein	**N**	**Sum of Scores**	**Expected Under H0**	**Std Dev Under H0**	**Mean Score**
FN	25	963.0	975.0	91.922673	38.520000
Coll1	8	495.0	312.0	59.899129	61.875000
BSA	30	984.0	1170.0	95.732748	32.800000
NLBSA	14	561.0	546.0	75.715582	40.071429
Average scores were used for ties.					

Kruskal-Wallis Test	
Chi-Square	10.7119
DF	3
Pr > Chi-Square	**0.0134**

The NPAR1WAY Procedure

Analysis of Variance for Variable Perimeter Classified by Variable Protein		
Protein	**N**	**Mean**
FN	25	307.089508
Coll1	8	435.192863
BSA	30	247.996376
NLBSA	14	257.026971

Source	DF	Sum of Squares	Mean Square	F Value	Pr > F
Among	3	243869.686550	81289.89552	7.6841	0.0002
Within	73	772260.582011	10578.91208		
Average scores were used for ties.					

Center celltype protein

The NPAR1WAY Procedure

Wilcoxon Scores (Rank Sums) for Variable Perimeter Classified by Variable Protein					
Protein	**N**	**Sum of Scores**	**Expected Under H0**	**Std Dev Under H0**	**Mean Score**
FN	25	1057.0	975.0	91.922673	42.280000
Coll1	8	520.0	312.0	59.899129	65.000000
BSA	30	940.0	1170.0	95.732748	31.333333
NLBSA	14	486.0	546.0	75.715582	34.714286
Average scores were used for ties.					

Kruskal-Wallis Test	
Chi-Square	15.3799
DF	3
Pr > Chi-Square	**0.0015**

The NPAR1WAY Procedure

Analysis of Variance for Variable RatioPA Classified by Variable Protein		
Protein	**N**	**Mean**
FN	25	0.234389
Coll1	8	0.181493
BSA	30	0.211341
NLBSA	14	0.176370

Source	**DF**	**Sum of Squares**	**Mean Square**	**F Value**	**Pr > F**
Among	3	0.037228	0.012409	1.1770	0.3244
Within	73	0.769625	0.010543		
Average scores were used for ties.					

This analysis is related to the Ratio of Perimeter to Area.

The NPAR1WAY Procedure

Wilcoxon Scores (Rank Sums) for Variable RatioPA Classified by Variable Protein					
Protein	**N**	**Sum of Scores**	**Expected Under H0**	**Std Dev Under H0**	**Mean Score**
FN	25	1038.0	975.0	91.922673	41.520000
Coll1	8	269.0	312.0	59.899129	33.625000
BSA	30	1254.0	1170.0	95.732748	41.800000
NLBSA	14	442.0	546.0	75.715582	31.571429
Average scores were used for ties.					

Kruskal-Wallis Test	
Chi-Square	2.7926
DF	3
Pr > Chi-Square	0.4247

The NPAR1WAY Procedure

Analysis of Variance for Variable RatioAP Classified by Variable Protein		
Protein	**N**	**Mean**
FN	25	5.256107
Coll1	8	5.848150
BSA	30	6.176070
NLBSA	14	6.316460

Source	DF	Sum of Squares	Mean Square	F Value	Pr > F
Among	3	15.026275	5.008758	0.4737	0.7016
Within	73	771.955608	10.574734		
Average scores were used for ties.					

This analysis is related to the Ratio of Area to Perimeter.

The NPAR1WAY Procedure

Wilcoxon Scores (Rank Sums) for Variable RatioAP Classified by Variable Protein					
Protein	**N**	**Sum of Scores**	**Expected Under H0**	**Std Dev Under H0**	**Mean Score**
FN	25	912.0	975.0	91.922673	36.480000
Coll1	8	355.0	312.0	59.899129	44.375000
BSA	30	1086.0	1170.0	95.732748	36.200000
NLBSA	14	650.0	546.0	75.715582	46.428571
Average scores were used for ties.					

Kruskal-Wallis Test	
Chi-Square	2.7926
DF	3
Pr > Chi-Square	0.4247

The NPAR1WAY Procedure

Analysis of Variance for Variable RatioAPSquare Classified by Variable Protein		
Protein	**N**	**Mean**
FN	25	0.021260
Coll1	8	0.014281
BSA	30	0.030205
NLBSA	14	0.026237

Source	**DF**	**Sum of Squares**	**Mean Square**	**F Value**	**Pr > F**
Among	3	0.002102	0.000701	1.7039	0.1737
Within	73	0.030024	0.000411		
Average scores were used for ties.					

This analysis is related to the Ratio of Area to Square of the Perimeter.

The NPAR1WAY Procedure

Wilcoxon Scores (Rank Sums) for Variable RatioAPSquare Classified by Variable Protein					
Protein	**N**	**Sum of Scores**	**Expected Under H0**	**Std Dev Under H0**	**Mean Score**
FN	25	836.0	975.0	91.922673	33.440000
Coll1	8	191.0	312.0	59.899129	23.875000
BSA	30	1308.0	1170.0	95.732748	43.600000
NLBSA	14	668.0	546.0	75.715582	47.714286
Average scores were used for ties.					

Kruskal-Wallis Test	
Chi-Square	8.5934
DF	3
Pr > Chi-Square	**0.0352**

The NPAR1WAY Procedure

Analysis of Variance for Variable Area Classified by Variable GroupProtein		
GroupProtein	**N**	**Mean**
UCHCFN	25	1565.91264
UCHCColl	8	2494.81800
UCHCBSA	5	2493.96240
WPIBSA	25	1291.91148
WPINLBSA	14	1607.49793

Source	DF	Sum of Squares	Mean Square	F Value	Pr > F
Among	4	12672995.55403	3168248.889	4.5741	0.0024
Within	72	49870559.61483	692646.661		
Average scores were used for ties.					

There is a significant differenc in the whole pot of them

The NPAR1WAY Procedure

Wilcoxon Scores (Rank Sums) for Variable Area Classified by Variable GroupProtein					
GroupProtein	**N**	**Sum of Scores**	**Expected Under H0**	**Std Dev Under H0**	**Mean Score**
UCHCFN	25	963.0	975.0	91.922673	38.520000
UCHCColl	8	495.0	312.0	59.899129	61.875000
UCHCBSA	5	248.0	195.0	48.372911	49.600000
WPIBSA	25	736.0	975.0	91.922673	29.440000
WPINLBSA	14	561.0	546.0	75.715582	40.071429
Average scores were used for ties.					

Kruskal-Wallis Test	
Chi-Square	14.0955
DF	4
Pr > Chi-Square	**0.0070**

The NPAR1WAY Procedure

Analysis of Variance for Variable Perimeter Classified by Variable GroupProtein		
GroupProtein	**N**	**Mean**
UCHCFN	25	307.089508
UCHCColl	8	435.192863
UCHCBSA	5	168.272034
WPIBSA	25	263.941244
WPINLBSA	14	257.026971

Source	DF	Sum of Squares	Mean Square	F Value	Pr > F
Among	4	282005.510475	70501.37762	6.9145	<.0001
Within	72	734124.758086	10196.17720		
Average scores were used for ties.					

The NPAR1WAY Procedure

Wilcoxon Scores (Rank Sums) for Variable Perimeter Classified by Variable GroupProtein					
GroupProtein	**N**	**Sum of Scores**	**Expected Under H0**	**Std Dev Under H0**	**Mean Score**
UCHCFN	25	1057.0	975.0	91.922673	42.280000
UCHCColl	8	520.0	312.0	59.899129	65.000000
UCHCBSA	5	75.0	195.0	48.372911	15.000000
WPIBSA	25	865.0	975.0	91.922673	34.600000
WPINLBSA	14	486.0	546.0	75.715582	34.714286
Average scores were used for ties.					

Kruskal-Wallis Test	
Chi-Square	18.5781
DF	4
Pr > Chi-Square	**0.0010**

The NPAR1WAY Procedure

Analysis of Variance for Variable RatioPA Classified by Variable GroupProtein		
GroupProtein	**N**	**Mean**
UCHCFN	25	0.234389
UCHCColl	8	0.181493
UCHCBSA	5	0.085315
WPIBSA	25	0.236546
WPINLBSA	14	0.176370

Source	DF	Sum of Squares	Mean Square	F Value	Pr > F
Among	4	0.132523	0.033131	3.5375	0.0108
Within	72	0.674330	0.009366		
Average scores were used for ties.					

The NPAR1WAY Procedure

Wilcoxon Scores (Rank Sums) for Variable RatioPA Classified by Variable GroupProtein					
GroupProtein	**N**	**Sum of Scores**	**Expected Under H0**	**Std Dev Under H0**	**Mean Score**
UCHCFN	25	1038.0	975.0	91.922673	41.520000
UCHCColl	8	269.0	312.0	59.899129	33.625000
UCHCBSA	5	24.0	195.0	48.372911	4.800000
WPIBSA	25	1230.0	975.0	91.922673	49.200000
WPINLBSA	14	442.0	546.0	75.715582	31.571429
Average scores were used for ties.					

Kruskal-Wallis Test	
Chi-Square	19.2046
DF	4
Pr > Chi-Square	**0.0007**

The NPAR1WAY Procedure

Analysis of Variance for Variable RatioAP Classified by Variable GroupProtein		
GroupProtein	**N**	**Mean**
UCHCFN	25	5.256107
UCHCColl	8	5.848150
UCHCBSA	5	13.586055
WPIBSA	25	4.694073
WPINLBSA	14	6.316460

Source	DF	Sum of Squares	Mean Square	F Value	Pr > F
Among	4	344.473514	86.118378	14.0122	<.0001
Within	72	442.508368	6.145950		
Average scores were used for ties.					

The NPAR1WAY Procedure

Wilcoxon Scores (Rank Sums) for Variable RatioAP Classified by Variable GroupProtein					
GroupProtein	**N**	**Sum of Scores**	**Expected Under H0**	**Std Dev Under H0**	**Mean Score**
UCHCFN	25	912.0	975.0	91.922673	36.480000
UCHCColl	8	355.0	312.0	59.899129	44.375000
UCHCBSA	5	366.0	195.0	48.372911	73.200000
WPIBSA	25	720.0	975.0	91.922673	28.800000
WPINLBSA	14	650.0	546.0	75.715582	46.428571
Average scores were used for ties.					

Kruskal-Wallis Test	
Chi-Square	19.2046
DF	4
Pr > Chi-Square	**0.0007**

The NPAR1WAY Procedure

Analysis of Variance for Variable RatioAPSquare Classified by Variable GroupProtein		
GroupProtein	**N**	**Mean**
UCHCFN	25	0.021260
UCHCColl	8	0.014281
UCHCBSA	5	0.083321
WPIBSA	25	0.019582
WPINLBSA	14	0.026237

Source	DF	Sum of Squares	Mean Square	F Value	Pr > F
Among	4	0.019030	0.004758	26.1550	<.0001
Within	72	0.013097	0.000182		
Average scores were used for ties.					

The NPAR1WAY Procedure

Wilcoxon Scores (Rank Sums) for Variable RatioAPSquare Classified by Variable GroupProtein					
GroupProtein	**N**	**Sum of Scores**	**Expected Under H0**	**Std Dev Under H0**	**Mean Score**
UCHCFN	25	836.0	975.0	91.922673	33.440000
UCHCColl	8	191.0	312.0	59.899129	23.875000
UCHCBSA	5	373.0	195.0	48.372911	74.600000
WPIBSA	25	935.0	975.0	91.922673	37.400000
WPINLBSA	14	668.0	546.0	75.715582	47.714286
Average scores were used for ties.					

Kruskal-Wallis Test	
Chi-Square	20.1142
DF	4
Pr > Chi-Square	**0.0005**

The GLM Procedure

Class Level Information		
Class	**Levels**	**Values**
Center	2	UCHC WPI
CellType	2	attached single
Protein	4	BSA Coll1 FN NLBSA

Number of Observations Read	77
Number of Observations Used	77

The GLM Procedure

Dependent Variable: RatioPA

Source	DF	Sum of Squares	Mean Square	F Value	Pr > F
Model	5	0.14106067	0.02821213	3.01	0.0161
Error	71	0.66579233	0.00937736		
Corrected Total	76	0.80685300			

R-Square	Coeff Var	Root MSE	RatioPA Mean
0.174828	46.25266	0.096837	0.209365

Source	DF	Type III SS	Mean Square	F Value	Pr > F
Center	1	0.09529521	0.09529521	10.16	**0.0021**
CellType	1	0.00853731	0.00853731	0.91	0.3432
Protein	3	0.10298184	0.03432728	3.66	**0.0163**

The GLM Procedure

Tukey's Studentized Range (HSD) Test for RatioPA

Note: This test controls the Type I experimentwise error rate.

Alpha	0.05
Error Degrees of Freedom	71
Error Mean Square	0.009377
Critical Value of Studentized Range	3.72071

Comparisons significant at the 0.05 level are indicated by *.**				
Protein Comparison	**Difference Between Means**	**Simultaneous 95% Confidence Limits**		
FN - BSA	0.02305	-0.04594	0.09204	
FN - Coll1	0.05290	-0.05059	0.15638	
FN - NLBSA	0.05802	-0.02703	0.14306	
BSA - FN	-0.02305	-0.09204	0.04594	
BSA - Coll1	0.02985	-0.07153	0.13122	
BSA - NLBSA	0.03497	-0.04749	0.11743	
Coll1 - FN	-0.05290	-0.15638	0.05059	
Coll1 - BSA	-0.02985	-0.13122	0.07153	
Coll1 - NLBSA	0.00512	-0.10779	0.11804	
NLBSA - FN	-0.05802	-0.14306	0.02703	
NLBSA - BSA	-0.03497	-0.11743	0.04749	
NLBSA - Coll1	-0.00512	-0.11804	0.10779	

10:16 Thursday, December 04, 2014 **43**

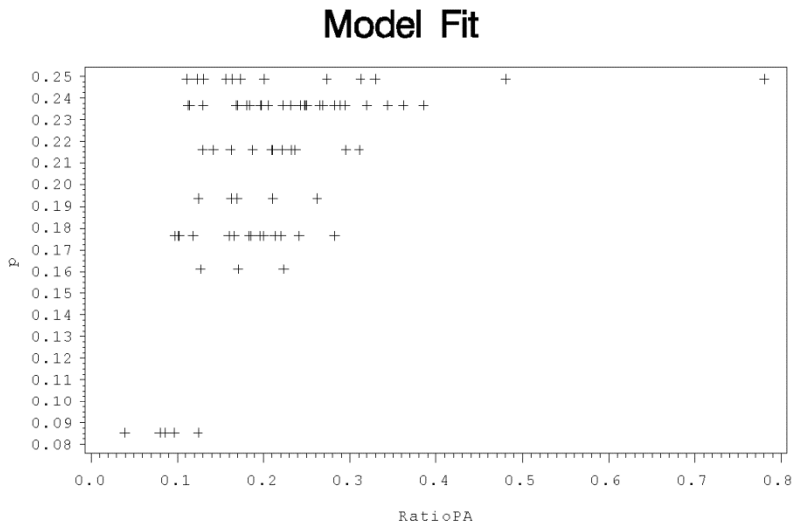

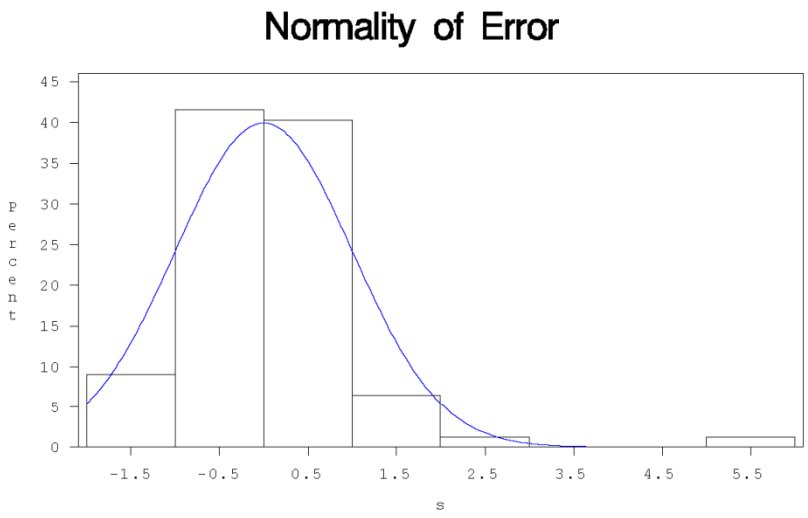
Normality of Error
percent
45
40
35
30
25
20
15
10
5
0
-1.5
-0.5
0.5
1.5
2.5
3.5
4.5
5.5
s

Normality of Error

The UNIVARIATE Procedure
Fitted Distribution for s

Parameters for Normal Distribution		
Parameter	**Symbol**	**Estimate**
Mean	Mu	0.00006
Std Dev	Sigma	0.999099

Goodness-of-Fit Tests for Normal Distribution				
Test	**Statistic**		**p Value**	
Kolmogorov-Smirnov	**D**	0.11053877	**Pr > D**	0.020
Cramer-von Mises	**W-Sq**	0.24289759	**Pr > W-Sq**	<0.005
Anderson-Darling	**A-Sq**	1.78414844	**Pr > A-Sq**	<0.005

Quantiles for Normal Distribution		
	Quantile	
Percent	**Observed**	**Estimated**
1.0	-1.46584	-2.32419
5.0	-1.29935	-1.64331
10.0	-0.98187	-1.28034
25.0	-0.61870	-0.67382
50.0	-0.05796	0.00006
75.0	0.39944	0.67394
90.0	0.87656	1.28046
95.0	1.32048	1.64343
99.0	5.67246	2.32431

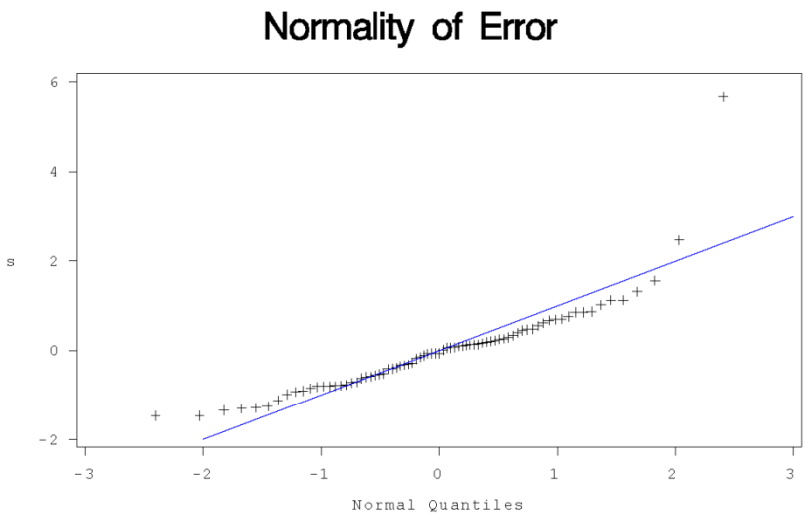
Normality of Error
6
4
2
0
-2
s
-3
-2
-1
0
1
2
3
Normal Quantiles

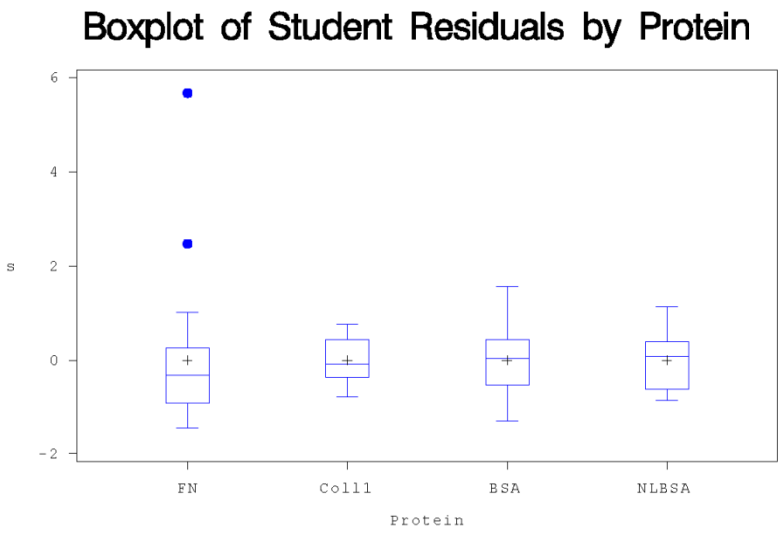
Boxplot of Student Residuals by Protein
s
6
4
2
0
-2
FN
Coll1
BSA
NLBSA
Protein

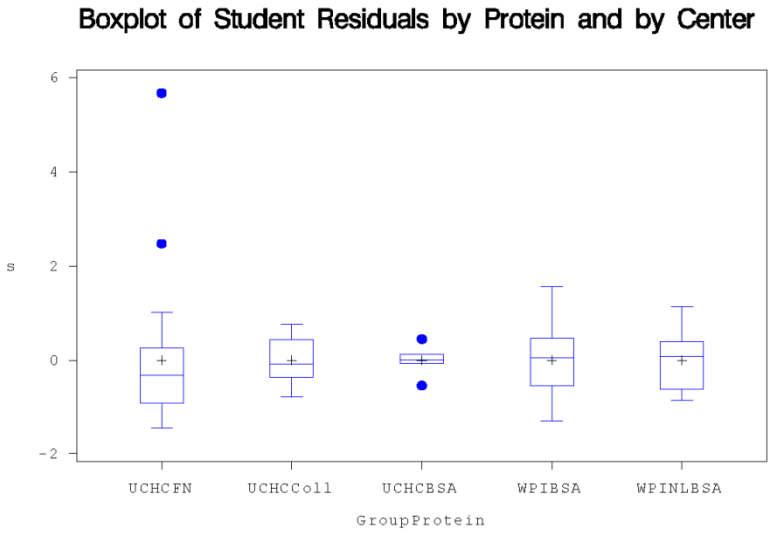
Boxplot of Student Residuals by Protein and by Center
s
6
4
2
0
-2
UCHCFN
UCHCColl
UCHCBSA
WPIBSA
WPINLBSA
GroupProtein

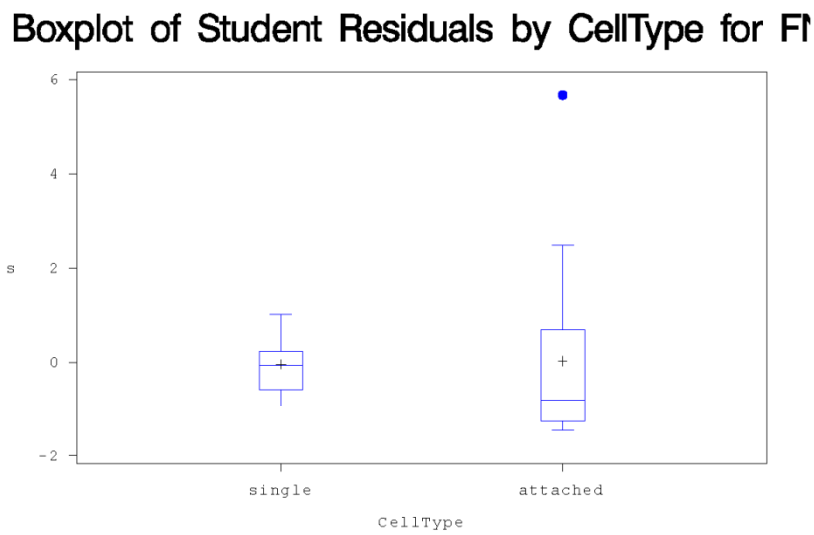
Boxplot of Student Residuals by CellType for Fl
6
4
2
0
-2
s
single
attached
CellType

The GLM Procedure

Class Level Information		
Class	**Levels**	**Values**
Center	2	UCHC WPI
CellType	2	attached single
Protein	4	BSA Coll1 FN NLBSA

Number of Observations Read	77
Number of Observations Used	77

The GLM Procedure

Dependent Variable: RatioAPSquare

Source	DF	Sum of Squares	Mean Square	F Value	Pr > F
Model	5	0.01934964	0.00386993	21.50	<.0001
Error	71	0.01277717	0.00017996		
Corrected Total	76	0.03212681			

R-Square	Coeff Var	Root MSE	RatioAPSquare Mean
0.602289	53.82111	0.013415	0.024925

Source	DF	Type III SS	Mean Square	F Value	Pr > F
Center	1	0.01692774	0.01692774	94.06	**<.0001**
CellType	1	0.00031947	0.00031947	1.78	0.1870
Protein	3	0.01735210	0.00578403	32.14	**<.0001**

This is also referenced as the isoperimetric quotient in the text.

The GLM Procedure

Tukey's Studentized Range (HSD) Test for RatioAPSquare

Note: This test controls the Type I experimentwise error rate.

Alpha	0.05
Error Degrees of Freedom	71
Error Mean Square	0.00018
Critical Value of Studentized Range	3.72071

Comparisons significant at the 0.05 level are indicated by *.**				
Protein Comparison	**Difference Between Means**	**Simultaneous 95% Confidence Limits**		
BSA - NLBSA	0.003968	-0.007456	0.015391	
BSA - FN	0.008944	-0.000613	0.018502	
BSA - Coll1	0.015924	0.001880	0.029967	***
NLBSA - BSA	-0.003968	-0.015391	0.007456	
NLBSA - FN	0.004976	-0.006805	0.016758	
NLBSA - Coll1	0.011956	-0.003687	0.027598	
FN - BSA	-0.008944	-0.018502	0.000613	
FN - NLBSA	-0.004976	-0.016758	0.006805	
FN - Coll1	0.006979	-0.007357	0.021316	
Coll1 - BSA	-0.015924	-0.029967	-0.001880	***
Coll1 - NLBSA	-0.011956	-0.027598	0.003687	
Coll1 - FN	-0.006979	-0.021316	0.007357	

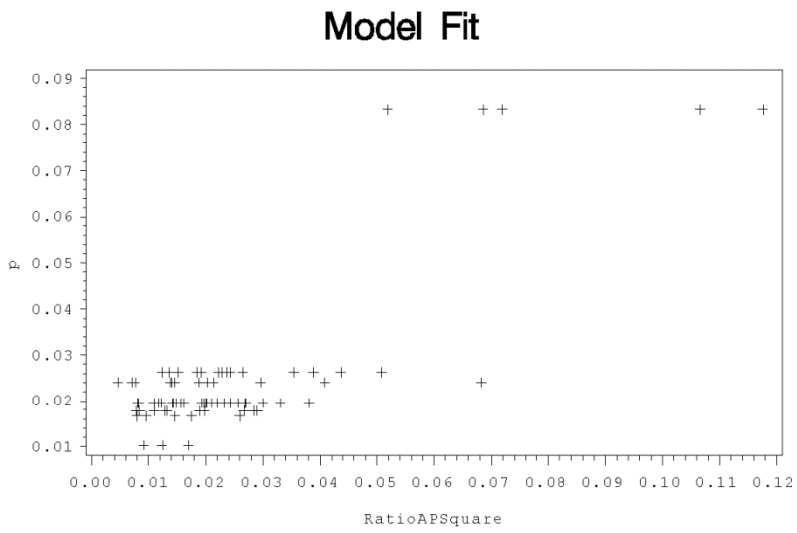
Model Fit
p
0.09
0.08
0.07
0.06
0.05
0.04
0.03
0.02
0.01
0.00 0.01 0.02 0.03 0.04 0.05 0.06 0.07 0.08 0.09 0.10 0.11 0.12
RatioAPSquare

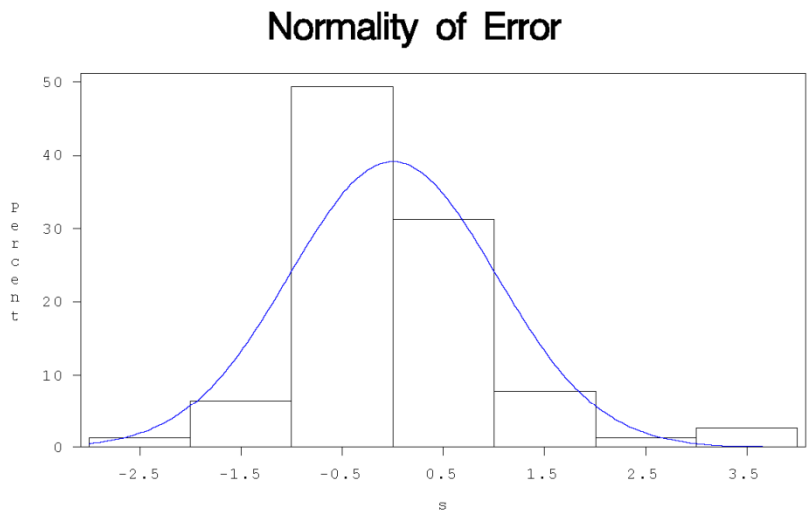
Normality of Error
50
40
30
20
10
0
Percent
-2.5
-1.5
-0.5
0.5
1.5
2.5
3.5
s

Normality of Error

The UNIVARIATE Procedure
Fitted Distribution for s

Parameters for Normal Distribution		
Parameter	**Symbol**	**Estimate**
Mean	Mu	0.000086
Std Dev	Sigma	1.019754

Goodness-of-Fit Tests for Normal Distribution				
Test	**Statistic**		**p Value**	
Kolmogorov-Smirnov	**D**	0.12913257	**Pr > D**	<0.010
Cramer-von Mises	**W-Sq**	0.31871365	**Pr > W-Sq**	<0.005
Anderson-Darling	**A-Sq**	1.98506433	**Pr > A-Sq**	<0.005

Quantiles for Normal Distribution		
	Quantile	
Percent	**Observed**	**Estimated**
1.0	-2.62139	-2.37222
5.0	-1.26013	-1.67726
10.0	-0.95012	-1.30678
25.0	-0.59587	-0.68773
50.0	-0.20103	0.00009
75.0	0.46836	0.68790
90.0	1.29845	1.30695
95.0	1.94487	1.67743
99.0	3.40921	2.37239

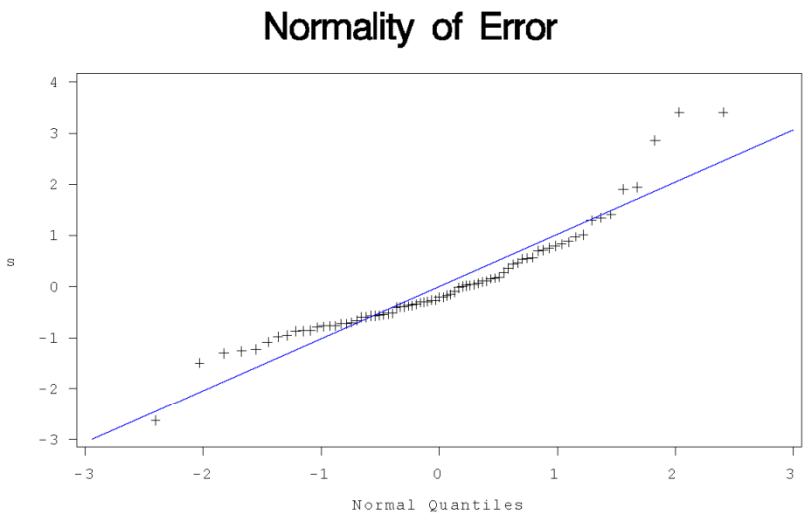
Normality of Error
s
4
3
2
1
0
-1
-2
-3
-3
-2
-1
0
1
2
3
Normal Quantiles

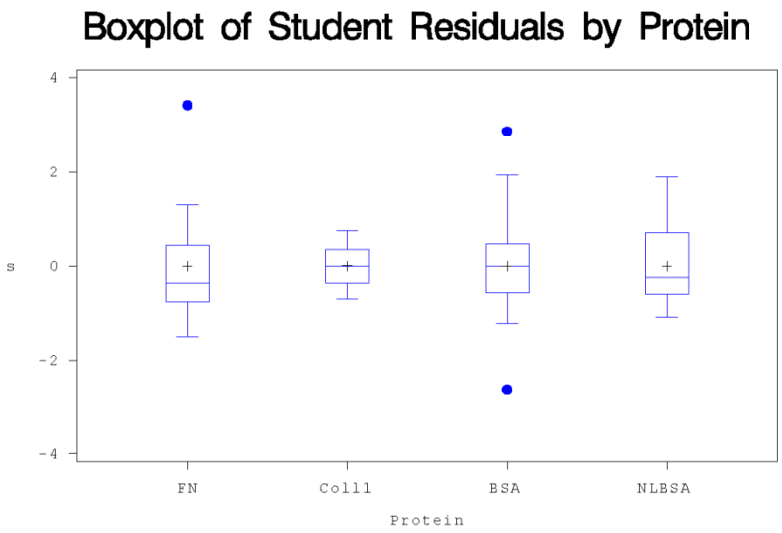
Boxplot of Student Residuals by Protein
s
4
2
0
-2
-4
FN
Coll1
BSA
NLBSA
Protein

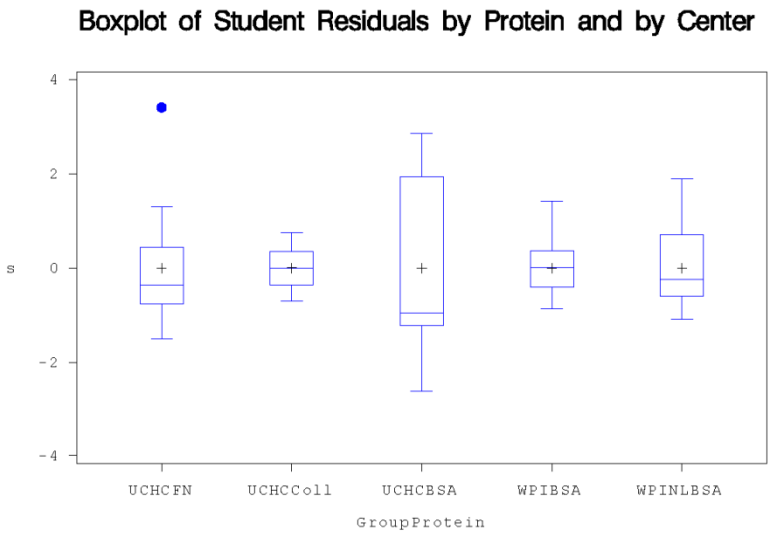
Boxplot of Student Residuals by Protein and by Center
s
4
2
0
-2
-4
UCHCFN
UCHCColl
UCHCBSA
WPIBSA
WPINLBSA
GroupProtein

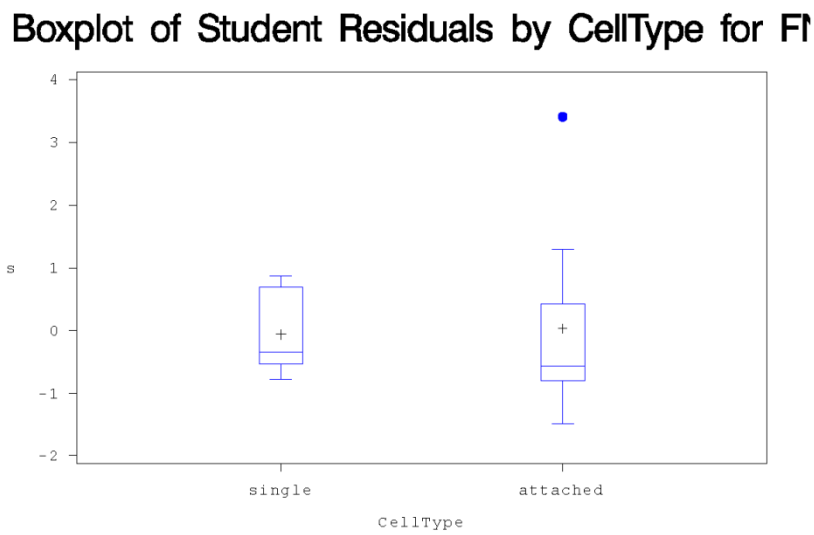
Boxplot of Student Residuals by CellType for Fl
4
3
2
s 1
0
-1
-2
single
attached
CellType

The GLM Procedure

Class Level Information		
Class	**Levels**	**Values**
Center	2	UCHC WPI
CellType	2	attached single
Protein	4	BSA Coll1 FN NLBSA

Number of Observations Read	77
Number of Observations Used	77

10:16 Thursday, December 04, 2014 **61**

The GLM Procedure

Dependent Variable: logAPS

Source	DF	Sum of Squares	Mean Square	F Value	Pr > F
Model	5	12.47620398	2.49524080	9.59	<.0001
Error	71	18.46677814	0.26009547		
Corrected Total	76	30.94298212			

R-Square	Coeff Var	Root MSE	logAPS Mean
0.403200	13.02099	0.509996	3.916718

Source	DF	Type III SS	Mean Square	F Value	Pr > F
Center	1	9.14141045	9.14141045	35.15	**<.0001**
CellType	1	0.20335322	0.20335322	0.78	0.3796
Protein	3	11.62846302	3.87615434	14.90	**<.0001**

This analysis is related to the log of the Ratio of Area by the Square of the Perimeter.

The GLM Procedure

Tukey's Studentized Range (HSD) Test for logAPS

Note: This test controls the Type I experimentwise error rate.

Alpha	0.05
Error Degrees of Freedom	71
Error Mean Square	0.260095
Critical Value of Studentized Range	3.72071

Comparisons significant at the 0.05 level are indicated by *.**

Protein Comparison	Difference Between Means	Simultaneous 95% Confidence Limits		
Coll1 - FN	0.2433	-0.3017	0.7884	
Coll1 - BSA	0.5554	0.0215	1.0893	***
Coll1 - NLBSA	0.5916	-0.0030	1.1863	
FN - Coll1	-0.2433	-0.7884	0.3017	
FN - BSA	0.3121	-0.0513	0.6754	
FN - NLBSA	0.3483	-0.0996	0.7962	
BSA - Coll1	-0.5554	-1.0893	-0.0215	***
BSA - FN	-0.3121	-0.6754	0.0513	
BSA - NLBSA	0.0363	-0.3980	0.4706	
NLBSA - Coll1	-0.5916	-1.1863	0.0030	
NLBSA - FN	-0.3483	-0.7962	0.0996	
NLBSA - BSA	-0.0363	-0.4706	0.3980	

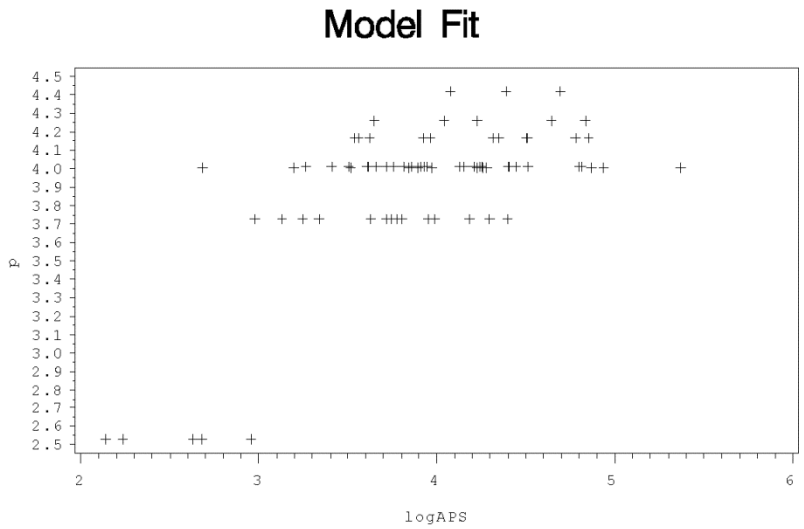
Model Fit
p
4.5
4.4
4.3
4.2
4.1
4.0
3.9
3.8
3.7
3.6
3.5
3.4
3.3
3.2
3.1
3.0
2.9
2.8
2.7
2.6
2.5
2
3
4
5
6
logAPS

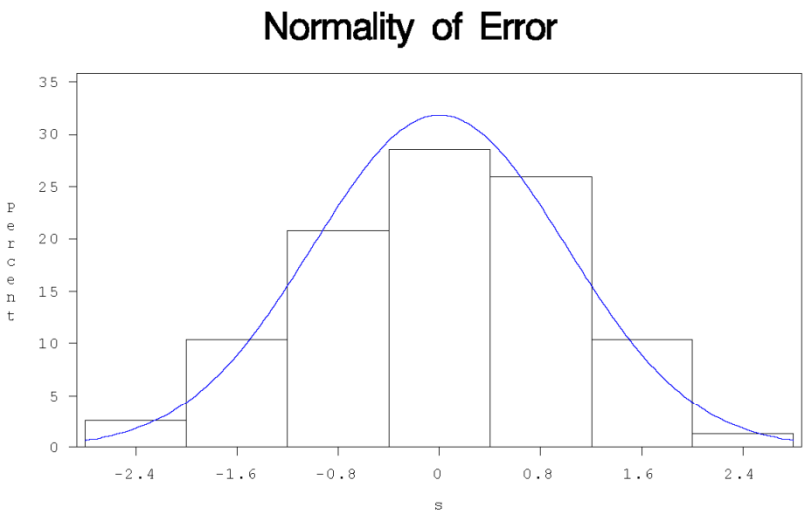
Normality of Error
Percent
35
30
25
20
15
10
5
0
-2.4
-1.6
-0.8
0
0.8
1.6
2.4
s

Normality of Error

The UNIVARIATE Procedure
Fitted Distribution for s

Parameters for Normal Distribution		
Parameter	**Symbol**	**Estimate**
Mean	Mu	-0.00003
Std Dev	Sigma	1.002851

Goodness-of-Fit Tests for Normal Distribution				
Test	**Statistic**		**p Value**	
Kolmogorov-Smirnov	**D**	0.04297258	**Pr > D**	>0.150
Cramer-von Mises	**W-Sq**	0.01963656	**Pr > W-Sq**	>0.250
Anderson-Darling	**A-Sq**	0.16882735	**Pr > A-Sq**	>0.250

Quantiles for Normal Distribution		
	Quantile	
Percent	**Observed**	**Estimated**
1.0	-2.67988	-2.33301
5.0	-1.52526	-1.64957
10.0	-1.23715	-1.28523
25.0	-0.70316	-0.67644
50.0	-0.02463	-0.00003
75.0	0.59061	0.67638
90.0	1.25415	1.28518
95.0	1.60538	1.64951
99.0	2.76618	2.33295

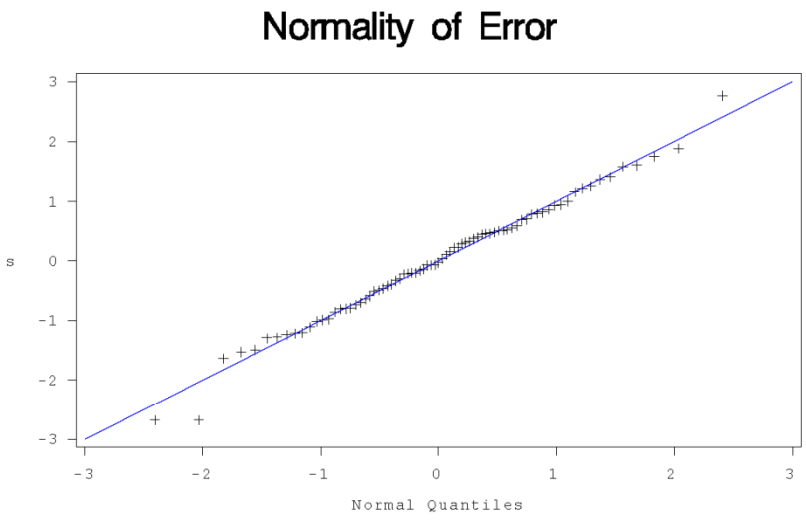
Normality of Error
s
3
2
1
0
-1
-2
-3
-3
-2
-1
0
1
2
3
Normal Quantiles

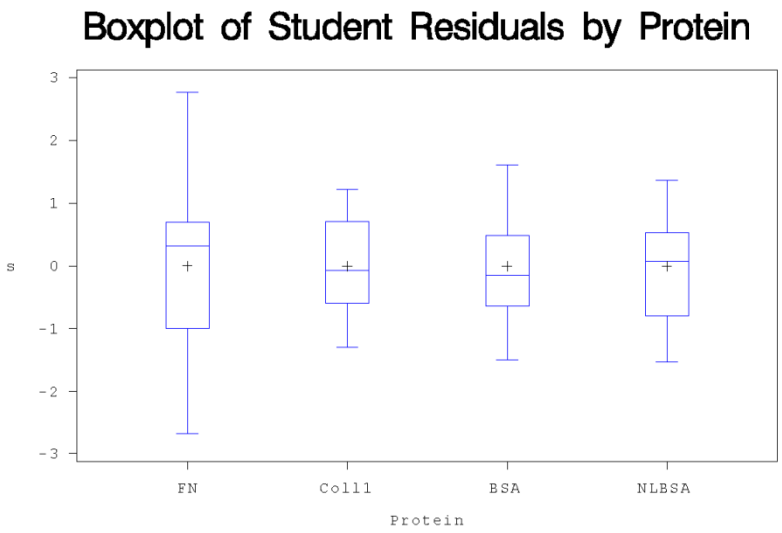
Boxplot of Student Residuals by Protein
s
3
2
1
0
-1
-2
-3
FN
Coll1
BSA
NLBSA
Protein

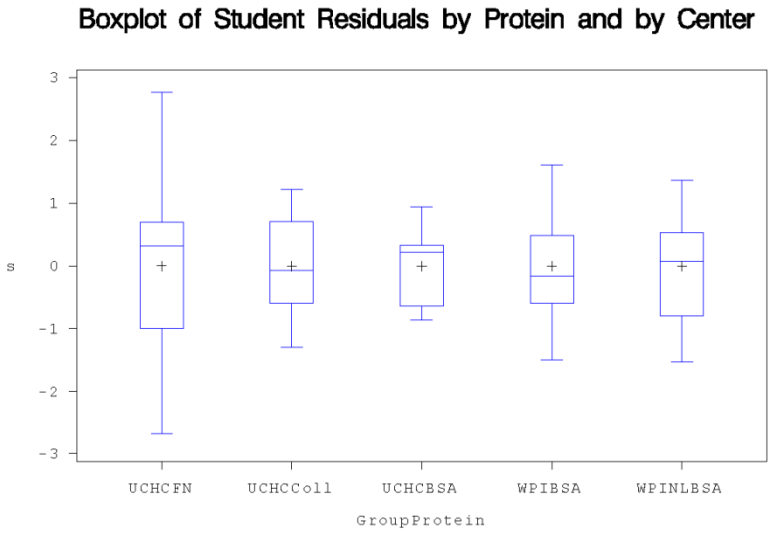
Boxplot of Student Residuals by Protein and by Center
s
3
2
1
0
-1
-2
-3
UCHCFN
UCHCColl
UCHCBSA
WPIBSA
WPINLBSA
GroupProtein

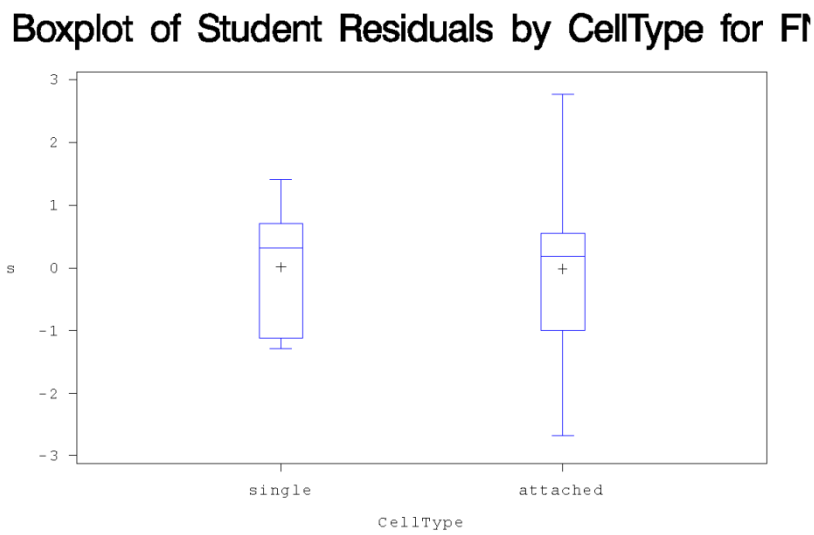
Boxplot of Student Residuals by CellType for Fl
3
2
1
s 0
-1
-2
-3
single
attached
CellType

Appendix B:

I wish to acknowledge the following publishers for their permission to reprint (adapt) for the following works below.

Chapter 2: American Chemical Society
Basu S, Cunningham LP, Pins GD, Bush KA, Taboada R, Howell AR, Wang J, Campagnola PJ., Multiphoton excited fabrication of collagen matrixes cross-linked by a modified benzophenone dimer: bioactivity and enzymatic degradation., Biomacromolecules. 2005 May-Jun;6(3):1465-74.

Chapter 3: John Wiley and Sons
Pins GD, Bush KA, Cunningham LP, Campagnola PJ., Multiphoton excited fabricated nano and micro patterned extracellular matrix proteins direct cellular morphology., J Biomed Mater Res A. 2006 Jul;78(1):194-204.

Chapter 5: The Optics Society
Cunningham LP, Veilleux MP, Campagnola PJ., Freeform multiphoton excited microfabrication for biological applications using a rapid prototyping CAD-based approach. Optics Express, 2006 Sep 18;14(19):8613-21.

Copyright permissions are provided from the three publishers whose publications are used in this work. Note that each permission references its respective citation.

PERMISSION/LICENSE IS GRANTED FOR YOUR ORDER AT NO CHARGE

This type of permission/license, instead of the standard Terms & Conditions, is sent to you because no fee is being charged for your order. Please note the following:

- Permission is granted for your request in both print and electronic formats, and translations.
- If figures and/or tables were requested, they may be adapted or used in part.
- Please print this page for your records and send a copy of it to your publisher/graduate school.
- Appropriate credit for the requested material should be given as follows: "Reprinted (adapted) with permission from (COMPLETE REFERENCE CITATION). Copyright (YEAR) American Chemical Society." Insert appropriate information in place of the capitalized words.
- One-time permission is granted only for the use specified in your request. No additional uses are granted (such as derivative works or other editions). For any other uses, please submit a new request.

BACK CLOSE WINDOW

JOHN WILEY AND SONS LICENSE TERMS AND CONDITIONS

Oct 31, 2014

This is a License Agreement between Lawrence P Cunningham ("You") and John Wiley and Sons ("John Wiley and Sons") provided by Copyright Clearance Center ("CCC"). The license consists of your order details, the terms and conditions provided by John Wiley and Sons, and the payment terms and conditions.

All payments must be made in full to CCC. For payment instructions, please see information listed at the bottom of this form.

License Number	3499511152737
License date	Oct 31, 2014
Licensed content publisher	John Wiley and Sons
Licensed content publication	Journal of Biomedical Materials Research
Licensed content title	Multiphoton excited fabricated nano and micro patterned extracellular matrix proteins direct cellular morphology
Licensed copyright line	Copyright © 2006 Wiley Periodicals, Inc.
Licensed content author	George D. Pins,Katie A. Bush,Lawrence P. Cunningham,Paul J. Campagnola
Licensed content date	Apr 24, 2006
Start page	194
End page	204
Type of use	Dissertation/Thesis
Requestor type	Author of this Wiley article
Format	Print and electronic
Portion	Full article
Will you be translating?	No
Title of your thesis / dissertation	Optically Micro-fabricated Linear and Freeform 3-D Extracellular Matrix Scaffolds for Tissue Engineering
Expected completion date	Jan 2015
Expected size (number of pages)	150
Total	0.00 USD
Terms and Conditions	

TERMS AND CONDITIONS

This copyrighted material is owned by or exclusively licensed to John Wiley & Sons, Inc. or one of its group companies (each a"Wiley Company") or handled on behalf of a society with which a Wiley Company has exclusive publishing rights in relation to a particular work (collectively "WILEY"). By clicking □accept□ in connection with completing this licensing transaction, you agree that the following terms and conditions apply to this transaction

(along with the billing and payment terms and conditions established by the Copyright Clearance Center Inc., ("CCC's Billing and Payment terms and conditions"), at the time that you opened your Rightslink account (these are available at any time at http://myaccount.copyright.com).

Terms and Conditions

- The materials you have requested permission to reproduce or reuse (the "Wiley Materials") are protected by copyright.
- You are hereby granted a personal, non-exclusive, non-sub licensable (on a stand-alone basis), non-transferable, worldwide, limited license to reproduce the Wiley Materials for the purpose specified in the licensing process. This license is for a one-time use only and limited to any maximum distribution number specified in the license. The first instance of republication or reuse granted by this licence must be completed within two years of the date of the grant of this licence (although copies prepared before the end date may be distributed thereafter). The Wiley Materials shall not be used in any other manner or for any other purpose, beyond what is granted in the license. Permission is granted subject to an appropriate acknowledgement given to the author, title of the material/book/journal and the publisher. You shall also duplicate the copyright notice that appears in the Wiley publication in your use of the Wiley Material. Permission is also granted on the understanding that nowhere in the text is a previously published source acknowledged for all or part of this Wiley Material. Any third party content is expressly excluded from this permission.
- With respect to the Wiley Materials, all rights are reserved. Except as expressly granted by the terms of the license, no part of the Wiley Materials may be copied, modified, adapted (except for minor reformatting required by the new Publication), translated, reproduced, transferred or distributed, in any form or by any means, and no derivative works may be made based on the Wiley Materials without the prior permission of the respective copyright owner. You may not alter, remove or suppress in any manner any copyright, trademark or other notices displayed by the Wiley Materials. You may not license, rent, sell, loan, lease, pledge, offer as security, transfer or assign the Wiley Materials on a stand-alone basis, or any of the rights granted to you hereunder to any other person.
- The Wiley Materials and all of the intellectual property rights therein shall at all times remain the exclusive property of John Wiley & Sons Inc, the Wiley Companies, or their respective licensors, and your interest therein is only that of having possession of and the right to reproduce the Wiley Materials pursuant to Section 2 herein during the continuance of this Agreement. You agree that you own no right, title or interest in or to the Wiley Materials or any of the intellectual property rights therein. You shall have no rights hereunder other than the license as provided for above in Section 2. No right, license or interest to any trademark, trade name, service mark or other branding ("Marks") of WILEY or its licensors is granted hereunder, and you agree that you shall not assert any such right, license or interest with respect thereto.
- NEITHER WILEY NOR ITS LICENSORS MAKES ANY WARRANTY OR REPRESENTATION OF ANY KIND TO YOU OR ANY THIRD PARTY,

EXPRESS, IMPLIED OR STATUTORY, WITH RESPECT TO THE MATERIALS OR THE ACCURACY OF ANY INFORMATION CONTAINED IN THE MATERIALS, INCLUDING, WITHOUT LIMITATION, ANY IMPLIED WARRANTY OF MERCHANTABILITY, ACCURACY, SATISFACTORY QUALITY, FITNESS FOR A PARTICULAR PURPOSE, USABILITY, INTEGRATION OR NON-INFRINGEMENT AND ALL SUCH WARRANTIES ARE HEREBY EXCLUDED BY WILEY AND ITS LICENSORS AND WAIVED BY YOU

- WILEY shall have the right to terminate this Agreement immediately upon breach of this Agreement by you.
- You shall indemnify, defend and hold harmless WILEY, its Licensors and their respective directors, officers, agents and employees, from and against any actual or threatened claims, demands, causes of action or proceedings arising from any breach of this Agreement by you.
- IN NO EVENT SHALL WILEY OR ITS LICENSORS BE LIABLE TO YOU OR ANY OTHER PARTY OR ANY OTHER PERSON OR ENTITY FOR ANY SPECIAL, CONSEQUENTIAL, INCIDENTAL, INDIRECT, EXEMPLARY OR PUNITIVE DAMAGES, HOWEVER CAUSED, ARISING OUT OF OR IN CONNECTION WITH THE DOWNLOADING, PROVISIONING, VIEWING OR USE OF THE MATERIALS REGARDLESS OF THE FORM OF ACTION, WHETHER FOR BREACH OF CONTRACT, BREACH OF WARRANTY, TORT, NEGLIGENCE, INFRINGEMENT OR OTHERWISE (INCLUDING, WITHOUT LIMITATION, DAMAGES BASED ON LOSS OF PROFITS, DATA, FILES, USE, BUSINESS OPPORTUNITY OR CLAIMS OF THIRD PARTIES), AND WHETHER OR NOT THE PARTY HAS BEEN ADVISED OF THE POSSIBILITY OF SUCH DAMAGES. THIS LIMITATION SHALL APPLY NOTWITHSTANDING ANY FAILURE OF ESSENTIAL PURPOSE OF ANY LIMITED REMEDY PROVIDED HEREIN.
- Should any provision of this Agreement be held by a court of competent jurisdiction to be illegal, invalid, or unenforceable, that provision shall be deemed amended to achieve as nearly as possible the same economic effect as the original provision, and the legality, validity and enforceability of the remaining provisions of this Agreement shall not be affected or impaired thereby.
- The failure of either party to enforce any term or condition of this Agreement shall not constitute a waiver of either party's right to enforce each and every term and condition of this Agreement. No breach under this agreement shall be deemed waived or excused by either party unless such waiver or consent is in writing signed by the party granting such waiver or consent. The waiver by or consent of a party to a breach of any provision of this Agreement shall not operate or be construed as a waiver of or consent to any other or subsequent breach by such other party.
- This Agreement may not be assigned (including by operation of law or otherwise) by you without WILEY's prior written consent.
- Any fee required for this permission shall be non-refundable after thirty (30) days

from receipt by the CCC.

- These terms and conditions together with CCC□s Billing and Payment terms and conditions (which are incorporated herein) form the entire agreement between you and WILEY concerning this licensing transaction and (in the absence of fraud) supersedes all prior agreements and representations of the parties, oral or written. This Agreement may not be amended except in writing signed by both parties. This Agreement shall be binding upon and inure to the benefit of the parties' successors, legal representatives, and authorized assigns.
- In the event of any conflict between your obligations established by these terms and conditions and those established by CCC□s Billing and Payment terms and conditions, these terms and conditions shall prevail.
- WILEY expressly reserves all rights not specifically granted in the combination of (i) the license details provided by you and accepted in the course of this licensing transaction, (ii) these terms and conditions and (iii) CCC□s Billing and Payment terms and conditions.
- This Agreement will be void if the Type of Use, Format, Circulation, or Requestor Type was misrepresented during the licensing process.
- This Agreement shall be governed by and construed in accordance with the laws of the State of New York, USA, without regards to such state□s conflict of law rules. Any legal action, suit or proceeding arising out of or relating to these Terms and Conditions or the breach thereof shall be instituted in a court of competent jurisdiction in New York County in the State of New York in the United States of America and each party hereby consents and submits to the personal jurisdiction of such court, waives any objection to venue in such court and consents to service of process by registered or certified mail, return receipt requested, at the last known address of such party.

WILEY OPEN ACCESS TERMS AND CONDITIONS

Wiley Publishes Open Access Articles in fully Open Access Journals and in Subscription journals offering Online Open. Although most of the fully Open Access journals publish open access articles under the terms of the Creative Commons Attribution (CC BY) License only, the subscription journals and a few of the Open Access Journals offer a choice of Creative Commons Licenses:: Creative Commons Attribution (CC-BY) license Creative Commons Attribution Non-Commercial (CC-BY-NC) license and Creative Commons Attribution Non-Commercial-NoDerivs (CC-BY-NC-ND) License. The license type is clearly identified on the article.

Copyright in any research article in a journal published as Open Access under a Creative Commons License is retained by the author(s). Authors grant Wiley a license to publish the article and identify itself as the original publisher. Authors also grant any third party the right to use the article freely as long as its integrity is maintained and its original authors, citation details and publisher are identified as follows: [Title of Article/Author/Journal Title and Volume/Issue. Copyright (c) [year] [copyright owner as specified in the Journal]. Links to the final article on Wiley□s website are encouraged where applicable.

The Creative Commons Attribution License

The Creative Commons Attribution License (CC-BY) allows users to copy, distribute and transmit an article, adapt the article and make commercial use of the article. The CC-BY license permits commercial and non-commercial re-use of an open access article, as long as the author is properly attributed.

The Creative Commons Attribution License does not affect the moral rights of authors, including without limitation the right not to have their work subjected to derogatory treatment. It also does not affect any other rights held by authors or third parties in the article, including without limitation the rights of privacy and publicity. Use of the article must not assert or imply, whether implicitly or explicitly, any connection with, endorsement or sponsorship of such use by the author, publisher or any other party associated with the article.

For any reuse or distribution, users must include the copyright notice and make clear to others that the article is made available under a Creative Commons Attribution license, linking to the relevant Creative Commons web page.

To the fullest extent permitted by applicable law, the article is made available as is and without representation or warranties of any kind whether express, implied, statutory or otherwise and including, without limitation, warranties of title, merchantability, fitness for a particular purpose, non-infringement, absence of defects, accuracy, or the presence or absence of errors.

Creative Commons Attribution Non-Commercial License

The Creative Commons Attribution Non-Commercial (CC-BY-NC) License permits use, distribution and reproduction in any medium, provided the original work is properly cited and is not used for commercial purposes.(see below)

Creative Commons Attribution-Non-Commercial-NoDerivs License

The Creative Commons Attribution Non-Commercial-NoDerivs License (CC-BY-NC-ND) permits use, distribution and reproduction in any medium, provided the original work is properly cited, is not used for commercial purposes and no modifications or adaptations are made. (see below)

Use by non-commercial users

For non-commercial and non-promotional purposes, individual users may access, download, copy, display and redistribute to colleagues Wiley Open Access articles, as well as adapt, translate, text- and data-mine the content subject to the following conditions:

- The authors' moral rights are not compromised. These rights include the right of "paternity" (also known as "attribution" - the right for the author to be identified as such) and "integrity" (the right for the author not to have the work altered in such a way that the author's reputation or integrity may be impugned).

- Where content in the article is identified as belonging to a third party, it is the

obligation of the user to ensure that any reuse complies with the copyright policies of the owner of that content.

- If article content is copied, downloaded or otherwise reused for non-commercial research and education purposes, a link to the appropriate bibliographic citation (authors, journal, article title, volume, issue, page numbers, DOI and the link to the definitive published version on **Wiley Online Library**) should be maintained. Copyright notices and disclaimers must not be deleted.

- Any translations, for which a prior translation agreement with Wiley has not been agreed, must prominently display the statement: "This is an unofficial translation of an article that appeared in a Wiley publication. The publisher has not endorsed this translation."

Use by commercial "for-profit" organisations

Use of Wiley Open Access articles for commercial, promotional, or marketing purposes requires further explicit permission from Wiley and will be subject to a fee. Commercial purposes include:

- Copying or downloading of articles, or linking to such articles for further redistribution, sale or licensing;

- Copying, downloading or posting by a site or service that incorporates advertising with such content;

- The inclusion or incorporation of article content in other works or services (other than normal quotations with an appropriate citation) that is then available for sale or licensing, for a fee (for example, a compilation produced for marketing purposes, inclusion in a sales pack)

- Use of article content (other than normal quotations with appropriate citation) by for-profit organisations for promotional purposes

- Linking to article content in e-mails redistributed for promotional, marketing or educational purposes;

- Use for the purposes of monetary reward by means of sale, resale, licence, loan, transfer or other form of commercial exploitation such as marketing products

- Print reprints of Wiley Open Access articles can be purchased from: corporatesales@wiley.com

Further details can be found on Wiley Online Library
http://olabout.wiley.com/WileyCDA/Section/id-410895.html

Other Terms and Conditions:

v1.9

Questions? customercare@copyright.com or +1-855-239-3415 (toll free in the US) or +1-978-646-2777.

Gratis licenses (referencing $0 in the Total field) are free. Please retain this printable license for your reference. No payment is required.

Cunningham, Lawrence

From: pubscopyright <copyright@osa.org>
Sent: Wednesday, November 05, 2014 5:31 PM
To: Cunningham, Lawrence
Subject: RE: permission request for dissertation

Dear Mr. Cunningham,

Thank you for contacting The Optical Society.

Because you are the author of the source paper from which you wish to reproduce material, OSA considers your requested use of its copyrighted materials to be permissible within the author rights granted in the Copyright Transfer Agreement submitted by the requester on acceptance for publication of his/her manuscript. It is requested that a complete citation of the original material be included in any publication. This permission assumes that the material was not reproduced from another source when published in the original publication.

Please let me know if you have any questions.

Kind Regards,

Susannah Lehman

Susannah Lehman
November 5, 2014
Authorized Agent, The Optical Society

From: Cunningham, Lawrence [_____]
Sent: Friday, October 31, 2014 2:09 PM
To: pubscopyright
Cc: Cunningham, Lawrence; _____
Subject: permission request for dissertation

Hi Suzanna

I just left you a voice mail. I am requesting permission for use the article below in my dissertation.
Please let me know what additional thing that might be involved.
I do know that an original letter is required by ProQuest who will be publishing the dissertation.
Thanks!

Opt Express. 2006 Sep 18;14(19):8613-21.

Freeform multiphoton excited microfabrication for biological applications using a rapid prototyping CAD-based approach.

Cunningham LP, Veilleux MP, Campagnola PJ.

Abstract

1

Multiphoton excited polymerization has attracted increasing attention as a powerful 3 dimensional nano/microfabrication tool. The nonlinear excitation confines the fabrication region to the focal volume allowing the potential to achieve freeform fabrication with submicron capabilities. We report the adaptation and use of a computer aided design (CAD) approach, based on rapid prototyping software, which exploits this potential for fabricating with protein and polymers in biologically compatible aqueous environments. 3D structures are drawn in the STL format creating a solid model that can be sliced, where the individual sections are then serially fabricated without overwriting previous layers. The method is shown for potential biological applications including microfluidics, cell entrapment, and tissue engineering.

Regards,

Lawrence (Larry) Cunningham